Damage Assessment of Conventional and Passively Controlled Buildings against Individual and Successive Earthquake and Wind Loads

（個別および連続する地震・風荷重に対する在来および応答制御建物の被害評価）

July 2021

Doctor of Philosophy (Engineering)

Ahmad Naqi

アフマド　ナキ

Toyohashi University of Technology

Dedication

I dedicate this Ph.D. dissertation to my beloved Parents and wife as well as my brothers and sisters. Who always encourages me to go on every adventure especially this one.

Abstract

In the region where more than one type of natural disaster is probable, the possibility of progressive damage of buildings due to successive hazards is a concern. The demand loads recommend by design manuals and guidelines are based on the maximum probable disaster, while the contribution of multi-hazard events to the progressive damage is not considered. Under the maximum loads, the design provisions allow a certain amount of damage to the load-carrying members expecting to absorb the input energy by inelastic deformation. However, the damaged members must be required, while demolishing or rebuilding damaged buildings is not economically feasible. Therefore, it is necessary to identify the buildings that will be damaged under natural disasters and take countermeasures. To examine the seismic capacity of existing buildings in the building service periods, a practical damage assessment method is essentially required. Also, the occurrence scenario of multi-hazards in the building design life is necessary, especially for earthquakes and strong winds.

To reduce the damage to structural members under dynamic loads such as earthquake and wind loads, the application of response control devices is an excellent solution to absorb the induced energy. Unlike the general structural elements, the seismic response control device can be replaced after getting damaged. This unique feature makes the devices popular and to be manufactured with different characteristics and shapes. Under the design loads, the performance of different passive control devices is examined extensively by researchers to point out the pros and cons. Although the response control techniques could minimize the damage to buildings, they may increase the building cost, and uncertain about future benefits because of the fatigue and deterioration problem of response control devices. The literature review indicates the effectiveness of the response control techniques under the combined application of low-cycle of high-strain earthquake loads and high-cycle of low-strain wind loads is less explored. Although the high-cycle of low-strain wind loads do not cause significant damage to structural and non-structural elements, it may cause cumulative damage to response control devices and correspondingly progressive damage to buildings.

To encounter the stated problems, first, this study examined the seismic damage of low- and mid-rise conventional buildings located in Afghanistan. In this regard, as a practical damage assessment method, the Japanese screening procedure was practiced to examine the building's performance and it was found out that the screen method is capable to determine the vulnerable buildings in Afghanistan by adjusting the damage criteria. In the next step, a simplified procedure was introduced to evaluate the seismic performance of the passively controlled building under design loads. Since the main objective of the research is to measure the progressive damage in the building's lifetime, the study introduced a practical methodology to model the occurrence of natural disasters. The procedure is based on the Poisson process which is using the

return period and intensity of earthquake and wind events. The proposed method enables the assessment of the building performance in the service period under possible successive earthquake and wind loads.

Then, under multi-hazard scenarios, the accumulative damage to high-rise buildings with passive control devices was examined in terms of the damage index, the plastic strain energy, the absorbed energy, and the maximum and accumulative ductility factors. It was revealed that under the successive analysis of multi-hazard events, the overall building damage was about 1.5~2.0 times larger than the damage under the individual design loads. Also, Moreover, it was found that the passive control device may reach its fatigue limit under multi-hazard scenarios.

Finally, the current research proposed a framework for the damage assessment of passive control buildings under multi-hazard scenarios.

Acknowledgments

I want to highly appreciate the Ministry of Education, Culture, Sports, Science and Technology of Japan, for providing the MEXT Scholarship to pursue the Ph.D. degree in the Toyohashi University of Technology. It was an amazing opportunity to research about earthquake engineering in the Department of Architecture and Civil Engineering under the talented Japanese Lecturer and Professors.

Especially, I would like to express my deepest gratitude to Professor Dr. Taiki Saito, first for giving me this unique adventure in his team, secondly for supervising me during the doctoral course. His endless efforts during the master course as well as the three years of doctoral course, enable me to accomplished the degree, which is highly appreciated.

Table of Contents

Contents

List of tables

List of figures

Chapter 1: Introduction

1.1 Research background

Natural disasters (such as earthquakes, tsunami, winds, floods, etc.) result in a sudden or progressive degree of damage to buildings located in the region which are prone to one or a couple of the disasters. The design manuals and guidelines are provided to encounter the effects of natural disasters and improve the building's performance based on damage observation after each disaster. While the existing buildings designed by previous provisions remain vulnerable and cannot comply with the updated design provisions. Demolition of existing buildings and construction of new structures to fulfill the present design provisions are not practically and economically feasible. Therefore, to identify the buildings that are at risk of partial damage or collapse under a single or couple of natural disasters is a feasible procedure to screen the vulnerable buildings which are not complying with the updated design provisions. To examine the building's reliability for future use and ensure the loading carrying capacity of the structure, damage assessment of existing buildings is essentially required. For the rehabilitation of vulnerable buildings, a well-planned assessment is required before strengthening the existing buildings. The simple and effective assessment method must be developed based on the characteristics of load-carrying elements. As for the retrofitting method for existing buildings or the advanced method for new buildings, response control techniques are widely studied by researchers and engineers. Although the response control techniques could minimize the damage degree of buildings, they may increase the building cost, and uncertain about future benefits because of the fatigue and deterioration problem of response control devices. Currently, there are very few research studies about passively control buildings under the successive or a combination of more than one type of natural disaster.

1.2 Statement of research

The structural and non-structural elements of conventional buildings may suffer significant damage during the wind or earthquake loads excitation. In the conventional building, the load-carrying members are allowed to yield and reach the inelastic deformation capacity to absorb the lateral load excitations. Since the design of conventional buildings relies on the inelastic behavior of flexural members, design provision accepts limited damage to the members. However, the structural damage because of inelastic deformation is quite difficult to be repaired.

The passively controlling technology becomes one of the frequently applied techniques to minimize the inelastic deformation of load-carrying elements. Unlike the general structural elements, the seismic

response control device can be replaced after getting damaged. This unique feature makes the devices popular and to be manufactured with different characteristics and shapes. After the pioneering work by Kobori in 1986 [1], the seismic performance of different passive control devices is examined extensively by researchers to point out the pros and cons. It is reported, the devices are capable to protect the main structure by absorbing the earthquake energy. The excellent performance of passive control technology under the low-cycle of high-strain earthquake loads makes this sort of device an alternative to protect the buildings. Although, under the high-cycle of low-strain wind loads, which may induce accumulative damage to the devices, few studies have been conducted so far.

On the other hand, considering the regions which are prone to more than one type of natural disaster (such as earthquake and wind loads), the possibility of a multi-hazard is probable. The current seismic provisions generally speculate the wind or earthquake loads as a single-hazard event with the maximum intensity in the region. It is demonstrated by researchers [2], the multi-hazard analysis provides a superior understanding of the possibility of building damage under low to high rates of a natural disaster during the building service period. The researchers also demonstrate the effectiveness of vibration control devices for the earthquake load [3].

The use of passive control technology is common in high-rise buildings [4-5] to improve the seismic performance, since the high-rise buildings may experience a large amplitude shaking by resonance with the long period component of earthquake ground motions. During the service period, high-rise buildings will experience frequent earthquakes and typhoons [6], therefore, the performance of the high-rise building with a response control system must be examined under the multi-hazard scenario of earthquakes and long-duration winds. Although the performance of passive control devices in high-rise buildings under either earthquake and wind loads is extensively studied, limited studies had been conducted to evaluate the cumulative damage of the damper devices under the successful application of wind and earthquakes. It is because most of the seismic provisions and design guidelines specify the design method for the single event of earthquakes and winds [7].

1.3 Objective of research

The objectives of this research are listed below.

- The screening method recommended in the Japanese standard for seismic evaluation of existing buildings, which is using the seismic damage index, is adopted for the vulnerability assessment of existed RC buildings in Afghanistan. Since the criteria of the damage index are decided according to the observed data of damaged buildings in Japan, the current research introduces a simplified

procedure to identify the new criteria of the seismic damage index for the regions which are severely prone to the earthquake and there is no observed data available.

- The seismic screening method is applied for conventional buildings (such as reinforced and unreinforced masonry walls) in Afghanistan to demonstrate that the screening method can be used as a simple method to screen the conventional masonry buildings as well.

- To evaluate the seismic performance of passively control buildings, a simplified Capacity Spectrum Method (CSM)-based method is proposed. In the method, a practical procedure is introduced to estimate the effective damping ratio of bi-linear type response control devices.

- To assess the probability of multi-hazard events over the building lifetime, a practical procedure to estimate the likelihood of the occurrence of multi-hazard scenarios in the building design life is developed. The procedure is based on the Poisson process, which uses the anticipated return period and intensity to generate the earthquake and wind events. It is expected that the proposed method enables the decision-makers to anticipate the likely recurrence of earthquake and wind events during the building lifetime to evaluate the building performance in the service period.

- Furthermore, the study aims to evaluate the effects of damper deterioration induces by preceding events in the multi-hazard timeline to the succeeding events. For this purpose, the effects of preceding wind on the succeeding earthquake loads and vice-versa are examined. It is illustrated that as a result of damper deterioration the overall performance of passive control building is modified. The amplification of this modification is dependent on the intensities and number of preceding events in the multi-hazard timelines.

- And lastly, corresponding to fatigue and deterioration of dampers the study aims to develop a seismic damage model of damping device performance in the building lifetime. For this purpose, the accumulative damage model of damping devices is studied in terms of Cumulative Damage Index, Plastic strain energy, Energy absorption rate, and ductility factor. It is indicated, the fatigue life and performance of dampers is a multi-criteria index that needs to be studied precisely.

1.4 Research organization

This dissertation consists of six chapters and one appendix. A brief description of each chapter is presented as follows.

Chapter one: This chapter describes an overview of the conventional and passively controlled building considering the multi-hazard scenarios. The research topics are reviewed following the previous studies. The objective and the expected outcome of the research are presented.

Chapter Two: This chapter discusses the seismic performance of conventional buildings in Afghanistan. Two cases-study are conducted to assess the seismic damage of the low- and mid-rise buildings. The application of the first screening method prescribed in Japanese standards is presented for the conventional concrete masonry and RC buildings. It is reported that the screening method can be applied to conventional buildings.

Chapter Three: In this chapter, a simplified method is presented to evaluate the seismic performance of passively controlled buildings. The proposed method is a CSM-based procedure that incorporates the equivalent damping ratio to assess the structural performance. The proposed equation to estimate the equivalent viscous damping ratio of the response control dampers is examined. It is observed that the proposed procedure is a practical method to assess the seismic performance of passively controlled buildings.

Chapter Four: In this chapter, the damage assessment of passive control building is examined considering the effects of preceding events in the multi-hazard timeline, to succeeding events. The damper deterioration and accumulative damage due to preceding events to the overall performance of a high-rise RC building with steel damper are analyzed. In this regard, two multi-hazard scenarios, wind-earthquake, and earthquake-wind cases are evaluated. It is observed, the passive control building performance under the successive application of multi-hazard scenarios is modified.

Chapter Five: In this chapter, the performance of response control devices in the high-rise building lifetime is investigated. The Poisson process is practiced anticipating the likely occurrence and recurrence of multi-hazard timelines. Based on the Poisson process a practical methodology is introduced to predict the probability and distribution of earthquake and wind loads. Moreover, the fatigue life of the damping device is modeled using the procedure recommended in the literature. It is observed, the proposed model is an efficient tool, enables architects and engineers to more precisely draw the distribution of multi-hazard events in the building lifetime and establish the cumulative damage and deterioration model of damping devices. The proposed cumulative damage and fatigue life model can be used as a maintenance plan to identify the vulnerable response control devices.

Chapter Six: The last chapter of this dissertation summarized the finding of the research and present the recommendation of the individual chapter. It has also included the research topic to be explored in the future.

Appendix A: In this section, the preliminary design procedure which was adopted in this dissertation to design the passive control device is presented. The preliminary design is based on the simplified procedure recommend in the Japanese manual for the Design of passively controlled buildings (JSSI) [8].

Chapter 2: Damage assessment of conventional buildings

2.1 Introduction

From the structural viewpoint, buildings are either conventional or controlled structures to resist lateral excitation. Conventional buildings are mainly constructed employing the traditional method of construction and common materials. Brick masonry, wooden structures, reinforced concrete, and steel elements are the common materials that are mainly practiced to construct buildings globally. In this method of construction, traditional knowledge is passed from one generation to the next, which is why new homes are built almost identically to those built over 25 years ago. Therefore, these buildings are mainly vulnerable to lateral excitation due to their material, design, and construction uncertainties.

2.2 Seismic index of conventional buildings

Seismic Index I_S is defined in the Japanese Standard, 2000, [9] to evaluate the seismic performance of low-rise and medium-rise RC buildings and is calculated by the **Eq. (2.1)** for each story and in each principal horizontal direction of a structure. As can be seen in the equation I_S is related to the basic seismic index E_0, time index T, and irregularity index S_D. The time index is a modification factor of the basic seismic index which evaluates the effects of cracks, deflection, and aging of building through screening procedure defined in Japanese standard for seismic evaluation of the existing building. The irregularity index is introduced to adjust the basic seismic index by measuring the effects of horizontal shapes, vertical shapes, mass, and stiffness-irregular distribution following engineering judgment.

$$I_S = E_0 \times S_D \times T \tag{2.1}$$

In the equation, E_0 is the basic seismic index which for the 1st level of screening, it is approximately obtained by multiplying the shear modification factor, Strength index, and ductility index of the load-carrying element in the story. The Japanese standard for seismic evaluation of existing buildings [9] introduces three levels of screening procedures, among them, 1st-Level with less amount of detail and 3rd-Level precisely evaluated the seismic performance of existing conventional buildings. Thus, the current work employee the 1st-Level of screening procedure to evaluate the low- and mid-rise conventional buildings. According to the first level of screening the vertical elements are classified into three categories as outlined in **Table 2.1**.

Table 2.1: Vertical member Classification and Ductility Index for 1st-Level of Screening.

Vertical Members	Definition	Ductility Index (*F*)
Column	$\frac{H_0}{D} > 2$	1.00
Extremely Short Column	$\frac{H_0}{D} \leq 2$	0.80
Wall	Walls including those without boundary Columns	1.00

whereas, H_0 is the clear height of the column and D is the depth of the column. And the basic seismic index is taken equal to the larger value of **Eqs. (2.2)** and **(2.3)**.

$$E_0 = \frac{n+1}{n+i}(C_W + \propto_1 C_C) F_W \quad (2.2)$$

$$E_0 = \frac{n+1}{n+i}(C_{SC} + \propto_2 C_W + \propto_3 C_3) F_{SC} \quad (2.3)$$

The parameter of the above equations is defined as bellow:

n	is number of stories.
i	is number of the concern story.
C_w, C_c, and C_{sc}	are strength indexes of walls, Columns, and extremely short columns.
F_w and F_{sc}	are ductility index of walls and extremely short columns, defined in **Table 2.1.**
α_1	is the effective strength factor of the columns at the ultimate deformation of walls, and it is equal to 0.70.
α_2	is the effective strength factor of the walls at the ultimate deformation of extremely short columns, and it is equal to 0.70.
α_3	is the effective strength factor of the columns at the ultimate deformation of extremely short columns, and it is equal to 0.50.

For the first level of screening, the strength Indices of wall, column, and short-column are calculated approximately by **Eqs. (2.4)**, (**2.5)** and (**2.6)**.

$$C_C = \frac{\tau_C \times A_C}{\sum W} \beta_C \quad (2.4)$$

$$C_{SC} = \frac{\tau_{SC} \times A_{SC}}{\sum W} \beta_C \quad (2.5)$$

$$C_w = \frac{\sum \tau_{wi} \times A_{wi}}{\sum W} \beta_C \quad (2.6)$$

where, A_C, A_{SC}, and A_W are the area of column, short-column, and wall in (mm^2), respectively. And τ_C, τ_{SC} & τ_W are the average shear strength of column, short-column, and wall in (MPa). β_C is a modification factor that is based on the nominal compression strength (f_C) of concrete. Where ($\beta_C = \frac{f_C}{20}$) in case ($f_C \leq 20$Mpa), and ($\beta_C = \sqrt{\frac{f_C}{20}}$) in case ($f_C$>20Mpa). The ΣW is the total permanent load sustained by the concerned story plus the live load for seismic calculation [9]. F_W and F_{SC} are ductility indices of wall and short-column, which in the case of the first level of screening, they are equal to (F_W= 1.0).

2.3 Case study 1: Low-rise reinforced masonry buildings.

In Afghanistan mainly, the low-rise structures are build using stone, clay, brick, or concrete block masonry, because of the low price and extensive availability. Since most of the regions in Afghanistan are prone to earthquake ground shaking, the building damage assessment is crucial. To evaluate the conventional building performance, fifteen reinforced masonry buildings, which are located in Kabul Afghanistan are selected. Low-rise masonry structures are very popular in Kabul and major cities in Afghanistan. Except for few buildings, most of the masonry buildings are constructed without consideration of the risk of earthquake, only following age-old methods without any modern building code or Afghanistan Structural Code (ASC) taken into consideration. The Kiran-wa-Munjan earthquake, with Magnitude 7.5 on 26 Oct 2015 which killed 115 people and injured 538 people [Statistics of the Afghanistan Government], shows that the life and lives could be under severe threat of earthquakes in Afghanistan due to the movement of the Indian plate over Eurasia being at a rate of 4 cm/year. Most of the casualties are due to the masonry building collapse. Therefore, one of the problems is the existing low-rise structures which essentially require seismic evaluation to screen vulnerable buildings. Among these 15 buildings; nine specimens are two-story existing buildings, and six specimens are three-story recently designed buildings. The buildings have different reinforcement details that are commonly used in Afghanistan. All the buildings have the same wall thickness of 200 *mm* but the masonry design compressive strengths f_m are different. The nominal yielding strengths of reinforcing bars are equal 345MPa for all the buildings. An outline of the buildings is presented in **Table 2.2**. It is assumed that all the specimens are located in very dense soil and soft rock that is classified as C-type in the Afghanistan Structural Code (ASC) [10].

Table 2.2: Outline of low-rise reinforced masonry buildings.

Building No.	Design f_m (MPa)	No. of Floor	Building Dimension		Shear Reinforcement of wall (single layer)	Story H. *(m)*
			L. (m)	*W. (m)*		
B01	10	2	20.8	20.6	D12@600mm	3.00
B02	12	2	24.7	10.95	D14@600mm	3.00
B03	13	2	29.6	27.2	D14@500mm	3.00
B04	10	2	41.5	8.95	D12@400mm	3.00
B05	12	2	35.2	14.00	D10@600mm	3.00
B06	10	2	66.00	10.95	D12@500mm	4.00
B07	10	2	46.20	10.95	D12@600mm	3.00
B08	10	2	22.00	12.00	D12@600mm	3.00
B09	10	2	44.00	10.00	D12@600mm	3.00
B10	10	3	11.33	10.83	D10@400mm	3.20
B11	10	3	13.00	10.80	D12@500mm	3.00
B12	12	3	12.38	8.60	D12@500mm	3.20
B13	10	3	12.38	11.50	D12@400mm	3.00
B14	12	3	10.25	9.75	D12@400mm	3.00
B15	12	3	24.70	10.95	D14@600mm	3.20

In the case of the reinforced masonry block, the masonry walls sustain the gravitational and seismic load and the building has no column (C_C=0) and beam. Thus the **Eq. (2.6)** is practiced to estimate the strength index of the walls C_W. In addition, the ductility index of the CMU wall F_W was assumed to be 1.0 because of the following reason. According to the study by Shing et al. [11], the deformation capacity of the masonry shear wall depends on the final damage mode. And in the case of shear failure mode, the deformation capacity is around 1/250 drift angle that corresponds to F_W=1.0. Since the vertical reinforcement ratio of the specimens of masonry buildings is relatively small, the study assumed the failure mode is shear and adopted F_W=1.0.

As for the average stress at the ultimate state of the wall, τ_W, the Akira Matsumura [12] concluded that the maximum shear stress is more than 1.6MPa for reinforced masonry walls. So, this study adopted (τ_W=1.0MPa) considering safety margin. Conventionally, the β_C applied for reinforced masonry wall structure based on nominal compression strength f_m of masonry. Besides, A_{wi} and α are the areas of wall and modification factor of the column at ultimate deformation [9]. The result of the seismic index for the target masonry buildings is presented in **Table 2.3**.

Table 2.3: Estimated seismic index of Low-rise reinforced masonry buildings.

Building No.	∑W	∑A_w (m^2)		β_C	Wall strength index (C_w)		I_S index	
	MN	*L. Dir*	*T. Dir*		*L. Dir*	*T. Dir*	*L. Dir*	*T. Dir*
01	10.2	9.44	8.88	0.50	0.46	0.43	0.46	0.43
02	7.1	10.08	9.87	0.60	0.84	0.83	0.84	0.83
03	19.3	14.08	14.10	0.68	0.47	0.47	0.47	0.47
04	12.0	18.80	14.07	0.50	0.45	0.45	0.45	0.45
05	11.8	10.78	7.32	0.60	0.55	0.37	0.55	0.37
06	17.3	12.70	5.07	0.50	0.37	0.15	0.37	0.15
07	13.0	12.24	9.87	0.50	0.47	0.38	0.47	0.38
08	6.3	4.85	5.66	0.50	0.38	0.45	0.38	0.45
09	11.4	7.48	4.20	0.50	0.33	0.18	0.33	0.18
10	3.6	5.57	2.30	0.50	0.76	0.32	0.76	0.32
11	5.7	4.08	4.78	0.50	0.36	0.42	0.36	0.42
12	4.2	3.52	2.47	0.50	0.50	0.35	0.50	0.35
13	5.5	6.00	2.96	0.50	0.54	0.27	0.54	0.27
14	5.5	5.95	3.50	0.60	0.65	0.38	0.65	0.38
15	10.7	10.08	9.87	0.60	0.56	0.55	0.56	0.55
Note 1: Time index and Irregularity index assumed 1.00 for all buildings.								

To evaluate the estimated seismic index the masonry building's performance was studied using the Capacity spectrum method. Therefore, the seismic performance of each building is calculated under the design response spectra defined by the Afghan Structural Code and scaled El Centro 1940 ground motion. **Figure 2.1** represents the design response spectrum and a scaled historical ground motion. The low-rise masonry buildings were modeled by STERA-3D software [13], to conduct the non-linear static pushover analysis. The software has the capability to input the force-deformation parameters directly for structural elements. Whereas, the hysteresis model of masonry elements defined as the poly-linear slip model, **Figure 2.2**. The yield shear force Q_y assumed equal to reinforced masonry wall shear capacity V_{um}. The ultimate shear capacity of the wall is speculated in the Building Code Requirements for Masonry Structure [14] as given in **Eq. (2.7)**. And the crack shear force (Q_c=1/3Q_y) is estimated as one-third of the yield shear force. Furthermore, the yield shear deformation and ultimate shear deformation (γ_y=1/250) and (γ_u=1/100) are assumed, respectively. And the cracked shear deformation is calculated relative to the initial stiffness, **Eqs. (2.8)** and **(2.9)**.

$$V_{um} = 0.083\left[4.0 - 1.75\left(\frac{M_u}{V_u d_v}\right)\right] A_v\sqrt{f'_m} + 0.25P_u \qquad (2.7)$$

$$\gamma_c = \frac{Q_c}{k_0} \qquad (2.8)$$

$$k_0 = \frac{2Q_y}{\gamma_y} \tag{2.9}$$

In **Eq. (2.7)**, M_u and V_u are the ultimate moment and the shear forces in (*N-mm*) and (*N*) respectively, f'_m and f_y are the nominal compressive strength of masonry and yield strength of reinforcement in (MPa), P_u is the ultimate axial load in (*N*), d_v and A_v are the depth of masonry wall in the direction of shear considered and the cross-sectional area of shear reinforcement in (*mm*) and (mm^2). M_u and V_u, due to gravity load and lateral load, calculated following ASC seismic section and $\left(\frac{M_u}{V_u d_v} \leq 1\right)$ should not exceed 1.0.

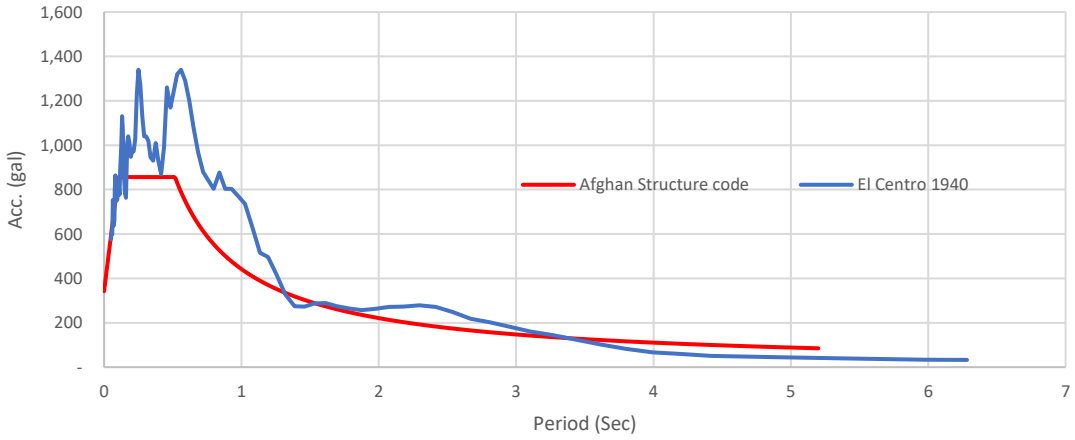

Figure 2.1: Design response spectrum and scaled El Centro Response Spectra.

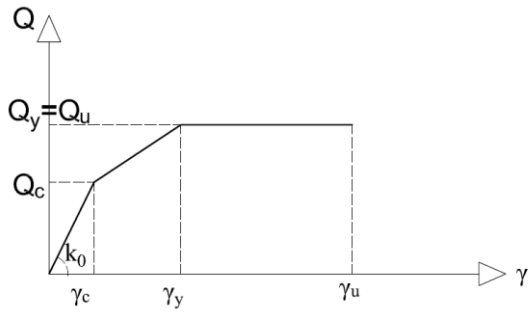

Figure 2.2: Shear-Deformation Relation of reinforcing masonry wall.

The capacity curves of masonry buildings in longitudinal and transverse directions, which represent the relationship of inter-story drift and story shear in acceleration divided by the mass, are presented in **Figure 2.3**. Following the Japanese Standard [16] for Capacity Spectrum Method (CSM), the target building's performance points are established, and accordingly, the maximum story displacements are determined.

It is observed, in most cases, buildings with a large seismic index are able to satisfy the safety design limit (1/250). However, in some rare cases, buildings with similar seismic indexes have different results. For instance, building No. 6 and building No. 8 with a similar seismic index of 0.37 and 0.38, respectively, in the longitudinal direction, have different seismic performances. Unlike building No. 8, which satisfies the safety drift limit, building No. 6 is not able to satisfy the limit. This difference in performance is related to the amount of shear capacity and reinforcement, and the architectural configuration of masonry walls. Since the I_s index for the first level of inspection neglects the reinforcement contribution, two buildings show a similar seismic I_s index. **Figure 2.4** shows the relationship between the maximum story drift and seismic index. From this figure, the buildings with a seismic index equal to or larger than (≥0.5) are able to confirm the Safety Drift Limit (1/250). Therefore, it is concluded the reinforced masonry buildings with the seismic index $I_S \geq 0.5$ are capable to withstand the earthquake demand loads in Afghanistan.

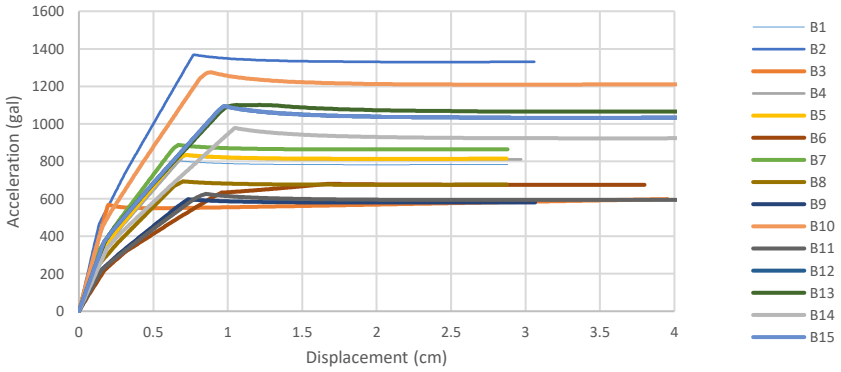

a) Longitudinal Direction

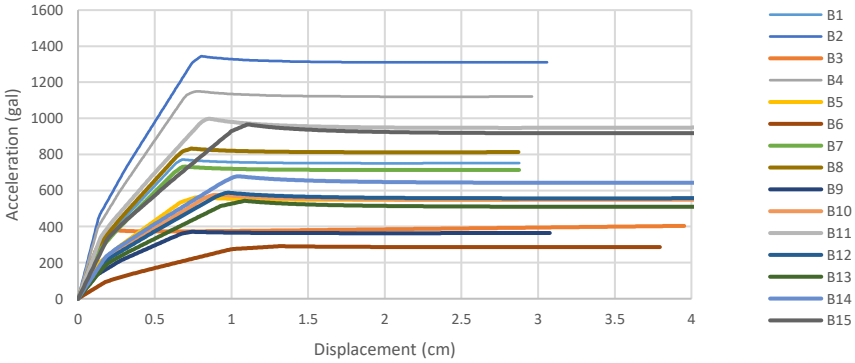

b) Transverse Direction

Figure 2.3: Capacity Curve of Low-rise reinforced masonry wall Buildings.

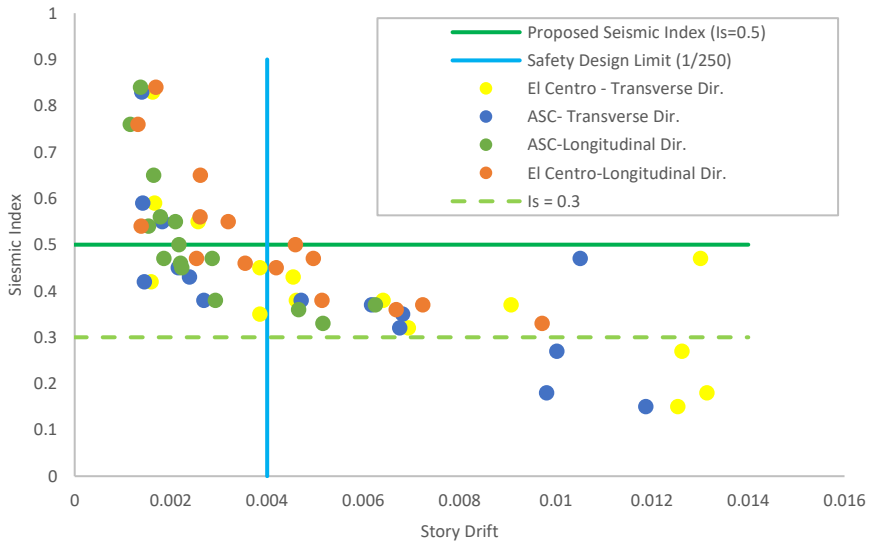

Figure 2.4: Comparison of the estimated seismic index and Inter-story Drift Angle of targe models.

2.4 Case study 2: Mid-rise RC moment-frame buildings.

To further elaborates the damage assessment of conventional buildings, in this section six mid-rise reinforced concrete moment-frame is selected. Since the mid-rise RC moment frames extensively constructed in the seismically active regions, the buildings are considered to more precisely investigate the target building performance. Similar to the low-rise structure the mid-rise buildings are existing buildings located in Kabul city of Afghanistan. The outline of target models is presented in **Table 2.4** for further information.

Table 2.4: Outline of Mid-rise RC moment-frame buildings.

Building No.	No. of Floor	F_C (MPa)	F_y (MPa)	Target Building Dimension (m)				Building Function
				Wide	Length	Typical F. Height	Total Height	
No.1	5 Story	20	295	15.00	31.00	3.24	16.20	Residential apartment
No.2	5 Story	20	295	12.00	16.20	3.00	15.20	Residential apartment
No.3	4 Story	21	295	10.30	16.00	3.00	12.00	Residential House
No.4	5 Story	20	295	16.00	46.00	3.20	16.00	Residential apartment
No.5	4 Story	24	295	17.10	51.00	3.60	14.40	Dormitory
No.6	3 Story	24	295	16.50	60.10	4.20	12.60	Classroom Building

Following **Section 2.2**, the seismic index of target buildings is calculated for both longitudinal and transverse directions. **Table 2.5** represents the calculated Seismic Indices according to the first level of screening at the ground floor level of the buildings. Whereas both the irregularity index and time index are assumed equal to (T=S_D=1.0).

Table 2.5: Estimated Seismic Index of Mid-rise RC moment-frame buildings.

Building No.	β_c	$\sum W$ (MN)	Seismic Index (I_S) of Ground Floor			
			Original Building		Retrofitted Building	
			Long. Axis	Trans. Axis	Long. Axis	Trans. Axis
No.1	1.00	27.90	0.19	0.20	0.40	0.44
No.2	1.00	13.68	0.15	0.20	0.33	0.42
No.3	1.02	7.95	0.17	0.15	0.41	0.39
No.4	1.00	44.10	0.12	0.13	0.31	0.29
No.5	1.09	47.59	0.30	0.30	0.39	0.49
No.6	1.09	31.39	0.33	0.26	0.45	0.46

Then following the capacity spectrum method and non-linear time history is practiced determining the maximum story drift ratio under the demand earthquake recommend in Afghanistan structural code. To conduct the time history analysis the historical earthquake ground motion was scaled to be compatible with the design response spectrum. Three sets of historical earthquake's phase angles, such as El-Centro 1940, Kobe 1995, and Tohoku 1987 Earthquakes, were selected. The result of CSM and THA revealed that the none of six selected buildings are capable to withstand the 1% (safety limit) of story drift ratio. It is observed, the maximum seismic index in the longitudinal direction is (Is=0.33) that belongs to Building no. 6, but in the transverse direction, it is (Is=0.30) that belongs to Building no. 5. From the result of CSM and THA it is determined, nor Building no. 5 and 6 can satisfy the safety design limit of (1/100).

Therefore, the building seismic performance is strengthened by considering reinforced concrete shear walls. The retrofitted shear walls have the same nominal concrete compression strength and steel yield strength as the original target building. The shear reinforcing detail (2 layers of D13 at 150mm) and wall thickness (150mm) are adopted for all shear walls. But the length and numbers of shear walls are different depending on the building spaces. Then, a similar procedure was applied for strengthened buildings and the results of the maximum inter-story drifts are compared for Capacity Spectrum Method and Time History Analysis, respectively, **Figure 2.5**. The seismic indices of strengthened buildings were recalculated and given in **Table 2.5**.

By strengthening the target buildings, through installing reinforced shear walls, the seismic index according to the first level of screening is increased about 150~200%. Parallel to the seismic index the results of CSM and time history were improved. Since the retrofitting was designed to enable the buildings to achieve the safety design limit of 1/100. Therefore, the result of retrofitted buildings represents that they are able to satisfy the safety design lime of 1/100, however, they are failed to satisfy the serviceability

design limit of 1/200. It is concluded, **Figure 2.5**, that mid-rise RC building with $I_s \leq 0.5$ has the potential the withstand the earthquake demand in the selected region.

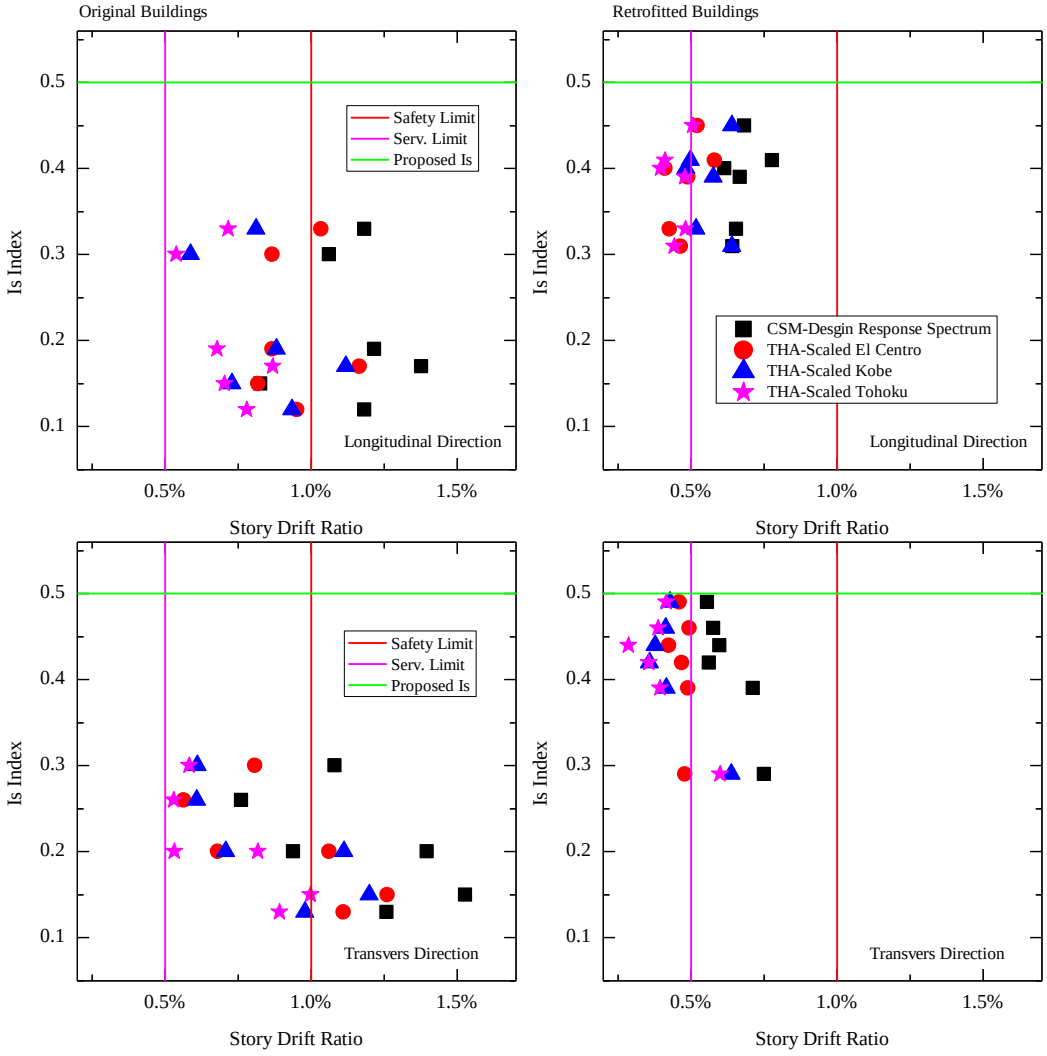

Figure 2.5: Comparison of the estimated seismic index and Inter-story Drift Angle of targe mid-rise RC frame buildings, before and after strengthening.

2.5 Conclusions

The Screening Procedure defined by "Japanese Standard for Seismic Evaluation of Existing Reinforced Concrete Building" is a useful tool that not enables the structural engineers to evaluate the seismic performance of the reinforced concrete building, but it is capable to determine the vulnerable conventional masonry as well. It is an appropriate procedure to be used to assess the seismic demands of low-rise and mid-rise buildings in Afghanistan. Among the three procedures defined by the standards, the study

estimates the seismic demand using the first level of the screening procedure. Consequently, besides the reinforced concrete buildings, this study made the procedure applicable in the case of reinforced masonry structures, as well.

Chapter 3: Damage assessment of passively controlled buildings

3.1 Introduction

Dissipating the earthquake energy by implementing damping devices along the height of the building is one of the recent technologies used frequently to mitigate earthquake damage. These types of buildings are rapidly expanding worldwide. For instance, in Japan, almost most of the recently constructed high-rise buildings are equipped with passive control technology [17]. In these sorts of buildings, damping devices are implemented to provide additional damping by dissipating the earthquake ground motion's energy. Various types of damping devices are manufactured and available in Japan [18-29]. For that reason, the Japan Society of Seismic Isolation (JSSI) classified the damping device into four major categories of Viscous Damper (VD), Viscous-Elastic Damper (VED), Oil Damper (OD), and Steel Damper (SD) [18]. Among the four major categories mentioned above, the damage assessment of bilinear type oil damper is studied and presented in this chapter.

Typically, the bilinear-type oil damper is consisting of a steel piston with an orifice head, piston rod, and steel cylinder which is infilled with low-viscosity oil [20]. The system is manufactured with a proportional valve and a relief valve of different characteristics. At the low velocity, the proportioning valve operates and produces the damping coefficient whereas the force-velocity relation is linear. Within a certain level of velocity, the relief valve starts to operate which produces the damping coefficient called post-relief damping coefficient. Because of the relief valve, the damping Force-Velocity (*F*-*V*) diagram bent which is known as the bi-linear characteristic of the system [20]. The bi-linear force-velocity (F-V) relation is fundamental for oil damper, which dissipates a huge amount of earthquake energy.

Generally, seismic assessment and design of the structure with added oil damper require non-linear time history analysis, which is extremely time-consuming. A couple of straightforward procedures, based on CSM, have been introduced by researchers to make the CSM applicable to passive control buildings. But, taking into account the force-displacement relationship in CSM and force-velocity relationship of the oil damper, a practical method is introduced to estimate the effective damping ratio of the building with the oil damper in this chapter.

3.2 Literature review

The CSM is a practical tool to evaluate the seismic performance of buildings using a response spectrum and an equivalent linear system. Since its original development by Freeman in 1975, it has been modified and adopted by different organizations [30]. For instance, in 1980, the Applied Technology Council (ATC) published the guideline to evaluate building performance using the CSM concept [31]. Similarly, in 1998, the Building Standard Law of Japan adopted the concept of CSM as one of the procedures for the seismic design of buildings [16]. Likewise, many researchers have assessed the accuracy of the method and applied it over a wide range of structural systems [32]. Consequently, several modifications have been proposed to improve the application of CSM depending on the structural type of buildings.

Generally, seismic assessment and design of structures equipped with damping devices require non-linear time history analysis, which is highly time-consuming. A couple of straightforward procedures have been proposed by researchers to evaluate the seismic performance of passively controlled buildings. Choi and Kim [33] developed a CSM-based procedure to estimate the amount of supplemental viscous damping for a multi-story building to reduce the roof displacement in the range of pre-defined target displacement. A similar concept is further illustrated by Kim et al. [34], and Li and Liang [35]. The study conducted by Chen et al. [36] introduced an improved version of CSM to estimate the number of metallic dampers under earthquake loads. In the case of buildings with viscoelastic dampers, Han et al. [37] employed CSM to analyze the performance of the passively controlled buildings. Benavent-Climent and Escolano-Margarit [38] compared the results of shaking table tests of the scaled-specimens equipped with the hysteretic dampers and those obtained by the improved CSM procedures, and it is reported that the improved CSM has the potential to estimate the maximum displacement with acceptable accuracy. Kim et al. [39] discussed the optimal distribution of steel dampers along with the height of the structures using the CSM procedure. Kosmas et al. [40] proposed an alternative CSM method using the constant ductility inelastic spectra to estimate the seismic performance of structures with viscous dampers. Joao Estevao [41] incorporated the CSM method to investigate the seismic risk of buildings in a seismically active region using the capacity curves of individual buildings. Furthermore, the effectiveness of CSM to design and evaluate the retrofitting of RC buildings is extensively discussed and reported by researchers [42-43]. Ramirez et al. [44] proposed two simplified procedures similar to CSM; the equivalent lateral force (ELF) and response spectrum procedures (RSP) which are adopted in the 2000 NEHRP and ASCE7 provisions for the design of passively controlled buildings. In the ELF method, the contributions of the first mode and residual mode are incorporated, wherein the RSP method, the contributions of higher modes are also considered to estimate the response of building with damping devices.

As the Oil Damper device (OD) is widely used due to its excellent performance, such as durability of aging, durability under repeated loading cycles, low-temperature dependence, high energy dissipation capacity, and stable mechanical properties [8,18,19,20]. Especially, the bilinear-type oil damper, which has a relief valve and reduces the rate of increase of damping force when the relief velocity is exceeded, is commonly used in Japan, especially for high-rise buildings. Adachi et al. [45,46] introduced a design procedure to minimize the story drift and acceleration of the high-rise building by optimizing the OD relief force distribution along with the height of the building. Ji et al. [47] reported about the contribution of OD in a real size 5-story steel building tested on the E-defense shaking table in Japan. Xie et al. [48] examined the performance of an eight-story steel building equipped with oil dampers damaged during the 2011 Great East Japan Earthquake. Takabatake and Kitada [49] proposed a simplified procedure to evaluate the seismic performance of a retrofitted building with OD installed inside and outside of the structural frame.

Although the seismic performance of buildings with hysteretic and viscous dampers are studied extensively, few studies have been done on the CSM methods for passively controlled buildings with bilinear type oil dampers. Therefore, this study proposes a CSM-based method to estimate the maximum responses of passively controlled buildings with bilinear type oil dampers, and the results are compared with those of nonlinear time history analysis.

3.3 Proposal of SRSS effective damping ratio

The equivalent damping ratio, h_h, of a hysteresis damper is defined [50] as,

$$h_h(\mu) = \frac{1}{4\pi}\frac{\Delta W_h}{W} \tag{3.1}$$

where ΔW_h is the hysteresis energy under one cycle of hysteresis and W is the area of elastic strain energy. For the bilinear hysteresis, as shown in **Figure 3.1a**, they are obtained as;

$$\Delta W_h = 4\,K\,\delta_y^2(\mu-1)(1-p) \tag{3.2}$$

$$W = \frac{1}{2}\,K\,\delta_y^2\,\mu^2 \tag{3.3}$$

in the **Eqs (3.2)** & **(3.3)**, δ_y is the yield displacement of the system, μ is a displacement ductility factor, K is the initial stiffness, and p is the ratio of post-yield to pre-yield stiffness.

In the same way, the equivalent damping ratio, h_V, of an oil damper is defined as,

$$h_v(\mu) = \frac{1}{4\pi}\frac{\Delta W_v}{W} \tag{3.4}$$

where ΔW_V is the area of one cycle of force-velocity relation of the oil damper given by.

$$\Delta W_v = \pi\, C\omega\ \mu^2\ \delta_y^2 \tag{3.5}$$

where C is the damping coefficient of the oil damper and ω is the equivalent circular frequency of the system.

In the case of the system with a hysteresis damper and an oil damper, according to the Building Standard Law of Japan [16], the effective damping ratio, h_{eff}, of a seismically isolated building is defined by the direct sum of three types of damping ratios as given in **Eq. (3.6)**.

$$h_{eff,Direct} = h_0 + h_h + h_v \tag{3.6}$$

where h_0 is the inherent damping ratio.

Kasai et al. [51] proposed a formula of the effective damping ratio as of the average of equivalent damping ratio in the range of (0 to μ) as given in **Eq. (3.7)**. It is reported that the accuracy of this formula is relatively high to estimate the earthquake response of the system. However, it is difficult to obtain an explicit analytical solution for the general hysteresis model.

$$h_{eff,Kasai} = \frac{1}{\mu}\int_0^{\mu} h_{eq}\,(\mu')d\mu' = \frac{1}{\mu}\int_0^{\mu} \left(h_h(\mu') + h_v(\mu')\right) d\mu' \tag{3.7}$$

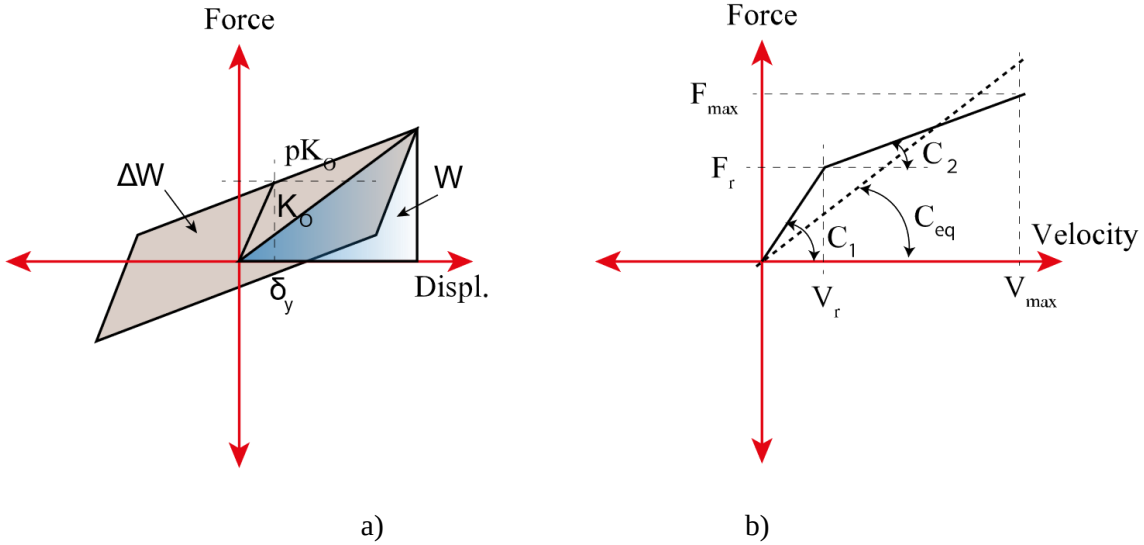

a) b)

Figure 3.1: a) The force-displacement relation of the bilinear hysteresis model; b) the force-velocity relation of bilinear type oil damper.

The current research study proposes a formula to calculate the effective damping ratio from the sum of the inherent damping and the Square Root of Sum of Square (SRSS) of the equivalent hysteresis and viscous damping ratios as given in **Eq. (3.8)**.

$$h_{eff,SRSS} = h_0 + \sqrt{h_h^2 + h_v^2} \tag{3.8}$$

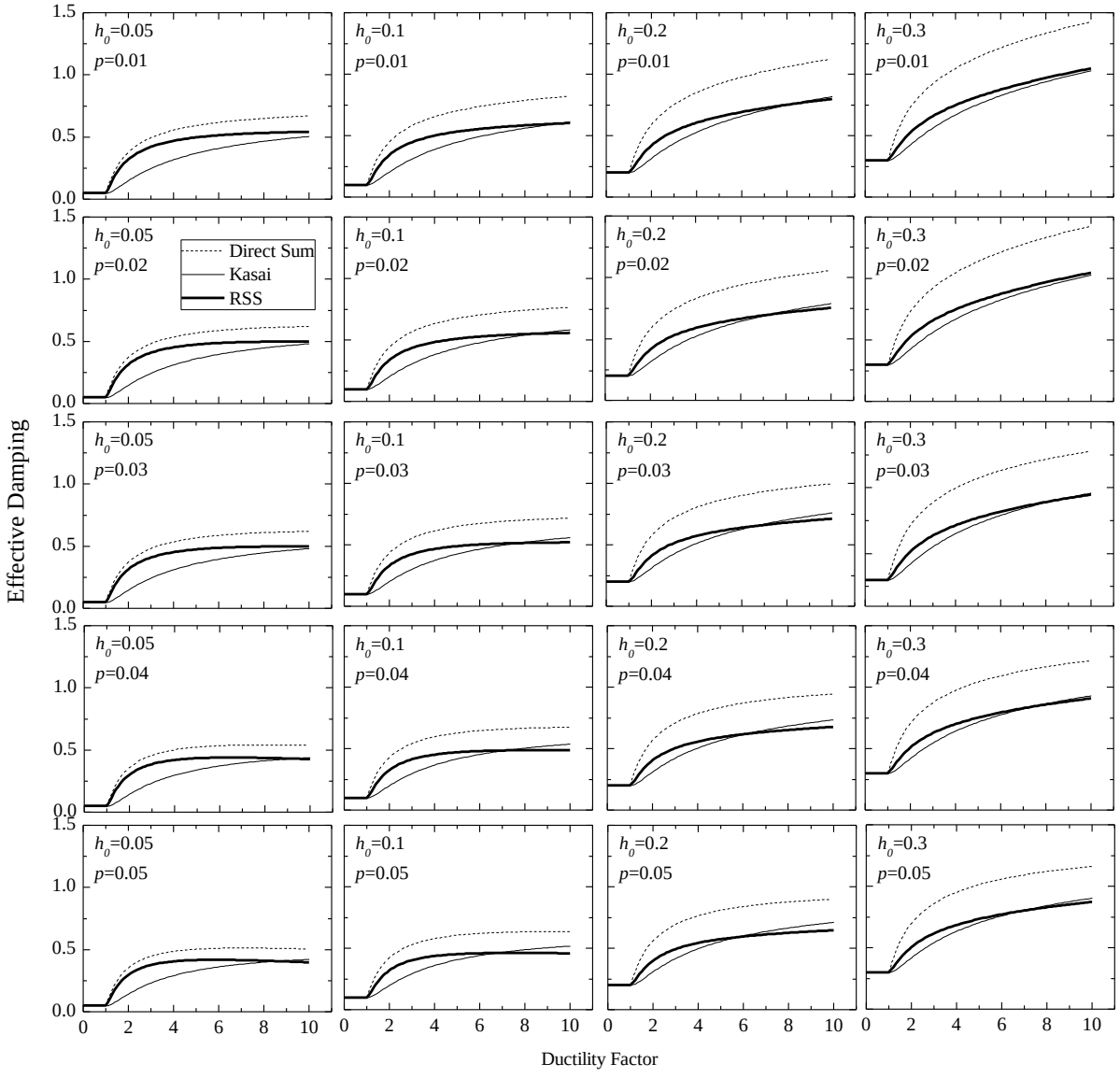

Figure 3.2: Comparison of different procedures to estimate the effective damping ratio.

The comparison of the values of effective damping ratio for the three procedures ($h_{eff,Direct}$, $h_{eff,SRSS}$, and $h_{eff,Kasai}$) with respect to the ductility factor is shown in **Figure 3.2**, where the post-yield stiffness ratio p

and the initial damping factor h_0 are varied as (p=0.01~0.05) and (h_0=0.05~0.3). It is depicted that the proposed $h_{eff,SRSS}$ is getting close to the value of $h_{eff,Kasai}$ as h_0 increases. On the other hand, $h_{eff,Direct}$ overestimates the effective damping ratio by 30% compared to $h_{eff,Kasai}$.

In the case of the bilinear-type oil damper, the equivalent damping coefficient C_{eq} is proposed in the JSSI manual so that the area under equivalent linear damping should be equal to the area of bilinear force-velocity relation as shown in **Figure 3.1b**, [8], and derived as;

$$C_{eq} = \frac{C_1}{\mu *^2} + C_2\left(1 - \frac{1}{\mu *}\right)^2 + \frac{2C_1}{\mu *}\left(1 - \frac{1}{\mu *}\right) \tag{3.9}$$

wherein **Eq. (3.9)**, C_1, and C_2 are the pre-relief and post-relief damping coefficients of bi-linear oil damper, and μ* is the ratio of maximum velocity to the relief velocity. In the subsequent sections, the proposed $h_{eff,SRSS}$, which is obtained from C_{eq}, is used to evaluate the maximum seismic performance of a steel building by CSM.

3.4 Proposed CSM procedure for buildings equipped with oil dampers

This section demonstrates the procedure of the proposed CSM using the Equivalent Single Degree of Freedom (ESDOF) system defined by Kuramoto et al. 2000 [53]. The ESDOF is consisting of a mass m, a frame damping coefficient C_f, and a stiffness, K_f. This study assumes that the natural period of the ESDOF is 0.5 sec and the base shear coefficient (i.e. the ratio of yielding force to the total weight) is 0.2. The ESDOF is equipped with the bilinear-type oil damper which has a damping coefficient, C_D, and a stiffness, K_D, as shown in **Figure 3.3a**. The ESDOF parameters are summarized in **Table 3.1** and **Table 3.2**.

Table 3.1: Technical parameters of ESDOF system**.**

Natural Period (*T*)	**Weight (*W*)**	**Damping (h_0)**	**Stiffness (K_F)**	**Yielding Force (F_y)**	$p = \frac{K_2}{K_1}$*
sec	***kN***	***%***	***kN/cm***	***kN***	
0.5	5,000.0	5.0	805.68	1,000.0	0.05

* K_1 and K_2 represent the pre-yield and post-yield stiffness of the ESDOF system, respectively.

The capacity curve of the system is shown in **Figure 3.3b**. The demand curve is presented in the form of the acceleration-displacement spectrum of the selected earthquake ground motion. In this study, the Level-2 earthquake defined in the Building Standard Law of Japan [16] is used to generate the design acceleration-displacement response spectrum with 5% damping factor. The latter one is adjusted according to the value of the effective damping using the reduction factor F_h in **Eq. (3.10)** adopted by the JSSI manual [8] from the study conducted by Kasai et al. [52].

$$F_h = \frac{\sqrt{1 + 25h_{5\%}}}{\sqrt{1 + 25h_{eff}}} \tag{3.10}$$

Table 3.2: Technical parameters of the supplemental story-equivalent oil damper.

Stiffness (K_D)	**Pre-relief Damping Coef. (C_1)**	**Relief velocity (V_r)**	$\frac{C_2}{C_1}^*$
kN/cm	***kN-sec/cm***	***cm/sec***	
805.68	22.0	5.0	0.05

* C_1 & C_2 represent the damping pre-relief valve & post-relief valve operation of oil-damper, respectively.

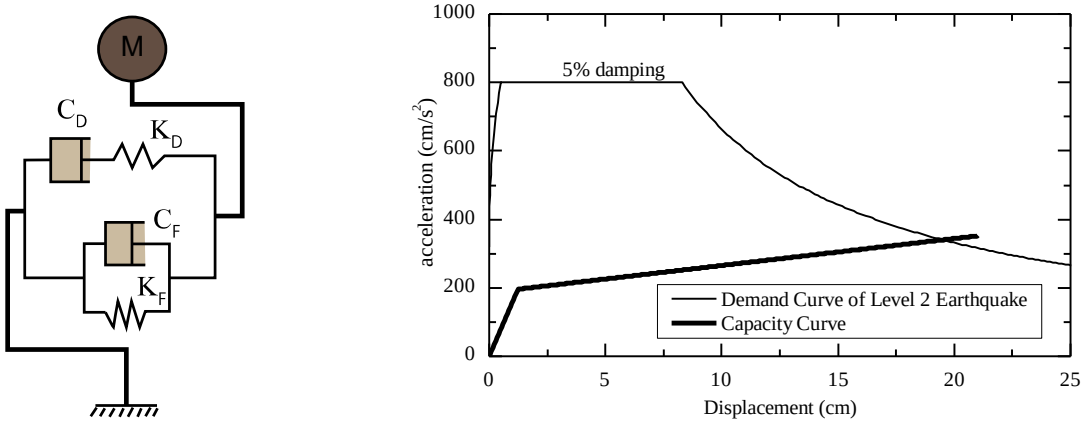

a) b)

Figure 3.3: a) The equivalent oil damper configuration in the ESDOF system; b) The initial demand curve (5% damping) and capacity curve of the ESDOF system.

The proposed CSM is performed as follows:

- The Multi Degree of Freedom (MDOF) is converted to the ESDOF [53].
- For selected ductility factor values (e.g. μ=1, 2, 3 …), the respective effective damping ratios (e.g. h_1, h_2, h_3 …), not including the contribution of the oil-damper devices, are computed using **Eq. (3.11)** [16], and the demand spectra are adjusted by **Eq. (3.10)** and plotted together with the capacity curve of the ESDOF as shown in **Figure 3.4a**.

$$h_{eq} = 0.8\frac{2}{\pi}\left(1 - \frac{1}{\mu}\right)\frac{1 - p}{1 + p(\mu - 1)} + 0.05 \tag{3.11}$$

- The spectral ordinates (spectral acceleration S_A and displacement S_D) of the demand spectrum at the intersection points with equivalent stiffness lines are determined and named as initial performance points.

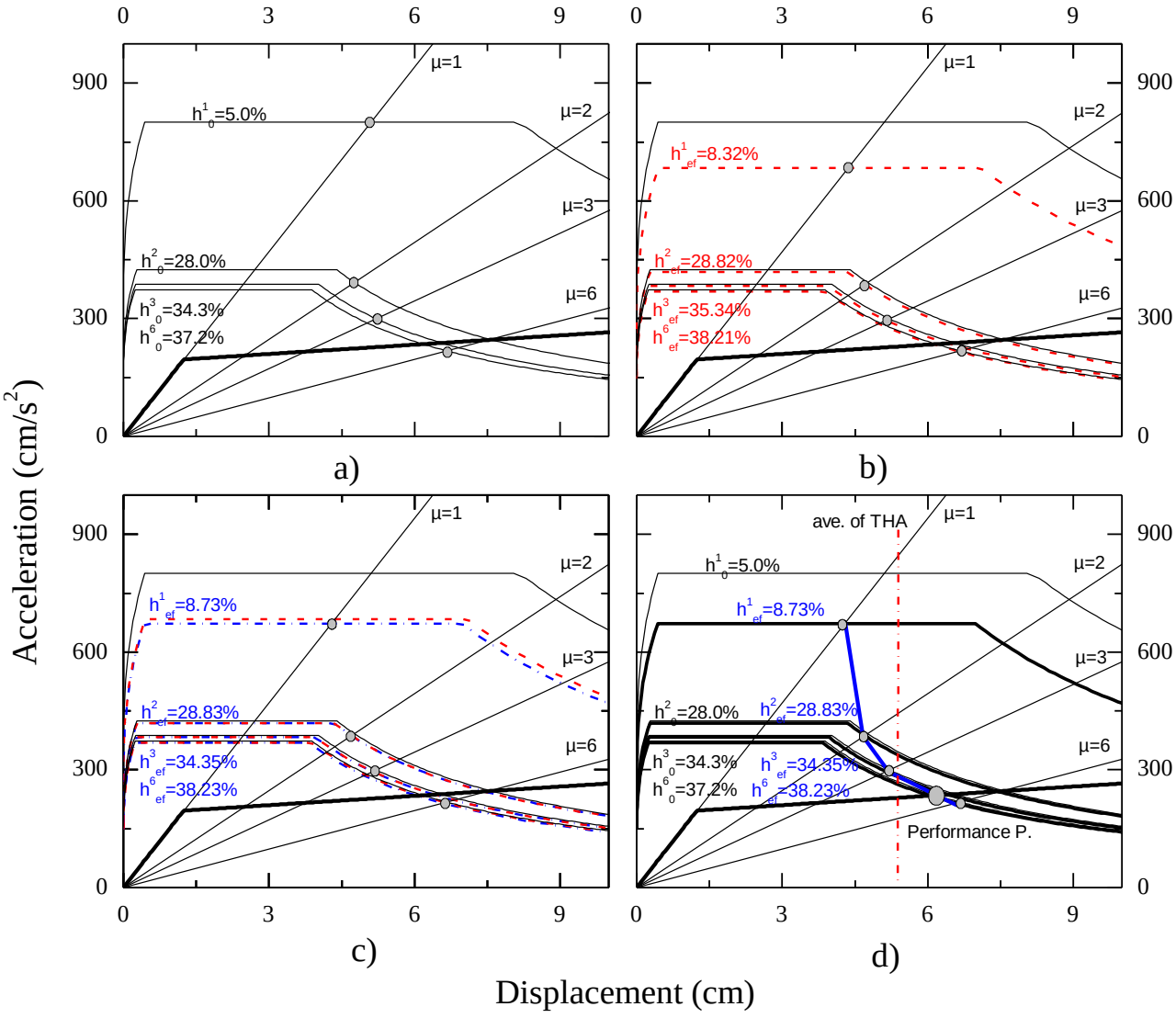

Figure 3.4: Steps of the proposed CSM applied to the ESDOF system using the damping-adjusted design spectra of Level-2 earthquake.

- For each initial performance point, the equivalent circular frequency of the ESDOF is estimated by **Eq. (3.12)**,

$$\omega_{eq}(\mu) = \sqrt{\frac{S_A}{S_D}} \tag{3.12}$$

- The corresponding story displacements (δ_1, δ_2, δ_3…) are computed from the ESDOF. Then, the maximum story velocities of the MDOF, V_{max}, are estimated as follows,

$$V_{max,i}(\mu) = \omega_{eq} \cdot \delta_i \tag{3.13}$$

- Using **Eqs. (3.8)**, **(39),** and **(3.16)** the effective damping of the system, $h_{eff,SRSS}$, the equivalent damping coefficient, C_{eq}, and the viscous damping of oil dampers, h_V, are estimated, respectively.

- Demand spectra are updated for each ductility factor as shown in **Figure 3.4b** (dashed-line response spectra).

- The next performance points are considered, and the same process is repeated until convergence (the difference between successive effective damping ratios becomes negligible), as shown in **Figure 3.4c** (dashed-dotted-line response spectra).

- The final performance points are connected and the intersection of the formed curve (blue solid line in **Figure 3.4d**) with the capacity curve is defined as the ultimate performance point of the ESDOF.

- The maximum seismic performance of the corresponding MDOF can be deducted from the ultimate performance point of its ESDOF.

For the ESDOF system presented in this section, the maximum displacement is estimated to 6.15 cm. In **Figure 3.4d**, the average maximum displacements from time history analysis (THA) of six selected Level-2 earthquakes (**Table 3.8**) is marked by a vertical broken line. A difference of 20% is observed from the proposed CSM result.

3.5 Application of the proposed CSM on steel frame buildings

3.5.1. Effective damping ratio of MDOF system

In case the oil dampers are arranged in a diagonal scheme with the inclination angle, θ, for a Multi-Degree of Freedom (MDOF) system as illustrated in **Figure 3.5**, the **Eq. (3.4)** and **Eq. (3.5)** can be used to incorporate the oil damper distribution along with the building height, as follow;

$$\sum \Delta W_j = \pi \cdot \omega_{eq} \sum C_j \, \phi_{rj}^2 \cos\theta_j^2 \tag{3.14}$$

$$W = \frac{1}{2}\omega_{eq}^2 \sum m_j \Delta_j^2 \tag{3.15}$$

where C_j, Δ_j, ϕ_{rj}, $\omega_{eq,}$ and m_j are the damping coefficient of the oil damper, the story drift of the first mode, the relative story drift, the equivalent circular frequency, and the mass of the j^{th} floor. Substituting **Eqs. (3.14)** and **(3.15)** in **Eq. (3.4)**, the viscous damping ratio of oil damper can be obtained as given in **Eq. (3.16)** for a MDOF system.

$$h_V = \frac{1}{2}\frac{\sum C_j \phi_{rj}^2 \cos\theta_j^2}{\omega_{eq} \sum m_j \Delta_j^2} \tag{3.16}$$

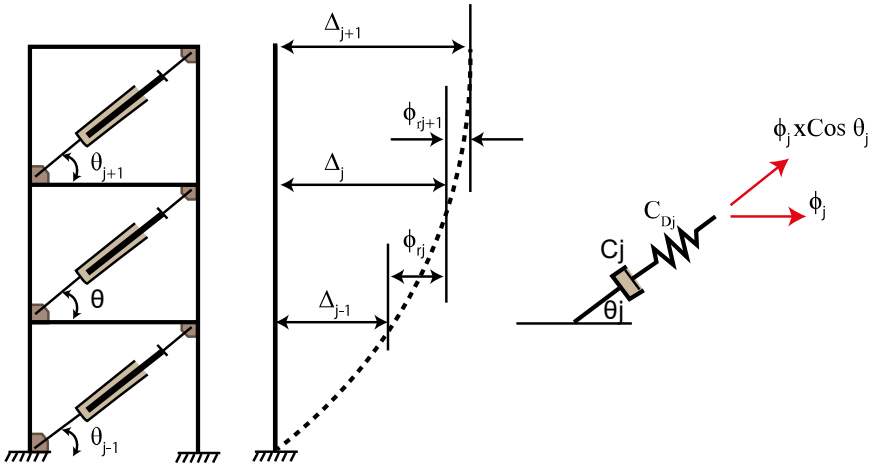

Figure 3.5. Multi Degree of Freedom (MDOF) with oil dampers corresponding to the first mode of vibration.

3.5.2. Description of target buildings

4-story and 10-story steel buildings are selected from the JSSI manual [8,54]. The buildings are designed as steel moment-resisting frames to resist the gravity loads, while oil dampers are considered to control the response under the earthquake ground motion. The plans and elevations of the buildings are shown in **Figure 3.6**. Except for the ground floor with 6 m height, the typical floor height is 4 m for both target buildings. The sizes of columns and beams are summarized in **Table 3.3** and **Table 3.4**.

The steel grade is SN490B with a yield strength of 325 MPa and tensile strength of 490 MPa. The arrangement of oil dampers in the plan and the evaluation of the building is shown in **Figure 3.6**. Since the oil dampers are diagonally installed in the longitudinal direction only, the following analysis is limited to the longitudinal direction. The technical parameters of oil dampers are presented in **Table 3.5** and **Table 3.6**.

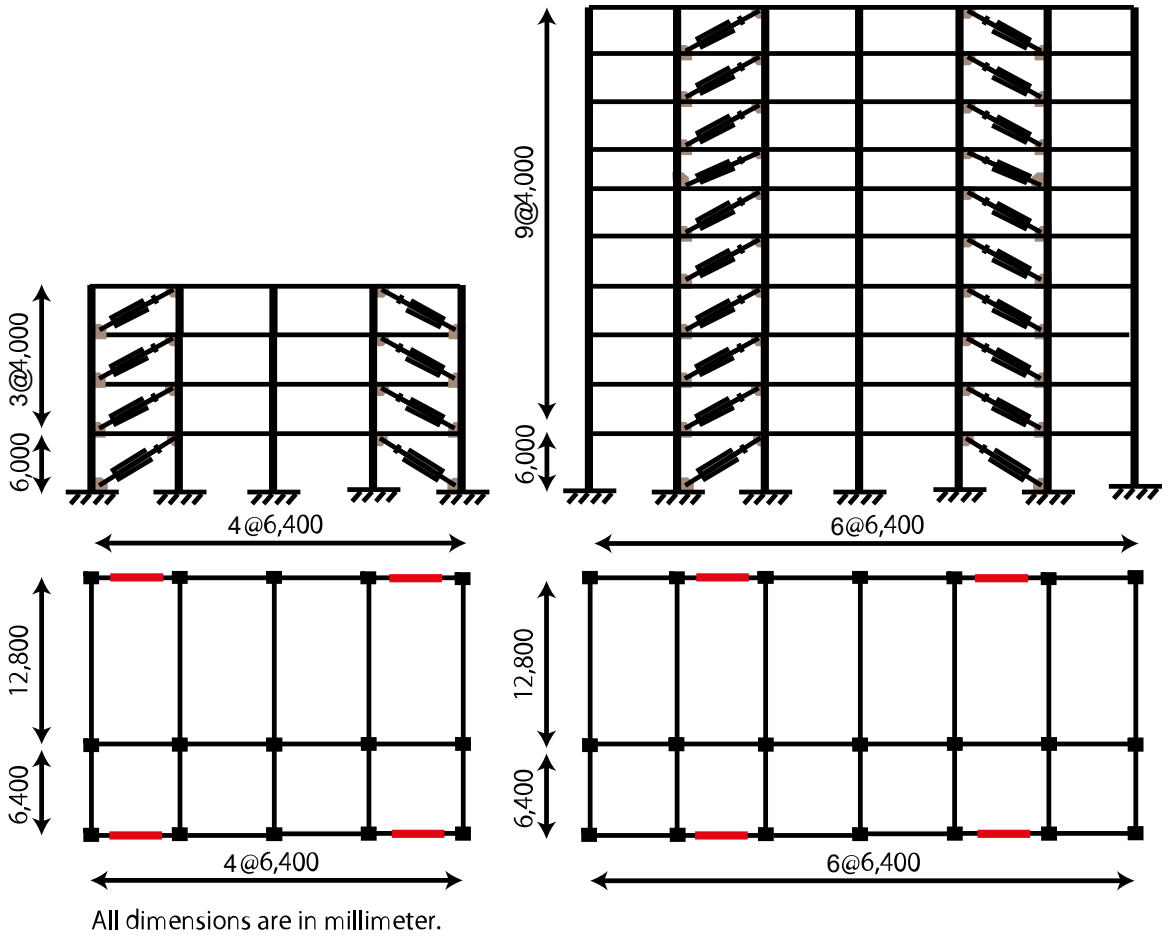

a) b)

Figure 3.6. Target buildings plan, elevation, and oil damper configuration: a) 4-story building; b) 10-story building.

Table 3.3: Detail and size of structural columns (*mm*).

Building	Story	Interior Column	Exterior Column	Corner Column
4-story	4	400×400×16	400×400×16	350×350×16
	3	450×450×19	400×400×19	350×350×16
	2	450×450×22	450×450×19	400×400×19
	1	500×500×22	500×500×19	400×400×19
10-story	7-R	550×550×22	500×500×22	500×500×19
	5-6	600×600×28	550×550×25	550×550×22
	3-4	650×650×28	600×600×25	600×600×22
	2	650×650×28	600×600×28	600×600×25

Table 3.4: Detail and size of structural beams (mm).

Building	Story	Longitudinal direction		Transverse direction	
		Interior beam	Exterior beam	Short span	Long span
4-story	4	550×200×9×16		550×250×12×22	700×300×12×22
	3	550×250×9×19		550×200×12×22	700×250×12×22
	2	600×250×12×22		600×200×12×25	750×250×14×25
	1	650×250×12×25		650×200×12×25	800×250×14×25
10-story	10-R	600×300×12×22	600×250×12×22	600×300×14×25	600×300×14×32
	8-9	700×300×12×22	700×250×12×22	700×300×14×25	700×300×16×32
	6-7	750×300×16×25	750×250×14×25	750×300×16×28	750×300×16×32
	4-5	750×300×16×28	750×250×16×28	750×350×16×28	750×350×16×32
	3	750×300×16×28	750×300×16×28	750×350×16×28	750×350×16×32
	2	800×300×16×32	800×300×16×28	800×300×16×32	800×300×16×32

Table 3.5: Technical parameters of oil dampers for the 4-story building**.**

Story	Height (H)	Weight (W_f)	Story Stiffness (K_F)	Damper Stiffness (K_D)	Damping (C_1)	Relief V. (V_r)	C_2/C_1
	m	*kN*	*kN/mm*	*kN/mm*	*kN-sec/mm*	*cm/sec*	
4	4.0	6,622.0	328.2	56.50	11.75	38.6	0.02
3	4.0	6,664.0	383.0	65.93	13.70	38.6	0.02
2	4.0	6,680.0	383.5	66.02	13.72	38.6	0.02
1	6.0	6,859.0	280.0	48.18	10.02	57.9	0.02

Table 3.6: Technical parameters of oil dampers for the 10-story building.

Story	Height (H)	Weight (W_f)	Story Stiffness (K_F)	Damper Stiffness (K_D)	Damping (C_1)	Relieve V. (V_r)	C_2/C_1
	m	*kN*	*kN/mm*	*kN/mm*	*kN-sec/mm*	*cm/sec*	
10	4.0	8,579.0	158.6	27.30	5.67	38.6	0.02
9	4.0	6,365.0	180.1	31.00	6.45	38.6	0.02
8	4.0	6,431.0	220.3	37.92	7.88	38.6	0.02
7	4.0	6,470.0	244.8	42.13	8.77	38.6	0.02
6	4.0	6,539.0	291.8	50.23	10.45	38.6	0.02
5	4.0	6,567.0	306.2	52.70	10.95	38.6	0.02
4	4.0	6,622.0	328.2	56.50	11.75	38.6	0.02
3	4.0	6,664.0	383.0	65.93	13.70	38.6	0.02
2	4.0	6,680.0	383.5	66.02	13.72	38.6	0.02
1	6.0	6,859.0	280.0	48.18	10.02	57.9	0.02

3.5.3. Frame models of target buildings

The 3D frame models of the buildings are analyzed by STERA_3D software, which is a finite element-based program developed for research purposes [55]. In the model, the steel beam element is presented by

a line element with two nonlinear flexural springs at both ends as shown in **Figure 3.7**. The steel column element is presented by a line element with the nonlinear axial springs in both end sections to consider nonlinear axial-moment interaction. The rebar strength is modified 1.1 times than the nominal strength and the ratio of post-yield stiffness is $\gamma=K_0/K_y=0.001$. The slab effects to amplify the flexural stiffness of the beam are assumed to be 1.2. The floor slab is considered to be rigid for in-plane deformation and free for out-of-plane deformation. The beam-column connection is assumed rigid, where the rigid zone length for the beam element is set to be half of the column width.

The bilinear-type oil damper is defined as a vertical line element with a shear spring in the middle. The shear spring is consisting of the Maxwell model with an elastic spring with stiffness, K_D, and a dashpot with bilinear type damping coefficient, C, connected in a series. The force-velocity relation of dashpot is shown in **Figure 3.8**.

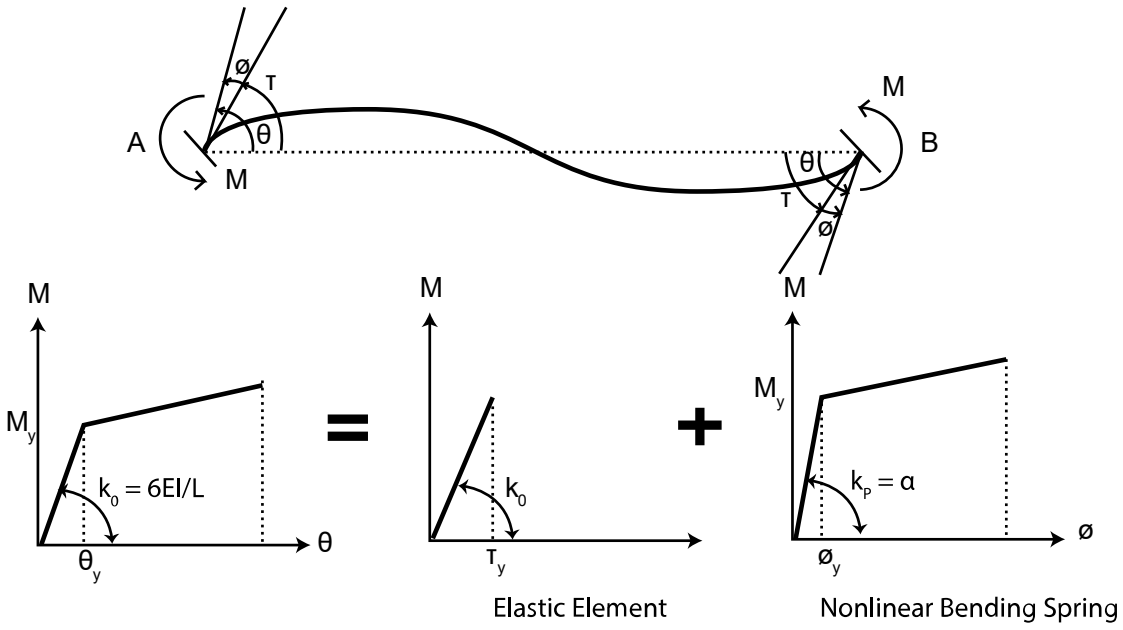

Figure 3.7: Moment-rotation relationship at bending spring of beam and column elements.

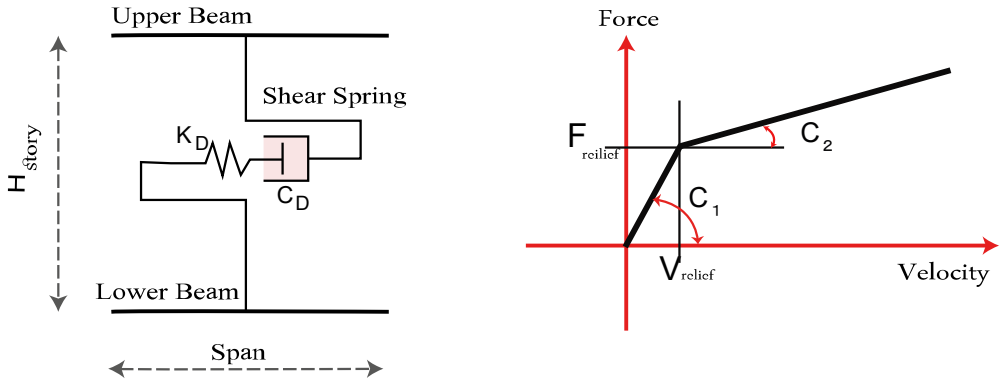

a) b)

Figure 3.8: a) Element model of bilinear-type oil damper, b) Force-velocity of oil damper.

Table 3.7 summarizes the natural periods and effective masses of the buildings obtained by the eigenvalue analysis. The capacity curves of ESDOF of the buildings are obtained by the non-linear static pushover analysis as shown in **Figure 3.9**.

Table 3.7: Dynamic characteristics of target buildings**.**

Building	Parameter	1st mode	2nd mode	3rd mode
4-story	Natural period (sec)	1.40	0.49	0.25
	Effective mass (%)	91.2	7.90	0.60
10-story	Natural period (sec)	2.03	0.75	0.44
	Effective mass (%)	82.8	11.3	3.40

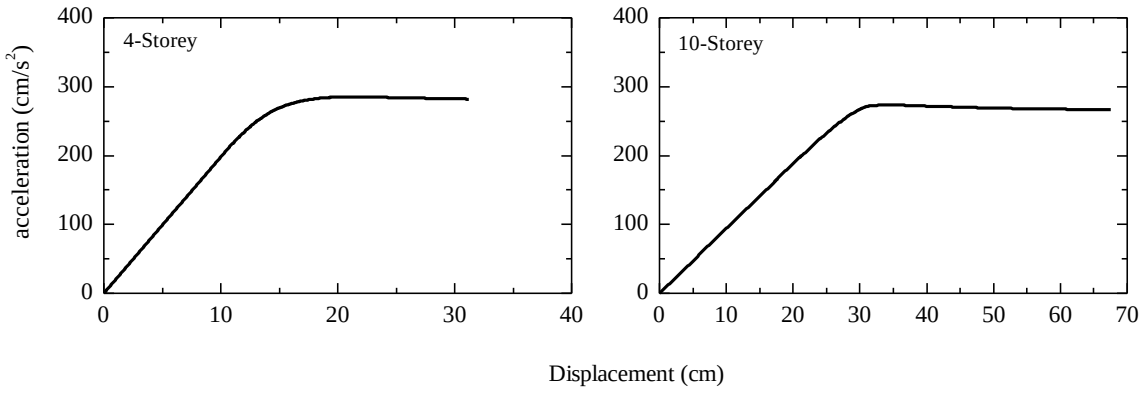

a) b)

Figure 3.9: The capacity curve of the ESDOF of target buildings: a) 4-story building, b) 10-story building.

3.5.4. Demand spectrum of earthquake ground motions

Six earthquake ground motions listed in **Table 3.8** have been selected as the extreme rare earthquakes defined by the Building Standard Law of Japan [16]. The earthquakes are generated using the algorithm developed by Pro. Taiki Saito [13]. Three of them (No. 1, 2, and 3) are the observed earthquake records scaled to have the maximum velocity of 50 cm/sec. Another three (No. 4, 5, and 6) are the artificially generated earthquake ground motions to have the response spectrum compatible with the design code and the phase spectrum of the observed earthquake records. **Figure 3.10** illustrates the acceleration response spectra with 5% damping factor of artificially generated earthquakes and the spectrum of design code (thick solid line).

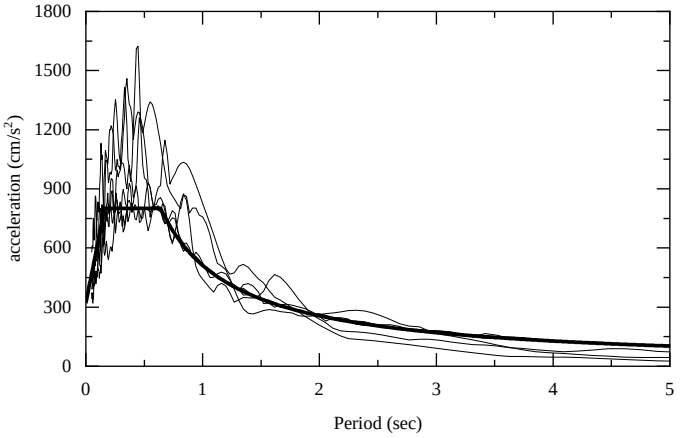

Figure 3.10: Response spectra of selected ground motions and design response spectrum of Level-2 earthquake with 5% damping factor.

Table 3.8. List of selected earthquake ground motions.

Categories	No.	Event	Year	Station
Scaled earthquake to be compatible of 50 cm/sec	1	Imperial Valley	1940	El Centro
	2	Kern County	1952	Taft
	3	Kobe	1995	JMA
Artificially generated earthquake to be compatible of L2	4	Tohoku	1978	Tohoku Univ.
	5	Tokachi Oki	1968	Hachinohe
	6	Kobe	1995	JMA

3.5.5. Comparison results between CSM and THA

The maximum responses of the target buildings under the earthquake ground motions are estimated by the proposed CSM and compared with the results of nonlinear Time History Analysis (THA). **Figures 3.11-**

3.14 shows the story drifts and story shear forces obtained by the proposed CSM and nonlinear THA for the selected ground motions along with the height of target buildings.

In the case of 4-story building, the average ratio of THA to proposed CSM (for story drift and story shear force) is 0.95 for the scaled 50 cm/sec earthquakes. While this ratio for artificially generated earthquakes generated to be compatible of Level-2 ground shacking is about 0.90. Similarly, the ratios of proposed CSM and THA for story drift and story shear force, in the case 10-story building, are 1.10 and 1.20 for the scaled and artificially generated ground motions, respectively. It was also noted for the 4-story building, the proposed CSM method overestimates the story shear force of the structure, although the story drift is underestimated for the 10-story building. Furthermore, the correlation between the performance result obtained from the proposed CSM method and THA is estimated as given in **Figure 3.15**. The estimated correlation is about 0.9 for the selected earthquakes in terms of story drift and story shear force for both steel buildings with oil dampers. The estimated correlation indicates the proposed CSM can be used as a practical procedure to estimate the maximum responses of passively control buildings equipped with bilinear oil damping devices.

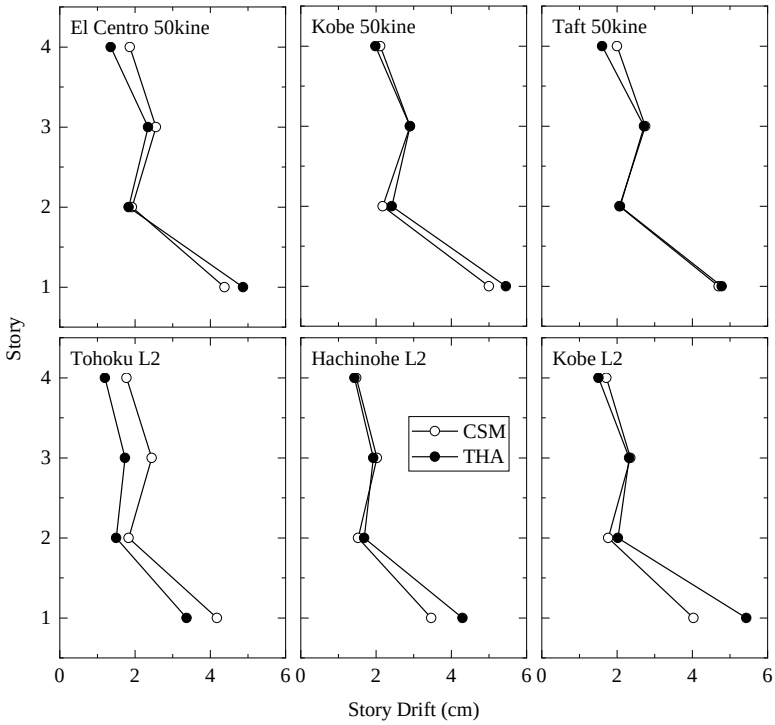

Figure 3.11: Comparison of story drifts between proposed CSM and THA for the 4-story building.

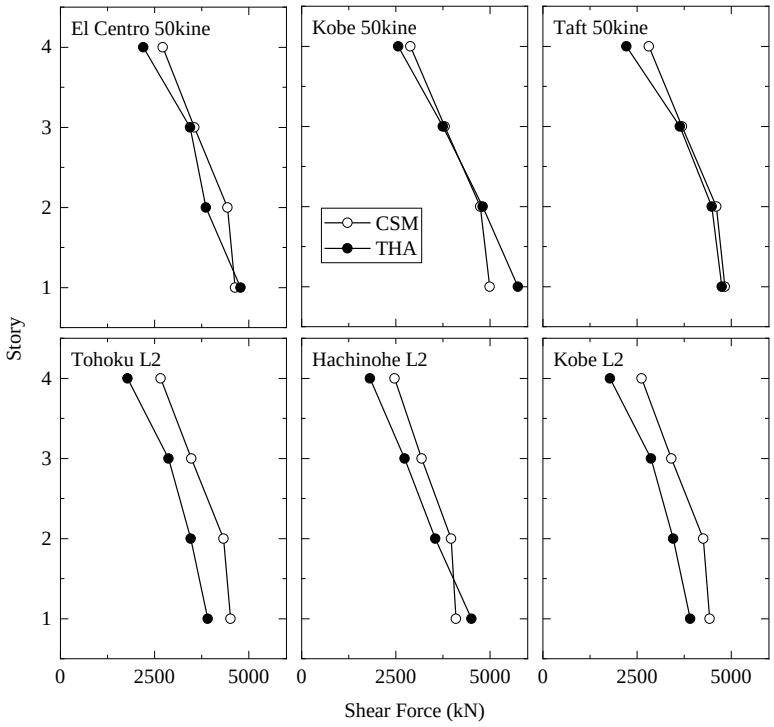

Figure 3.12: Comparison of story shear forces between proposed CSM and THA for 4-story building.

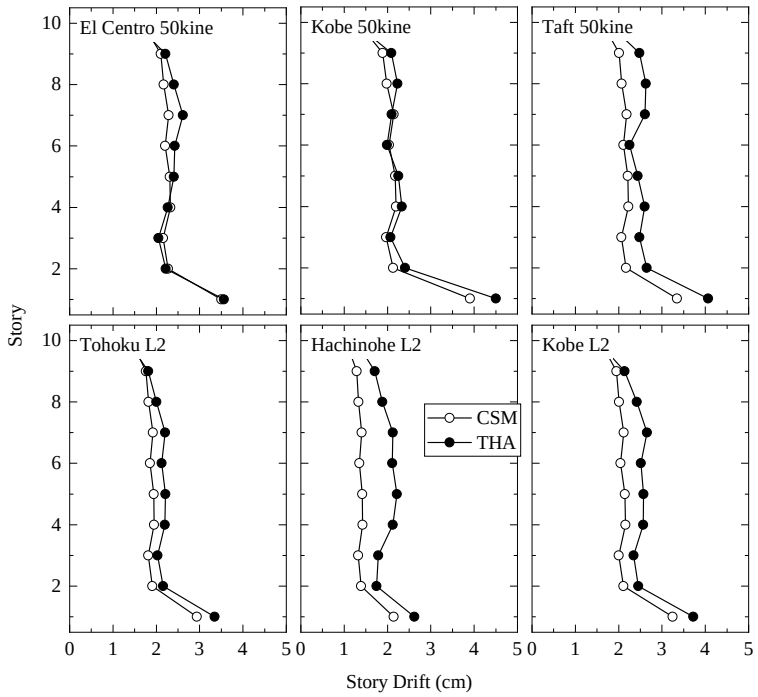

Figure 3.13: Comparison of story drifts between proposed CSM and THA for the 10-story building.

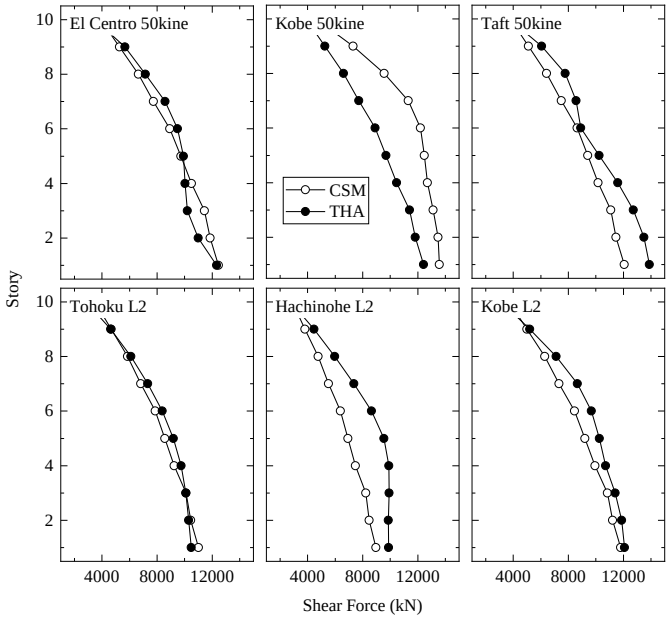

Figure 3.14: Comparison of story shear forces between proposed CSM & THA for the 10-story building.

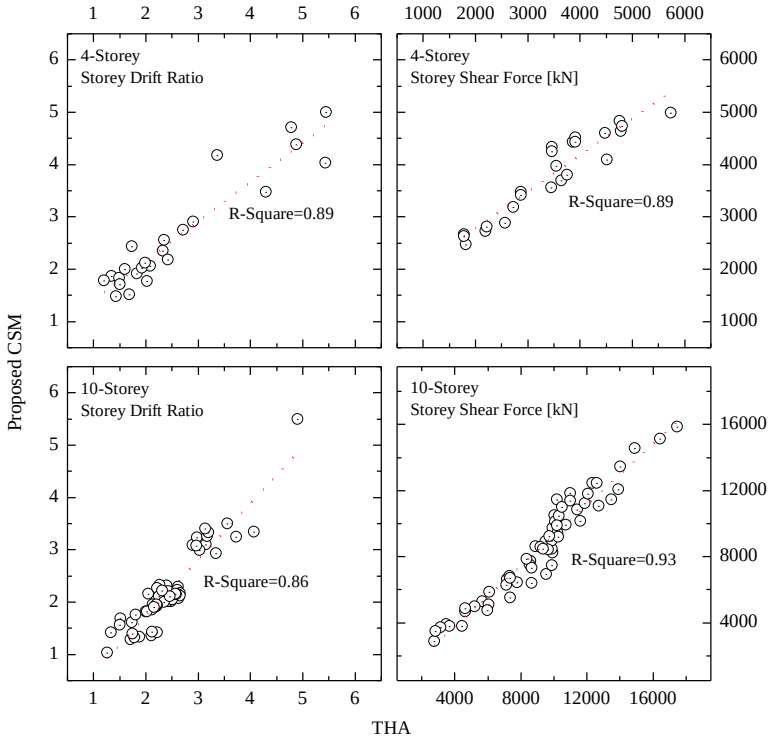

Figure 3.15 Story drift and shear force correlation of the proposed CSM & nonlinear THA for 4- and 10-story steel buildings.

Chapter 4: Damage assessment of passively controlled building under multi-hazard scenarios

4.1. Introduction

For earthquake and wind loads, most worldwide building codes consider the single hazard (SH) for the structural design and do not consider the successive events because of its low occurrence probability and cumbersome calculation [7]. However, when hysteresis dampers such as buckling-restrained braces (BRBs) are used as vibration control devices for high-rise buildings, fatigue due to the accumulation of plastic energy against successive events cannot be ignored. Therefore, multi-hazard (MH) scenarios involving winds and earthquake ground motions are considered in this chapter, and the structural performance of a 20-story RC building enhanced with BRBs is examined to clarify the effect of the sequence of hazards to the damage of both the building and the BRB devices.

4.2. Case study: RC frame enhanced with BRBs

A 20-story RC moment-resisting frame is designed to resist the gravitational loads and then the BRB devices are selected to minimize the inter-story drift ratio below 1% under lateral excitation of Level-2 earthquakes [16]. It is assumed that the prototype building is located in Aichi Prefecture, Japan. As presented in **Figure 4.1**, the prototype building is a plane frame consisting of a 5-span with a total length of 27.2 m and the story height is 4.5 m on the first floor and 4 m on the other floors. Structural parameters of the RC columns and beams are summarized in **Table 4.1**. The prototype building is enhanced on each floor by two diagonal BRBs installed symmetrically. The parameters of BRB devices are summarized in **Table 4.2**.

The earthquake response of the frame model is calculated by STERA_3D (STructural Earthquake Response Analysis 3D) software, which is a finite element-based software [13]. In the software, the beam elements are presented by two nonlinear flexural springs at both ends and one shear spring at the middle. The column elements have nonlinear axial springs distributed in the sections of both ends and two nonlinear shear springs in the middle to represent the directional properties of the element. The hysteresis model of nonlinear bending springs for column and beam elements is the degrading trilinear model as shown in **Figure 4.2a**. The beam-column connection is assumed rigid, where the rigid zone length for the beam element is set to be half of the column width. For both beam and columns, the steel strength is modified 1.1 times than the nominal strength and the ratio of post-yield stiffness is $\gamma=K_0/K_y=0.001$. The BRB element is

defined as a shear spring in a frame with the bi-linear hysteresis with initial stiffness, K_1, and secondary stiffness of, K_2, as shown in **Figure 4.2b**. The wind loads in STERA-3D are applied at the center of gravity at each floor, while the load distribution factor according to the Japanese standard is used to distribute the load along with the height.

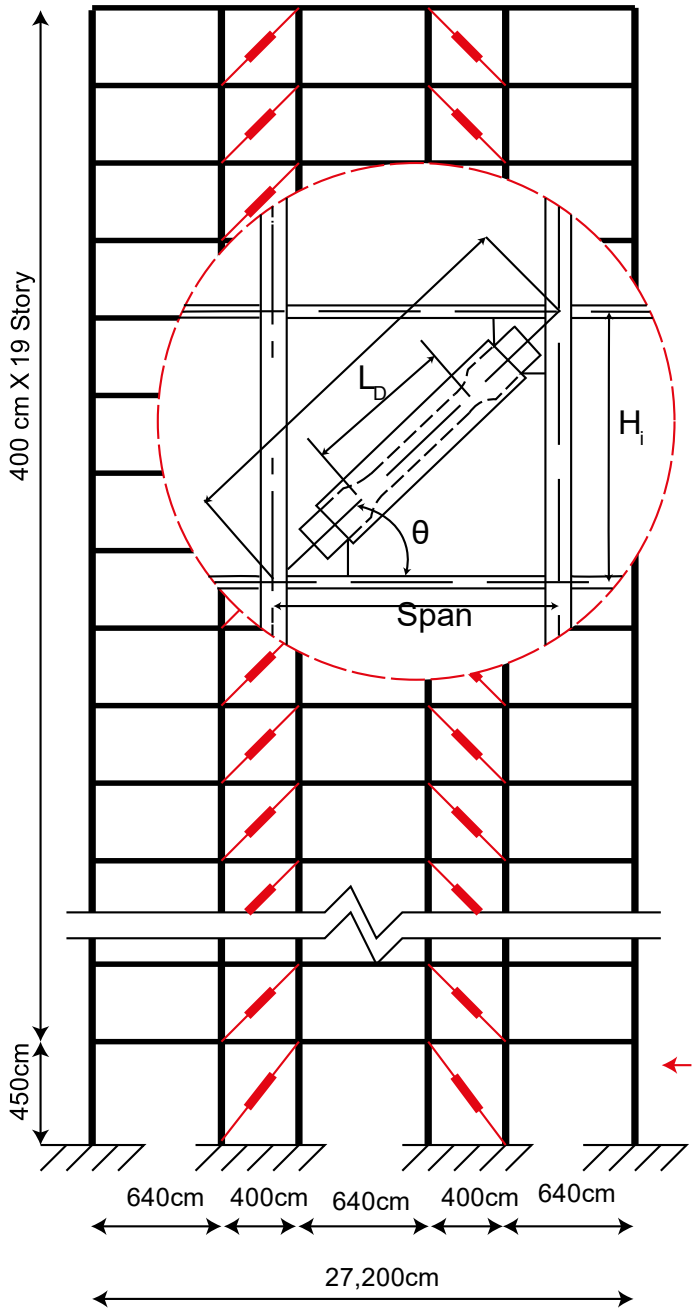

Figure 4.1: The prototype building elevation and BRB configuration.

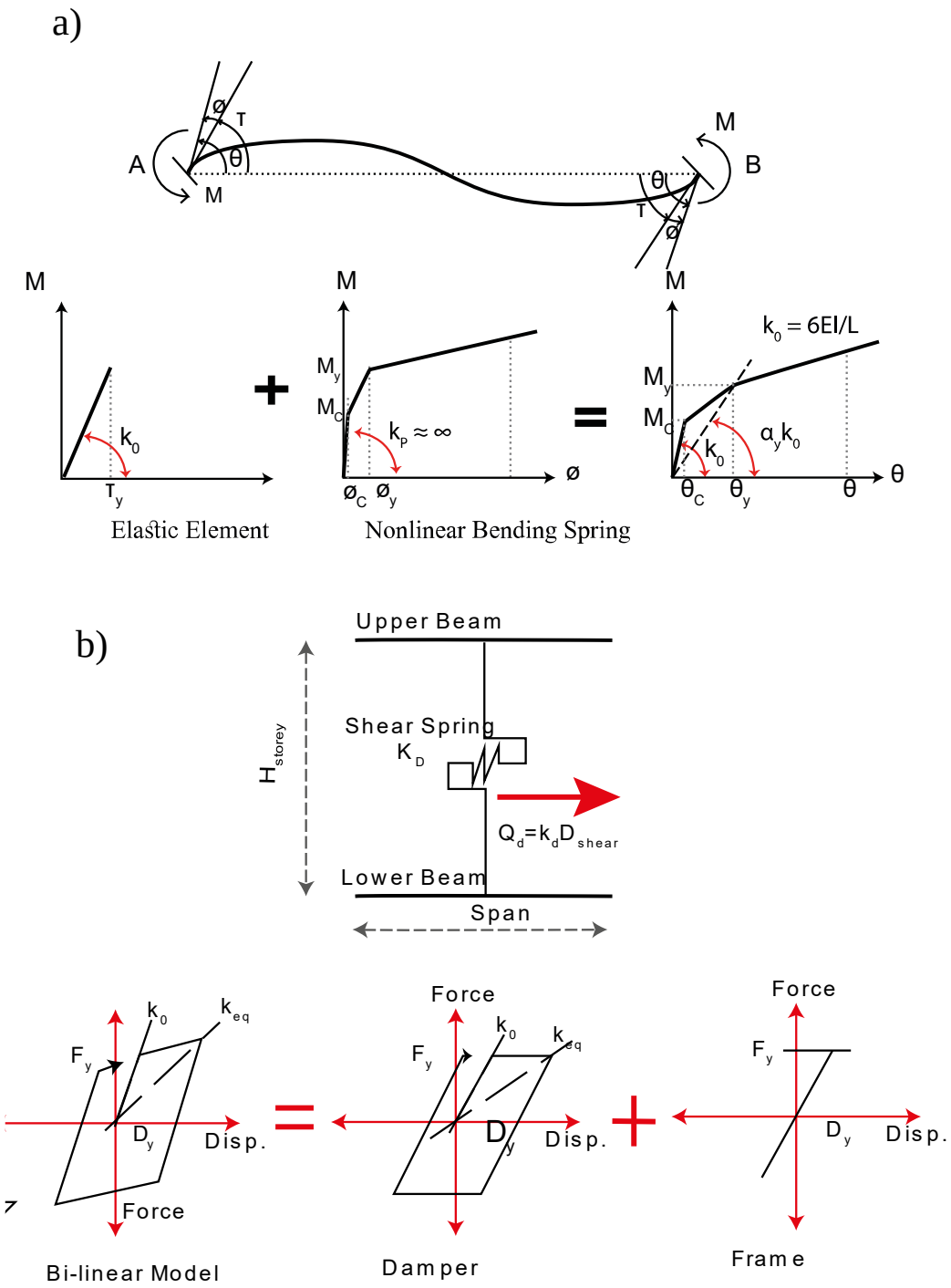

Figure 4.2: a) Hysteresis model of nonlinear bending spring of beam and column elements; b) Bi-linear hysteresis model of nonlinear shear spring for BRBs.

Table 4.1: Structural parameters of RC columns and beams in prototype Building.

Story	Column			Story	Beam			
	Fc	D×B	Main Reinforcement		Fc	D×B	Main Reinforcement	
	MPa	cm			MPa	cm	Top	Bottom
18-20	32	50×50	16-D19	16-20	32	60×50	5-D20	5-D20
13-17	36	55×55	16-D20	11-15	36	60×50	5-D22	5-D22
8-12	42	60×60	16-D22	6-10	42	65×55	5-D22	5-D22
4-7	48	65×65	16-D22	2-5	42	65×55	5-D22	5-D22
1-3	52	70×70	16-D25	1	48	65×60	4-D25	4-D25
	1) For the entire beams and columns, the shear reinforcement is D13@100mm. 2) For both column and beams the tensile strength of main & shear reinforcement are 490MPa & 295MPa, respectively.							

Table 4.2: Structural parameters of BRB members.

Story	Story Weight	Story Height	K_0	F_y	K_1/K_0
	kN	***cm***	***kN/mm***	***kN***	
20	2275.0	400	80	520	0.02
18-19	2082.5	400	80	520	0.02
14-17	2082.5	400	100	650	0.02
11-13	2082.5	400	120	780	0.02
8-10	2082.5	400	130	845	0.02
5-7	2082.5	400	120	780	0.02
2-4	2082.5	400	110	715	0.02
1	2187.5	450	80	520	0.02

4.3. Multi-hazard scenarios (MH)

During the lifetime of a building, the possibility of earthquake events preceded by wind events, or vice-versa, is significantly high in the area like Japan which is prone to earthquakes and typhoons [6]. The objective of the current study is to evaluate the performance of the target building under different scenarios of successive wind and earthquake loadings. **Figure 4.3** shows two different scenarios; one is the wind comes first followed by the earthquake (wind-earthquake), and the other is the order is reversed

(earthquake-wind). Four sets of earthquake ground motions are combined with four sets of winds of different intensities. **Table 4.3** presents the detail of four selected earthquakes. The earthquakes are consisting of two observed earthquake ground motions scaled to match the maximum velocity of 50 cm/sec [15, 16] and two ground motions artificially generated from the phase spectrum of historical earthquakes to be compatible with the extreme rare earthquake (Level-2) acceleration response spectrum defined by Building Standard Law of Japan [16]. In case of wind events, four sets of wind excitation are generated according to the Architectural Institute of Japan (AIJ) 2019 recommendation [15], namely; the weak winds (17m/sec of frequent occurrence), moderate winds (20m/sec of 1-year return period), rare wind (25m/sec of 10-years return period), and extremely rare wind (31m/sec of 50-years return period). For each of the four wind intensities, a 10-minutes fluctuating component of the wind time-history profile is generated using the von Karman spectrum which is recommended in AIJ 2019 [15].

Table 4.3: List of selected earthquake ground motions**.**

No.	Categories	Event	Date	Station	Abbreviation
1	Scaled earthquake to be compatible of 50 (cm/sec)	Imperial Valley	1940	El Centro	ELC
2		Kern County	1952	Taft	TAF
3	Artificially generated earthquake to be compatible of L2	Tokachi Oki	1968	Hachinohe	HAC
4		Kobe	1995	JMA	KOB

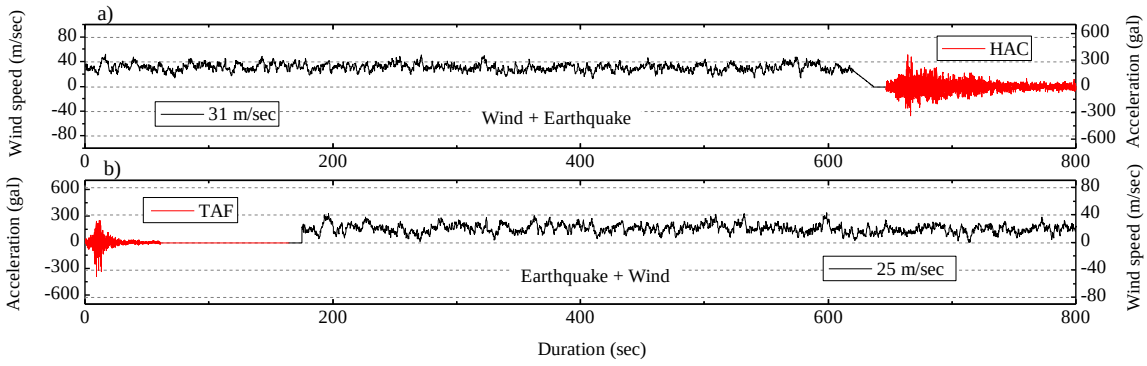

Figure 4.3: Multi-hazard scenarios, a) wind-earthquake (W31-HAC); b) earthquake-wind (TAF-W25).

4.4 Results of successive analysis of prototype building

4.4.1 Natural period of the building

The difference of the natural period of the building between pre- and post-earthquake or wind excitation due to the damage and stiffness degradation of structural members is examined [56]. As presented by the dotted line in **Figure 4.4**, the natural periods of 1st, 2nd, and 3rd modes under the free vibration (pre-event)

are 2.379, 0.797, and 0.430 sec, respectively. As presented by the event number 1, 2, 3, and 4 in **Figure 4.4**, the natural periods after application of four earthquakes are 3.588~3.704 sec for the 1st mode, 1.107~1.119 sec for the 2nd mode, and 0.527~0.558 sec for the 3rd mode of vibration which indicates the natural period is elongated about 50~55% for the 1st mode, 38~40% for the 2nd mode, and 28~30% for 3rd mode, respectively. Similarly, as presented by the event number 5, 6, 7, and 8 after individual application of wind events, it is observed the natural period is elongated 2.621~ 3.377 sec for the 1st mode, 0.842 ~1.027 sec for the 2nd mode, and 0.45 ~0.52 sec for the 3rd mode, respectively. There is a noticeable difference in the natural period due to the wind intensity.

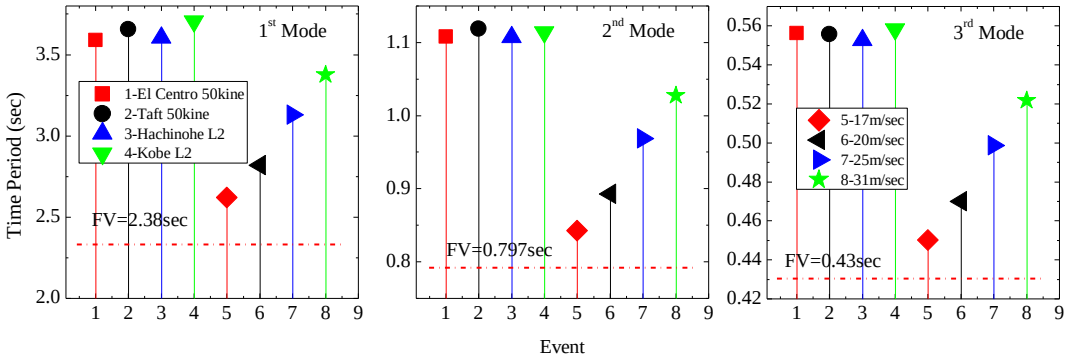

Figure 4.4: Comparison of natural periods between pre-event (FV) and post-event of earthquake or wind.

The post-event natural periods of MH scenarios are compared with the free vibration and SH as well. **Figure 4.5** shows the 1st mode natural periods of SH of earthquake and MH of wind-earthquake. It can be seen that the difference in natural periods between SH is MH is small. **Figure 4.6** shows the 1st mode natural periods of SH of wind and MH of earthquake-wind. Although the post-event natural period of SH increases in wind intensity, it does not affect the natural period of MH. This means that the effect of wind is small concerning the change of the natural period.

4.4.2 Maximum story drift of the building

The maximum inter-story drift ratios, which are obtained from the time history analyses of SH and MH, are compared. **Figure 4.7** shows the maximum story drift ratios of SH of earthquake and MH of wind-earthquake. It is interesting to note that when the wind precedes the earthquake, the subsequent earthquake does not necessarily increase the response, but may even decrease it. It is assumed that the change of natural period after wind event affects the subsequent earthquake response.

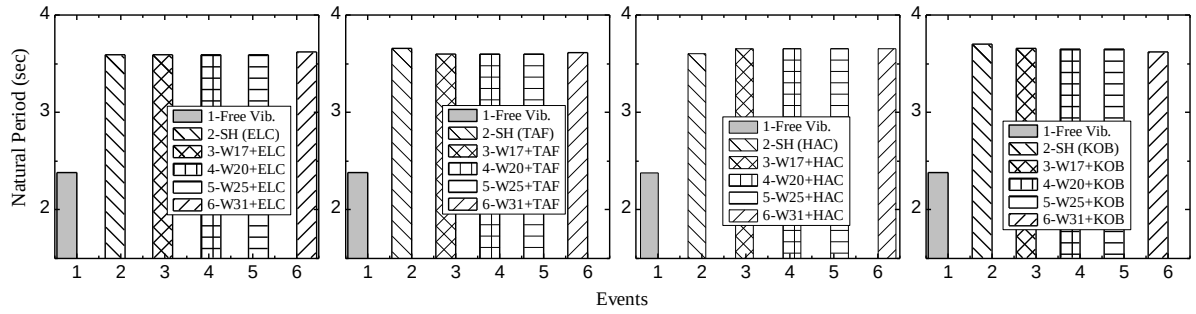

Figure 4.5: Comparison of the natural period between SH (earthquake) and MH (wind-earthquake).

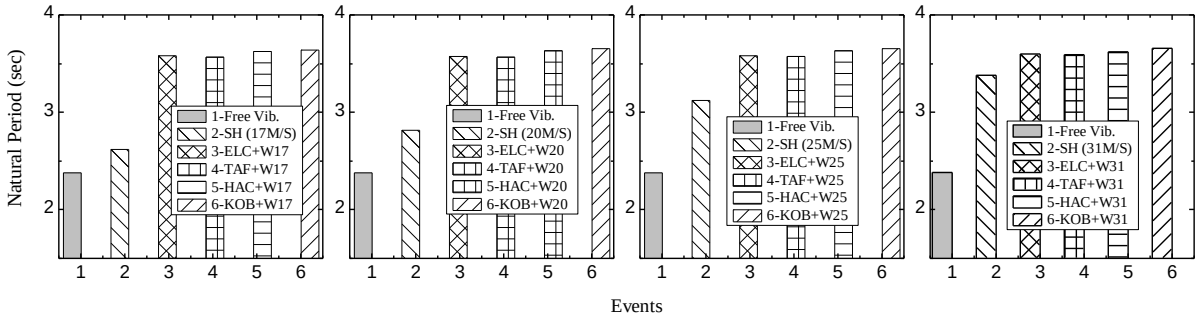

Figure 4.6: Comparison of the natural period between SH (wind) and MH (earthquake-wind).

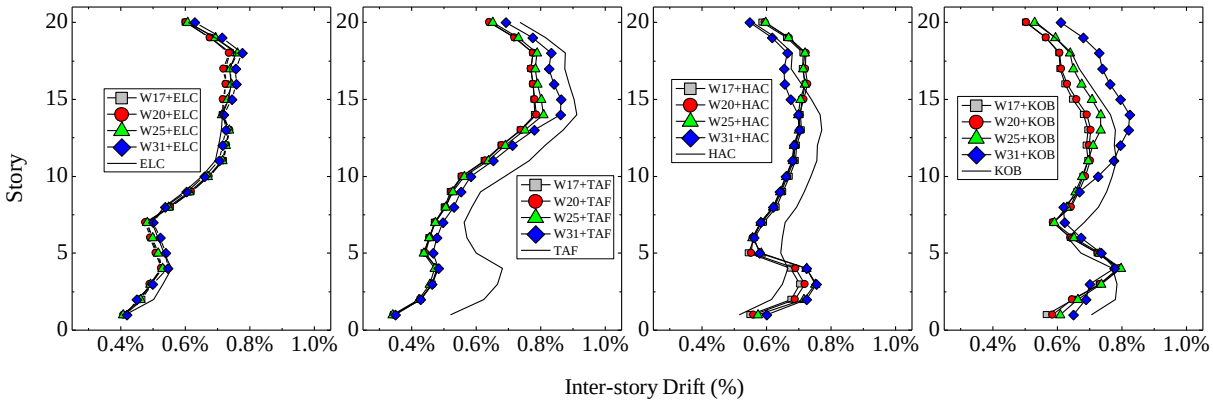

Figure 4.7: Comparison of the maximum story drift ratio between SH (earthquake) and MH (wind-earthquake).

Figure 4.8 shows the maximum story drift ratios of SH of wind and MH of earthquake-wind. When the earthquake precedes the wind, the change in the maximum response due to the subsequent earthquake is large. It increases in the order of KOB, ELC, HAC, and TAF.

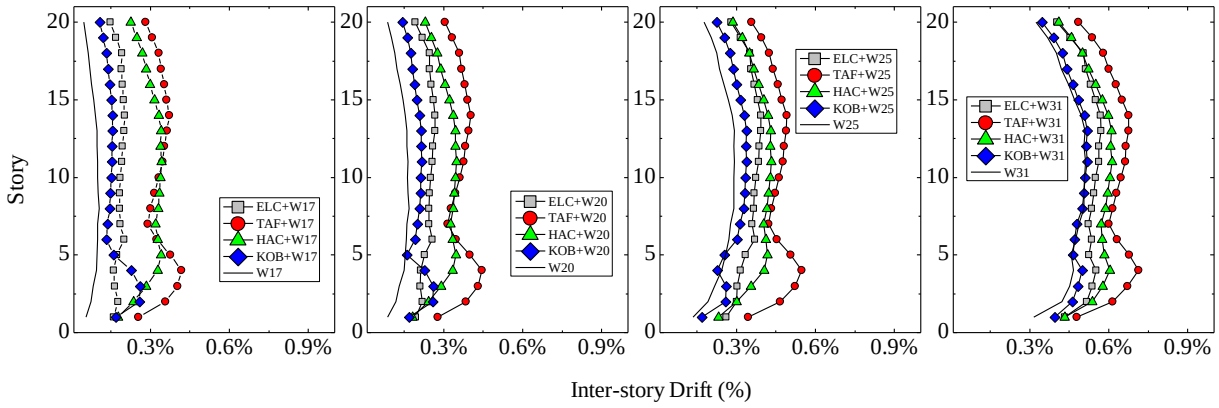

Figure 4.8: Comparison of the maximum story drift ratio between SH (wind) and MH (earthquake-wind).

4.4.3 Roof displacement profile

Figure 4.9 compares the maximum roof deformation between SH and MH. It is seen from **Figure 4.9a**, the maximum roof displacement of SH (earthquake) is larger than MH (wind-earthquake) except ELC. In the case of MH of earthquake-wind, as shown in From **Figure 4.9b**, the maximum roof displacements increase with wind intensity. The same trend can be seen for the residual deformation as presented in **Figure 4.10**.

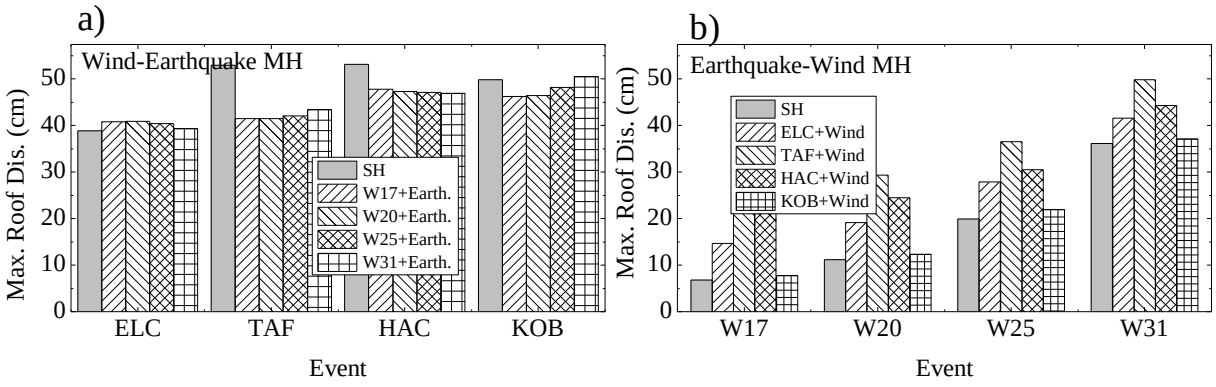

Figure 4.9: Comparison of the maximum roof displacement between SH and MH, a) SH (earthquake) and MH (wind-earthquake), b) SH (wind) and MH (earthquake-wind).

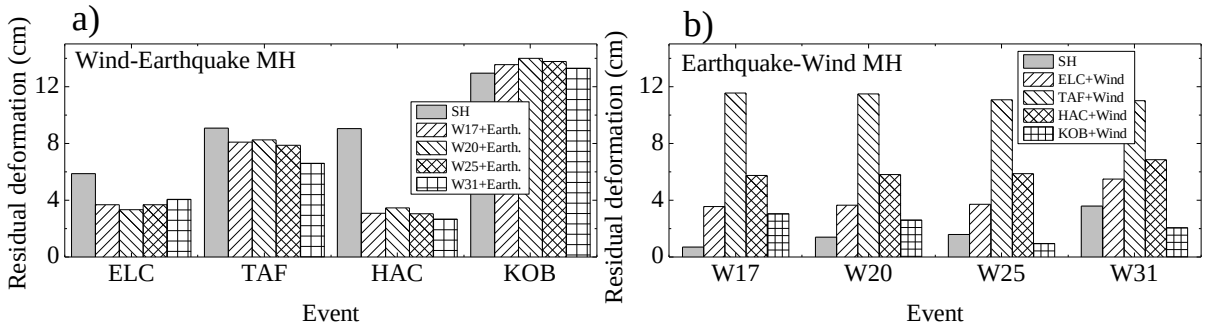

Figure 4.10: Comparison of the residual deformation between SH and MH, a) SH (earthquake) and MH (wind-earthquake), b) SH (wind) and MH (earthquake-wind)

4.4.4 Energy absorption rate

Figure 4.11 shows the amount of hysteresis energy absorbed by load-resisting members (columns, beams, and dampers) of the building under the SH and MH events. From **Figure 4.11a**, the cumulative energy dissipation of MH (wind-earthquake) increases in comparison to SH (earthquake) by ~3%, ~7%, ~50%, and ~149% corresponding to the preceding wind loads of 17, 20, 25 and 31m/sec. A similar trend is observed for MH (earthquake-wind) scenarios as well as shown in **Figure 4.11b**.

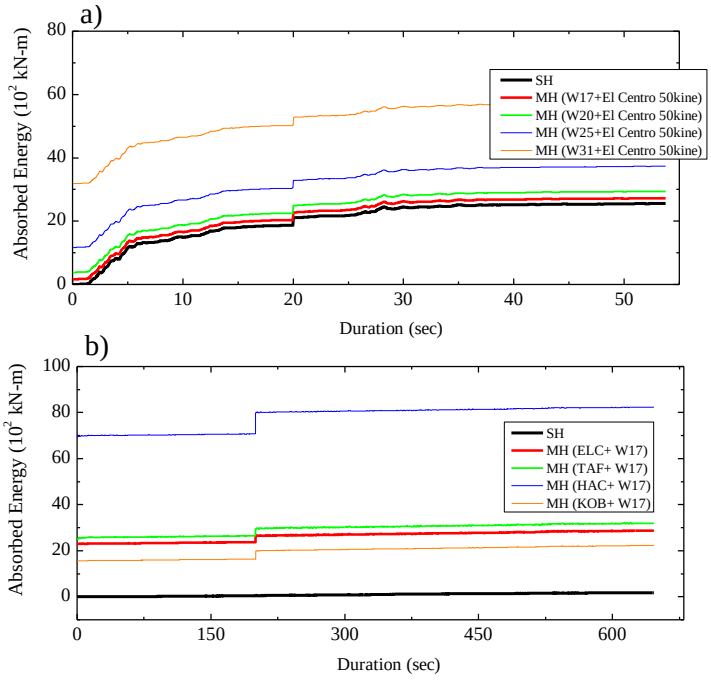

Figure 4.11: Energy absorption rate of load-resisting elements, a) SH (earthquake) and MH (wind-earthquake), b) SH (wind) and MH (earthquake-wind).

4.4.5 Cumulative ductility factor and plastic strain energy of BRBs

The accumulative damage of BRBs is evaluated in the term of the cumulative ductility factor (CDF) and the plastic strain energy (PSE) [57]. As presented in **Figure 4.12**, the plastic strain energy is defined as the ratio of the area of plastic strain energy by the triangular area shaped by the yield and deformation strengths of RBR. The cumulative ductility factor is the normalized summation of total plastic deformation to the yield deformation of BRB.

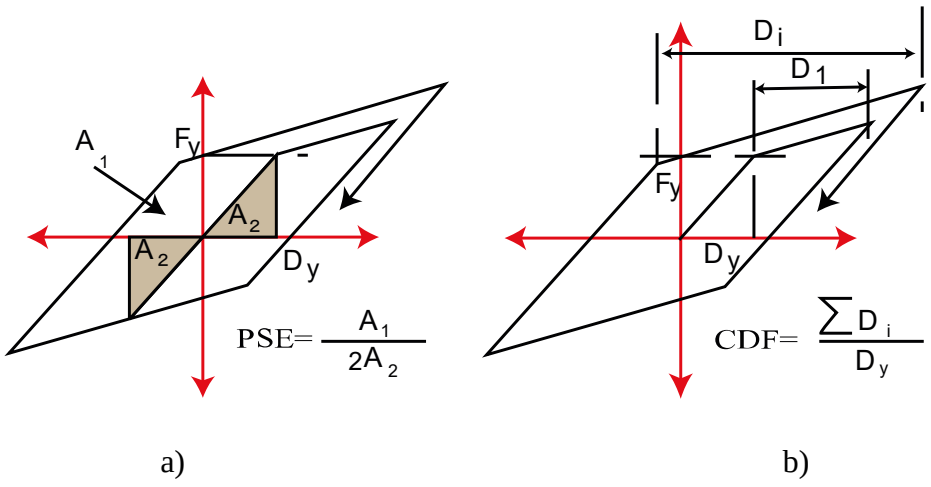

Figure 4.12: a) Plastic Strain Energy (PSE), b) Cumulative Ductility Factor (CDF).

Figure 4.13 presents the force-deformation (strain) relationship of the BRB installed on the first floor of the building. From **Figure 4.13a**, under the successive analysis of MH (wind-earthquake), the shape of the force-deformation relationship is different from SH (earthquake), and PSE and CDF are increased about 1~5% and 50~300% corresponding to the preceding wind intensity. As shown in **Figure 4.13b**, the value of PSE for SH (wind of 31m/sec) is small at 0.02, while the value of CDF is large at 20.54. This is related to the long duration of the wind.

The performance of the high-rise RC building with BRB dampers is investigated under successive application of MH scenarios of earthquakes and winds. It is observed, although the effect of wind load is small concerning the overall performance of prototype building, its effect on the cumulative ductility factor and plastic strain energy of BRBs cannot be neglected.

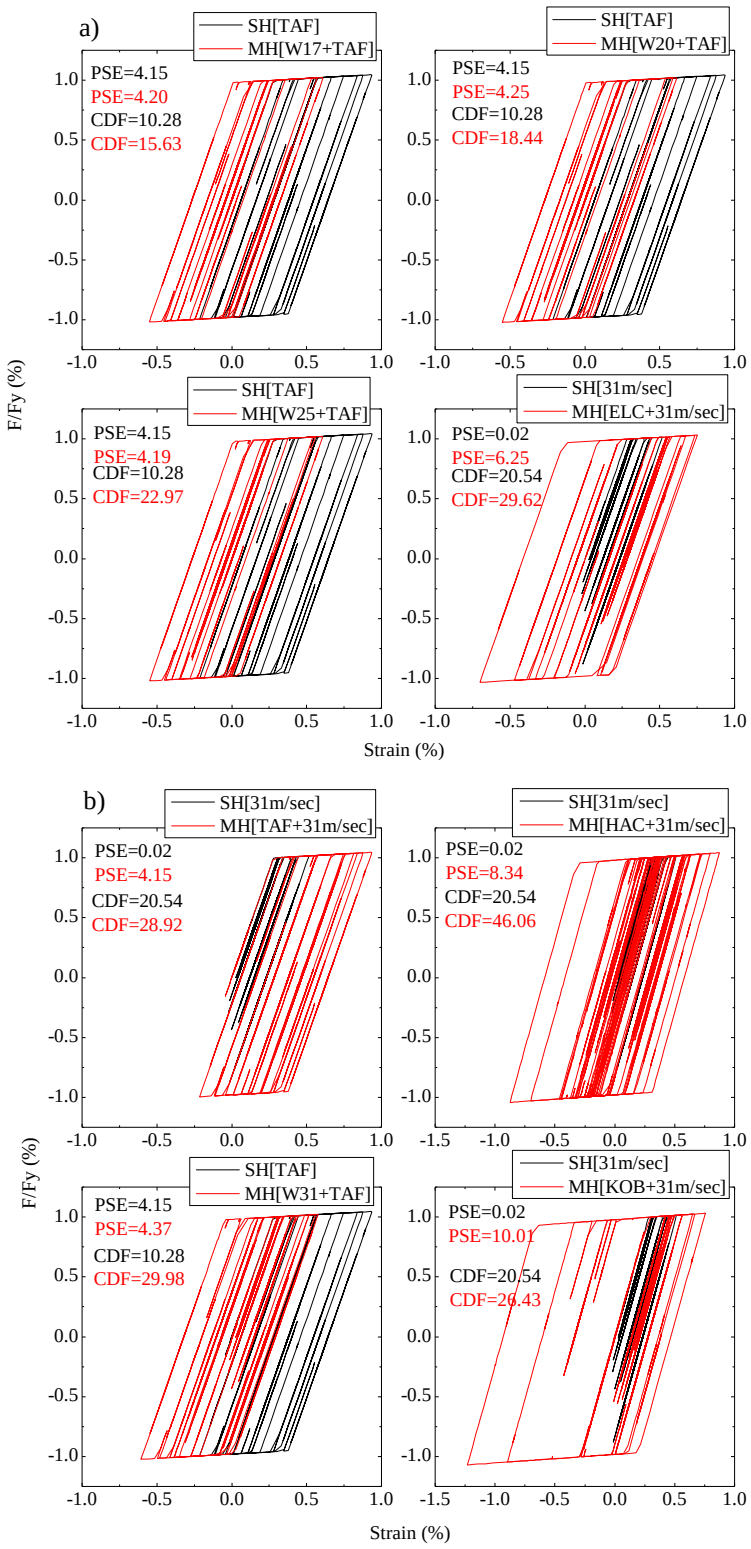

Figure 4.13: Force-deformation relationship of BRBs, a) SH (earthquake) and MH (wind-earthquake), b) SH (wind) and MH (earthquake-wind).

Chapter 5: Lifetime damage assessment of passively controlled building

5.1 Introduction

It is indicated in Chapter Four, that the successive analysis of multi-hazard scenarios induces accumulative damage to the response control device which in response modifies the high-rise building's performance. Therefore, in this chapter considering the contribution of successive events on each other, a cumulative damage model is presented to evaluate the high-rise building performance.

5.2 Literature review

The buckling-restrained brace (BRB) is an energy-absorbing device that consists of a detached steel core brace inside a steel restrainer infilled with concrete mortar. This unique combination enables the BRB to exhibit stable hysteresis behavior both in compression and tension. The BRB was originally invented in Japan and the first practical application was reported by Fujimoto et al. in 1988 [58]. Since the first successful application of BRB for 10- and 15-story steel frame buildings in 1989, the device has gained popularity in seismically active regions around the world [59]. The excellent performance of BRB as an energy absorbing device has been proved by many experimental tests [60- 67]. The use of BRB has become one of the efficient measures to minimize the effects of seismic loadings in low- to high-rise buildings [5,68]. Moreover, the BRB is extensively employed to retrofit the existing buildings to increase the building strength and energy dissipation capacity [69-73].

The use of BRBs is common in Japan for high-rise buildings [4, 5] to mitigate their performance since the high-rise buildings experience a large amplitude shaking due to the effect of resonance with the long period component of earthquake ground motions. Since Japan is a country that experiences frequent earthquakes and typhoons [6], the performance of the high-rise building with BRBs must be examined under the multi-hazard scenario of earthquakes and long-duration winds. Although the performance of BRBs in high-rise buildings under either earthquake and wind loads is extensively studied in Japan and worldwide, limited studies had been conducted to evaluate the cumulative damage of BRBs in the successful application of wind and earthquakes. It is because most of the seismic provisions and design guidelines specify the design method for the single event of earthquakes and winds [7].

Under the multi-hazard scenario, high-rise buildings are exposed to series of high-cycle low-strength dynamic wind loads and low-cycle high-strength earthquake loads. The literature review of BRB's fatigue life under the low-cycle excitation [74-78] indicates the devices are capable to withstand the design load and endure the design threshold successfully. The effect of low-cycle fatigue of BRBs for three consecutive Level-2 earthquakes is investigated by Usami et al. [74] and the BRBs fatigue performance is found to be in an acceptable range. On the other hand, although the failure mechanism of wind-induced fatigue for steel buildings has been examined by researchers [79-82], there are few studies to discuss the BRBs under the combination of low- and high-cycle excitations in high-rise buildings.

The objective of this research is to evaluate the cumulative deformation capacity of BRBs installed along with the height of a 20-story steel frame building under multi-hazard scenarios. The target building is designed to satisfy the design criteria recommend in Japanese regulation. The performance of the building and the cumulative deformation of BRBs are then evaluated under successive application of multi-hazards in the building lifetime, consisting of the low-cycle earthquake and high-cycle wind loadings.

5.3 Procedure to generate probable multi-hazard scenarios in building lifetime.

The likely recurrence of earthquake and wind events during the building lifetime is crucial to be addressed, as it enables the decision-makers to evaluate the building performance in any specific service period. Thus, a practical procedure to estimate the likelihood of the occurrence of multi-hazard scenarios in the structural design life is developed and presented in this section. The procedure is based on the Poisson process, which uses the anticipated return period and intensity to generate the earthquake and wind events.

From the Gutenberg-Richter equation, the annual occurrence rate, *N(I)*, of earthquake loads with an intensity more than, *I*, is given as,

$$\ln N(I) = a - bI \tag{5.1}$$

The average recurrence period, *T(I)*, satisfies the following relationship,

$$N(I) = {}^{1}/_{T(I)} \tag{5.2}$$

If we consider two earthquake events having the intensity of, I_{100}, and I_{500}, with the correspondent return period of 100 and 500 years, respectively, the constants, *a* and *b*, of the Gutenberg-Richter can be obtained as given in **Eqs. (5.4)** and **(5.5)** and **Table 5.1**.

$$\left.\begin{matrix}\ln(0.01) = a - bI_{100} \\ \ln(0.002) = a - bI_{500}\end{matrix}\right\} \tag{5.3}$$

$$b = \frac{\ln(0.01) - \ln(0.002)}{I_{500} - I_{100}} \tag{5.4}$$

$$a = \ln(0.01) + bI_{100} \tag{5.5}$$

Now, if $N(I_0)$ is an earthquake event with intensity more than the I_0, the cumulative distribution function (CDF) of the intensity I is given as,

$$F(i) = P(I \leq i) = 1 - \frac{N(i)}{N_0} \tag{5.6}$$

where; $N_0 = N(I_0)$

Once the probability of earthquake intensity is determined, the probability of earthquake occurrence, $P(t)$, assuming that the earthquake events occur individually with an average occurrence rate $N(I)$ can be estimated. The probability of n earthquake events of intensity more than I in the t-years is expressed as the Poisson process as,

$$P_n(t) = \{N(I)t\}^n \ \frac{e^{-N(I)t}}{n_!} \tag{5.7}$$

In **Eq. (5.7)**, setting, n=0, the probability of no earthquake events of intensity more than I in the t-years can be determined as,

$$P_0(t) = e^{-N(I)t} \tag{5.8}$$

Similarly, the probability of occurrence of more than one earthquake event exceeding intensity, I, in the t-years could be given as;

$$P(t) = 1 - P_0(t) = 1 - e^{-N(I)t} \tag{5.9}$$

The probabilistic model of the occurrence of wind events is created in the same way.

To generate the events in the expected lifetime, the proposed procedure initially consists of estimation of the probable earthquake and wind intensity, and subsequently, for the estimated intensity, calculating the probable occurrence with the generation of earthquake and wind events. In the first step, the sample of wind or earthquake intensity, I_i $(i=1,2,..,L)$, is generated from the CDF, **Eq. (5.6)**, using the uniform random variable F_i, where $F_i \in [0,1]$. In conjunction, the sample of the returned period of intensity, ${}_iT_j$ $(j=1,2,..,M)$, is generated from the CDF, **Eq. (5.8),** using the uniform random variable P_i, where $P_i \in [0,1]$.

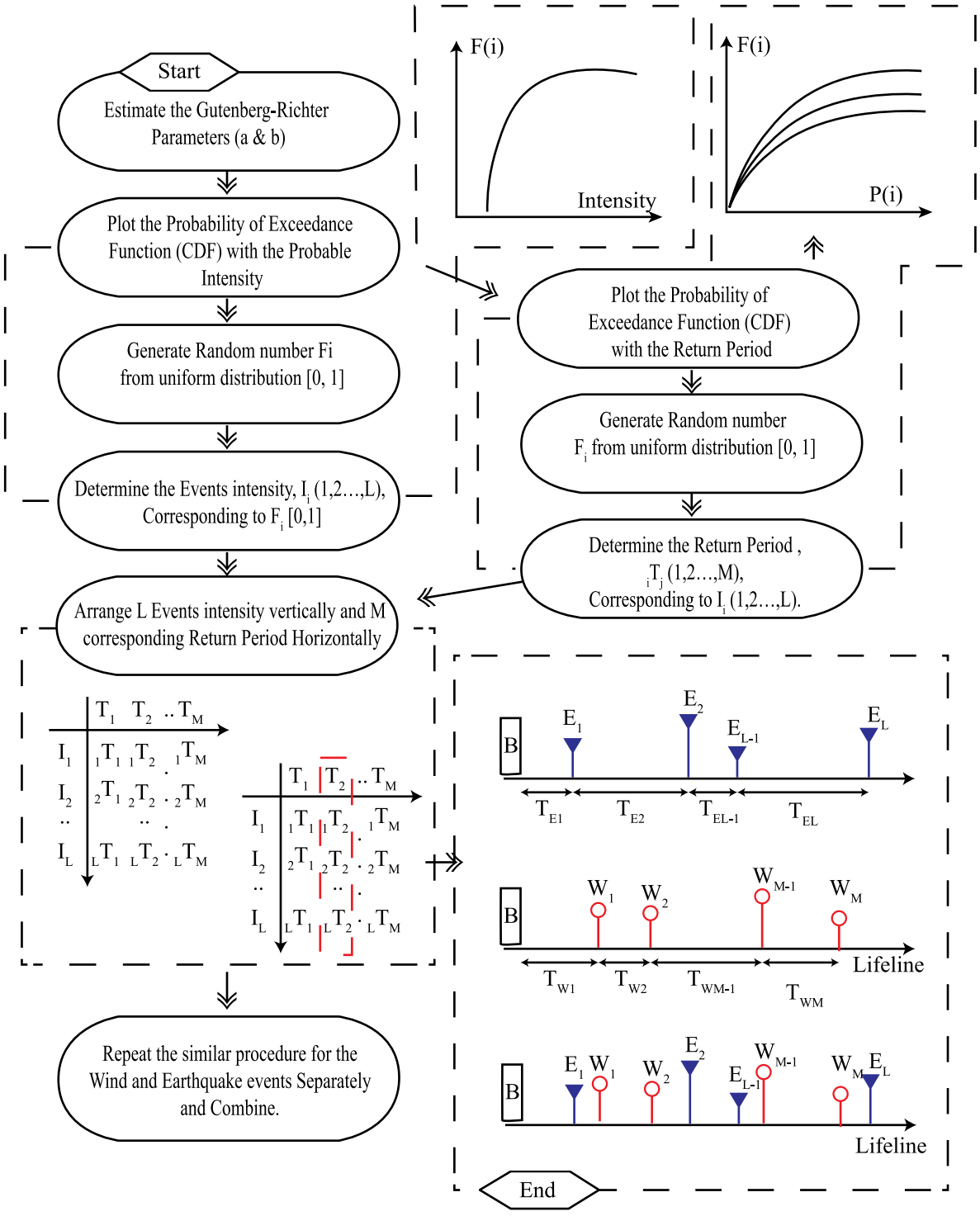

Figure 5.1. Flowchart of probable earthquake and wind events generation in the project lifetime.

Lastly, the L events with different intensity, I_i $(i=1,2,..,L)$ is arranged corresponding to M return period, ${}_iT_j$ $(j=1,2,..,M)$. For the multi-hazard scenarios, the earthquake and wind events are assumed to be occurred independently, where the final timeline is added together, as further illustrated in the proposed procedure flowchart **Figure 5.1**.

Table 5.1. Parameters of the probabilistic distribution of earthquake and wind intensity for Aichi Prefecture Japan.

Event	Intensity I[1,2]	Unit	Return P. years	Recurrence rate	Parameters	
					a	***b***
Earthquake	600	gal	100	0.01	-1.7898	0.0047
	943	gal	500	0.002		
Wind	16	m/sec	1	1	4.9717	0.3107
	36	m/sec	500	0.002		

[1] *in case of an earthquake: "I" denotes zero-period (PGA) acceleration from the response spectrum.*
[2] *in case of wind: "I" denotes the mean wind speed.*

5.4 Multi-hazard events

5.4.1 Earthquake loads

Once the probable earthquake events are sampled for the project lifetime, the next task is to generate the ground motion time history data to be compatible with sampled earthquake intensities. In this regard, the Uniform Hazard Spectrum (UHS) provided in the AIJ (2019) for Nagoya City is used, as shown in **Figure 5.2**. The recommended UHS are the acceleration response spectrum of 5% damping in the engineering bedrock (Vs=292 m/s) level, with the probability of exceedance of 39%, 10%, 5%, and 2% in the 50 years. In case the intensity (PGA) of the probable earthquake is not matching the intensity of recommended UHSs, the interpolation technique is used to generate the appropriate response spectra. **Figure 5.4**, illustrates the steps required to generate spectrum-compatible ground motions using the Fourier and Phase spectrum, following the algorithm developed by one of the authors, STERA_WAVE, [83]. For the phase spectrum, corresponding to the PGA intensity of estimated probable earthquakes in the project lifetime, the historical earthquake has been carefully selected from **Table 5.2** which has a similar PGA. The sequence of selected phase spectrum to generate the sampled earthquake ground motion in each case is presented in **Figure 5.3**. Only in the case, the probably estimated intensity is smaller than 250 *gal*, the uniform random phase angle is adopted, and the ground motion is generated by multiplying the envelope function proposed by Jennings et al. [84].

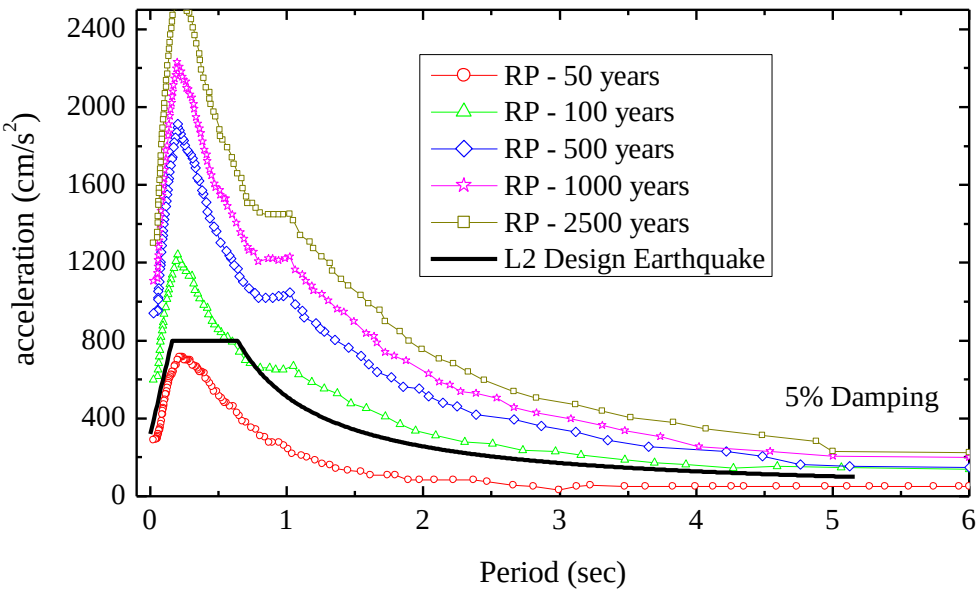

Figure 5.2. Uniform hazard spectrum provided in AIJ (2019) for Nagoya city, Aichi, Japan.

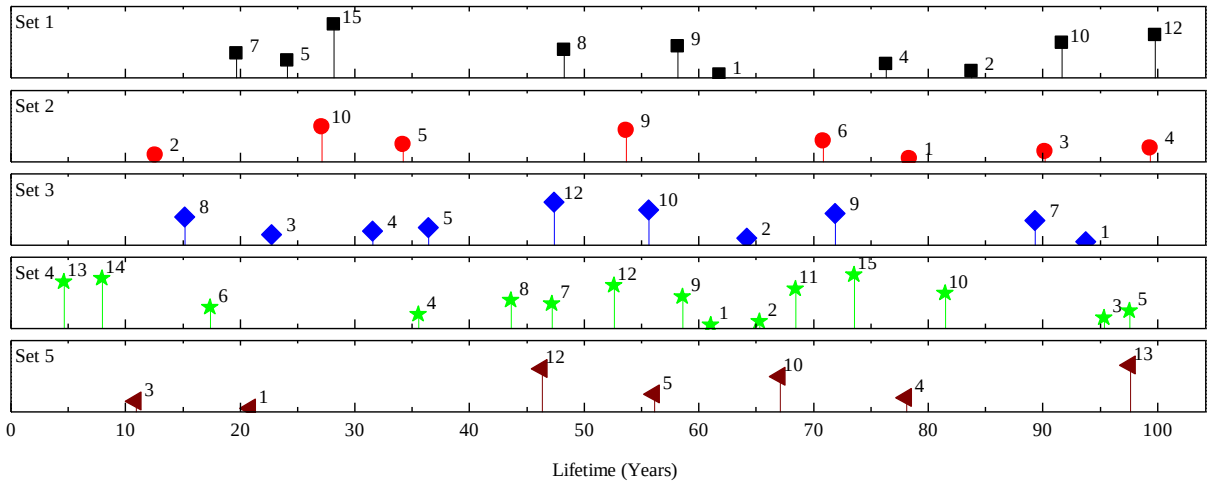

Figure 5.3. The sequence of the phase spectrum earthquakes used to generate compatible earthquakes in multi-hazard scenarios.

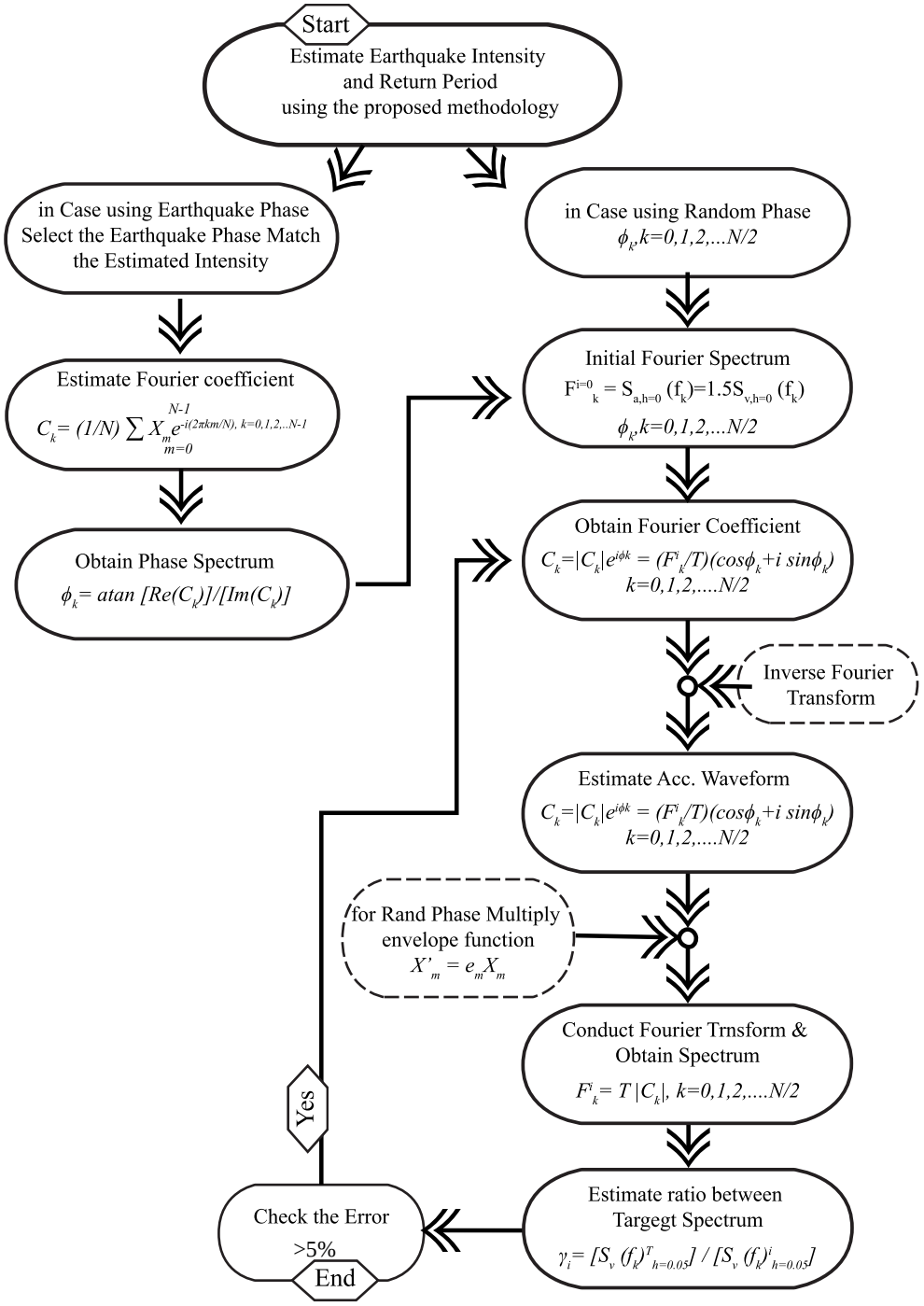

Figure 5.4. Flowchart of STERA_Wave algorithm to generate spectrum compatible earthquakes.

Table 5.2. List of the earthquake used for phase spectrum to scale the probable earthquake events.

No.	Phase Spectrum	Component	Date	Station	Recorded PGA (gal)
1	Random Phase	-	-	-	>250.000
2	Kumamoto	NS	3rd Jan. 2019	Wadamachi Eda	261.697
3	Tottori	NS	6th Oct. 2000	Yonago City	280.233
4	Tottori	EW	21st Oct. 2016	Kurayoshi City	285.811
5	Toho-Oki	NS	4th Oct. 1994	Honamachi	454.975
6	Noto Hanto	NS	25th March, 2007	Wajima City	463.544
7	Miyagi	EW	26th May, 2003	Izumimachi	655.161
8	Iburi	NS	6th Sep. 2018	Atsuma Kananuma	662.241
9	Osaka	NS	18th June, 2018	Hirakata City	690.169
10	Tokachi-Oki	NS	26th Sep. 2003	Makuhetsu-cho	754.2
11	Niigata-Chuetsu	NS	23rd Oct. 2004	Ojiya City Castle	779.244
12	Kushiro Oki	NS	15th Jan. 1993	Kushiro	814.906
13	Kobe	NS	17th Jan. 1995	JMA	818.066
14	Tohoku	EW	11th March, 2011	Ofunato	944.072
15	Yamagata	EW	18th June, 2019	Murakami City	1184.581

5.4.2 Long-duration wind loads

Similar to the earthquake, after the wind events in the project lifetime are sampled, the wind load time-history data are generated following the AIJ (2015) recommendations. The natural wind speed is consisting of the mean wind speed component ($\bar{U}(z)$) and the fluctuating component ($u(t)$) in the longitudinal direction which is changing with time. The AIJ (2015) adopted the von Karman power spectrum to present the power spectral density of the fluctuating component of wind events, as given;

$$S_u(f) = \frac{4\sigma_u^2\{L_z/\bar{U}(z)\}}{[1+70.8\{fL_z/\bar{U}(z)\}^2]^{5/6}} \tag{5.10}$$

wherein the equation, f is the frequency spectrum of wind loads, σ_u is the standard deviation of fluctuating component, $\bar{U}(z)$ is the mean wind speed at 10 m of ground level and L_Z is the turbulence scale.

Co-coherence of wind turbulence along with the structure height, which defines the frequency-dependent spatial correlation of wind speed fluctuation, is also considered as given below;

$$\gamma(f,d_j) = \frac{\mathrm{Re}\left[S_{i_1,i_2}(f,d_j)\right]}{\sqrt{S_{i_1}(f)\cdot S_{i_2}(f)}} = exp\left(-C_{ij}\frac{fd_j}{\bar{U}(z)}\right), i=u,v,w; j=v,w \tag{5.11}$$

$$\gamma(f, d_j) = exp\left(-\frac{\sqrt{(C_{uy} \cdot f d_y)^2 + (C_{uz} \cdot f d_z)^2}}{\bar{U}(z)}\right) \quad (5.12)$$

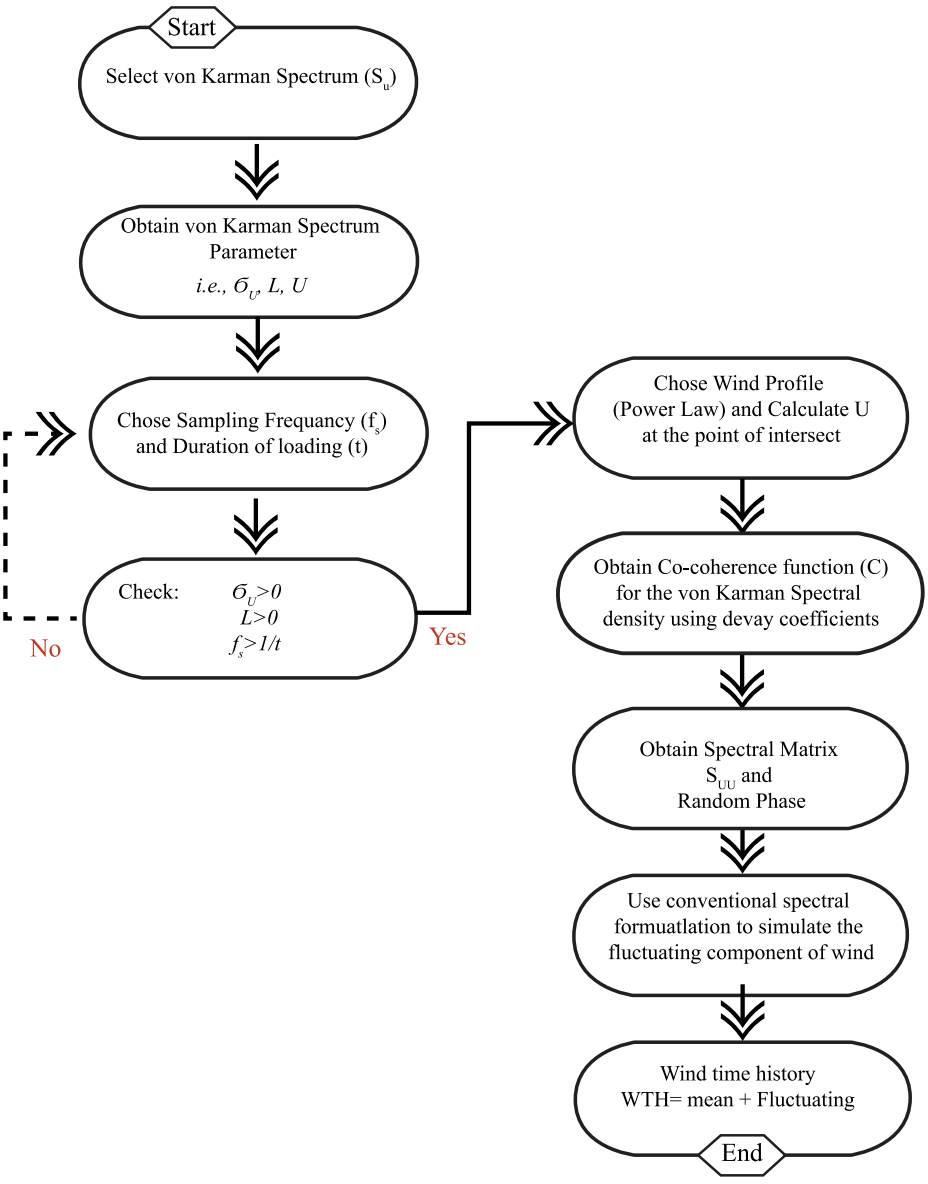

Figure 5.5. Flowchart for generating wind loads time history.

where d_j is the distance of two referenced nodes of Euclidian distance, S_u is power spectral density of turbulence in the longitudinal direction of a single point, C_{ij} is decay coefficients. The current work employed the decay coefficients from the Norwegian Public Roads Administration (NPRA) Handbook N400 [40], as well as, the power law is employed to estimate the wind speed force at story levels. Furthermore, the conventional spectral method introduced by Deodatis and Shinozuka (1991) [85] and Deodatis (1996) [86] is adopted to estimate the fluctuating component of wind load by simulating the multivariate random process in the time domain. The entire process discussed in this section is further illustrated in the flowchart, **Figure 5.5**, and the corresponding parameters are summarized in **Table 5.3**.

Table 5.3. Corresponding parameters of long-duration wind loads.

No.	Description	Parameter	Unit
1	Turbulence Length Scale	75.27	m
2	Standard Deviation of Fluctuating Component	6.73	m/sec
3	Cutoff Frequency	5.00	Hz
4	Mean of duration	7,500.00	sec
5	Coefficient of variation	10.00	%

5.5. Cumulative damage model

5.5.1 Fatigue evaluation of BRBs device

The fatigue life of BRBs is originated with the initiation of first fatigue cracks, and it grows slowly and gradually under each cyclic loadings until reaches the failure thresholds. Thus, the fatigue life can be defined from the number of cycles N_f of specific intensity which a BRB can sustain before failures happened. For the earthquake and wind loads, which induce cyclic load with variable intensity, the strain-based estimation of fatigue life is suitable. For this purpose, first, the random cyclic-loads are sorted in bins of similar strain, then, for each of the bins the cumulative damages are computed from the *S-N* curves, and finally, using the Miner's rule the contribution of individual variable strains are combined.

5.5.2 Variable-load cycle counting

The BRBs member under earthquake and wind events experience variable-load cycles over the time of excitation. This necessitates a proper procedure to estimate the number of cycles and classify the time-varying load history to a constant and equivalent load of similar amplitude. Among the typical variable-load counting the rainflow counting method, which was developed by Matsuishi and Endo (1968), demonstrated good agreement with the observed fatigue damage and was widely adopted by researchers [87]. Thus, the current work practiced the rainflow counting technique to estimate the number of variable

loads, strain amplitude, and range for the random cyclic load imposed as a result of wind and earthquake excitations.

5.5.3 Strain-cycle relationship of BRBs

Coffin (1962) and Manson (1966) defined the relationship between the number of cycles until failure, N_f, and strain amplitude, $\Delta\varepsilon_t$, which leads to fatigue failure, as given in **Eq. (5.13)**. Usually, this relationship is derived from experimental results or empirical formulas based on statistical data. The fatigue life of BRBs element, manufactured in Japan, has been studied extensively under different loading scenario such as; shaking table test [89], constant amplitude fatigue test [90], BRB frame shaking table test under random amplitude [91], and truss frame test under gradually increasing amplitude [92]. Takeuchi et al. [93], observed that the fatigue properties of BRBs are not considerably changed for different types of steel material, wherein the approximate strain-failure cycle relation is given as below,

$$\begin{aligned} \Delta\varepsilon_t[\%] &= 0.5N_f^{-0.14}\ (\Delta\varepsilon_t < 0.1\%) \\ \Delta\varepsilon_t[\%] &= 20.48N_f^{-0.49}(0.1\% \le \Delta\varepsilon_t < 2.2\%) \\ \Delta\varepsilon_t[\%] &= 54.0N_f^{-0.71}(\Delta\varepsilon_t \le 2.2\%) \end{aligned} \tag{5.13}$$

5.5.4 Miner's damage rule

According to the Miner rule, if in a strain profile there are *j* number of the strain of different intensity, where each of them contributes n_i cycles in the profile, and if the number of cycle to failure point is N_i, the cumulative damage failure index (CDI) occurs when the total ratio of $\frac{n_i}{N_i}$ reaches 1, which is given as

$$CDI = \sum_{i=1}^{j} \frac{n_i}{N_i} \le 1 \tag{5.14}$$

Now by substituting the BRBs strain-cycle relation, **Eq. (5.13)**, into the Miner rule, **Eq. (5.14)**, the cumulative damage of BRBs subjected to random cyclic-loads of earthquake and wind excitations, can be presented as given below,

$$CDI = \sum_{i=1}^{j} \frac{n_i}{\left(\frac{\Delta\varepsilon_t}{0.50}\right)^{-\frac{1}{0.14}}} \ (\Delta\varepsilon_t < 0.1\%)$$
$$CDI = \sum_{i=1}^{j} \frac{n_i}{\left(\frac{\Delta\varepsilon_t}{20.48}\right)^{-\frac{1}{0.49}}} (0.1\% \le \Delta\varepsilon_t < 2.2\%) \quad (5.15)$$
$$CDI = \sum_{i=1}^{j} \frac{n_i}{\left(\frac{\Delta\varepsilon_t}{54.0}\right)^{-\frac{1}{0.71}}} (\Delta\varepsilon_t \le 2.2\%)$$

5.6 Case study: Steel building with BRB devices

5.6.1 Building description

The target building is a 20-story steel moment-resisting frame designed according to Japanese standards [8,15,16]. It is assumed the target building is located in the Aichi Prefecture, Japan, with a 100-years service period. The elevation of the frame and the configuration of BRBs along the height of the frame are presented in **Figure 5.6**. The total height of the frame is 71 m, while the ground floor height is 4.5 meters, and the remaining floor height is 3.5 m. There are 5 spans, with 3 spans of 6.4 m and 2 spans of 4 m. The hollow square-box and wide flange of SN490B steel type are selected for the column and beam elements, with the yield strength of 325 MPa and tensile strength of 490 MPa. The member size and thickness of the elements in each story are summarized in **Table 5.4**.

Table 5.4. Structural details of beam and column elements (*mm*).

Steel Beam				***Steel Box Column***		
Story	***H×B***	t_W	t_F	***Story***	***H×B***	***t***
19-20	450×250	9	16	-	-	-
17-18	450×250	9	16	17-20	350×350	19
14-16	500×250	12	22	13-16	400×400	19
11-13	500×300	12	16	9-12	450×450	19
8-10	500×300	12	25	6-8	450×450	22
5-7	550×300	12	16	4-5	500×500	22
2-4	550×300	12	25	2-3	500×500	25
1	600×300	12	19	1	550×550	35

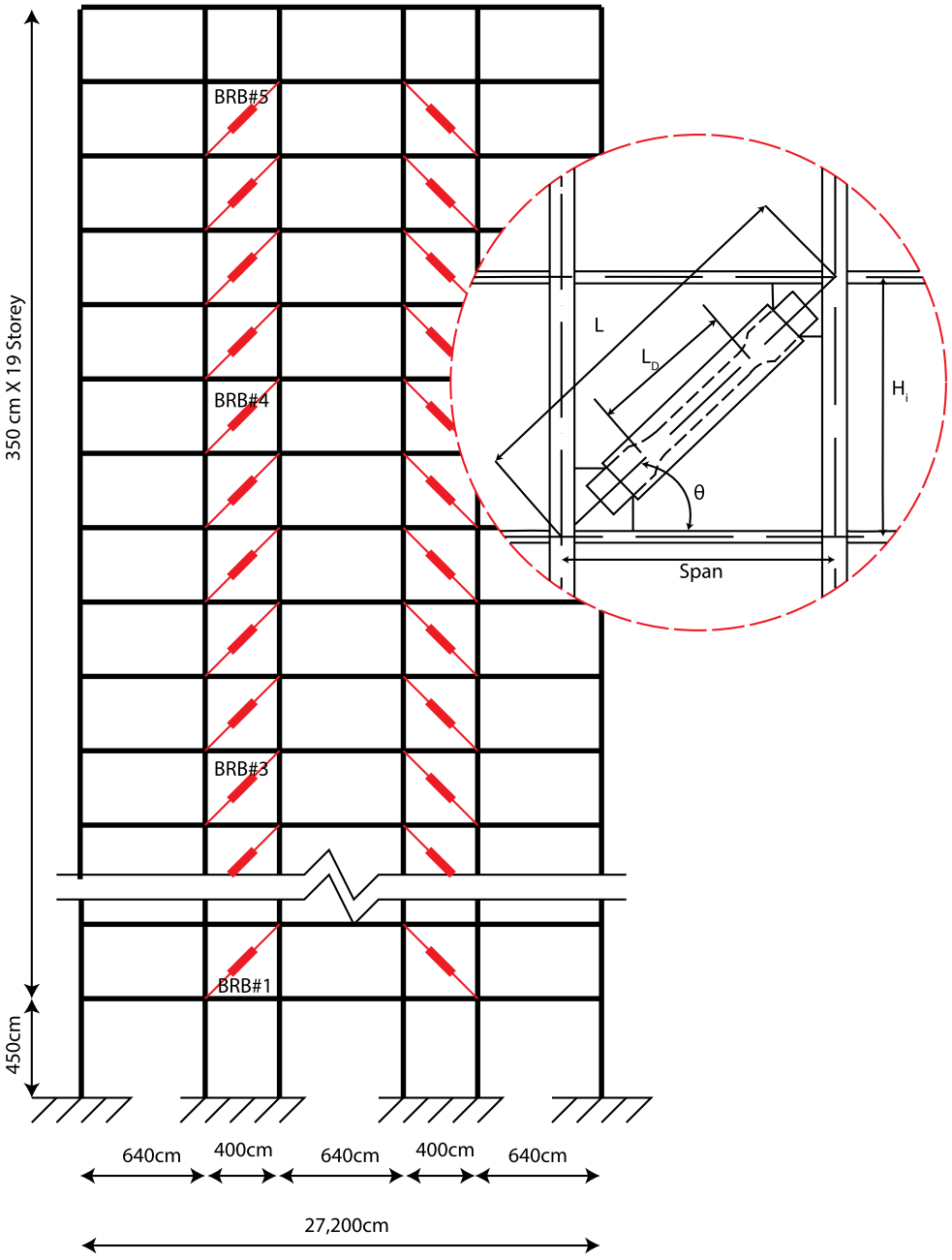

Figure 5.6. 20-story steel prototype building elevation and BRB configuration.

The design guideline of buildings with passive control devices (JSSI, 2014) [8] is used to determine the size and number of BRBs. The JSSI guideline adopts the procedure developed by Kasai et al. (1998) [17] to obtain the necessary stiffness and damping of additional BRBs. The method idealizes the building as an equivalent single degree of freedom (SDOF) system and estimates the amount of additional stiffness and

damping of passive control devices according to the target performance level under design earthquake. For the current example, the target performance levels are the maximum inter-story drift ratio of less than 1% and the ductility factor of BRBs of less than 7, under the design earthquake and wind loads. **Table 5.5** presents the estimated parameters of BRBs, while device configuration is shown in **Figure 5.6**.

Table 5.5. Technical parameters of design BRBs.

Story	F_{iy}	K_{ai}	K_1/K_{ai}[1]
	kN	*kN/mm*	
20	-	-	-
17-19	250	100	0.02
14-16	345	140	0.02
11-13	435	175	0.02
8-10	430	172	0.02
5-7	460	185	0.02
2-4	385	155	0.02
1	-	-	-

[1] *Ratio of post-yield to pre-yield stiffness.*

5.6.2 Numerical model of the target building

The 20-story steel frame is modeled by a finite element software, STERA_3D (STructural Earthquake Response Analysis 3D), developed by Prof. T. Saito [13]. The beam elements are presented by two nonlinear flexural springs at both ends. The column elements have nonlinear axial springs distributed in the sections of both ends. The steel strength is modified 1.1 times than the nominal strength and the ratio of post-yield stiffness to the initial stiffness is 0.001. **Figure 5.7** represents the hysteresis behavior of the nonlinear bending spring which is defined as the moment-rotation relationship under cyclic loadings. The beam-column connection is assumed rigid, where the rigid zone length for the beam element is set to be half of the column width. The BRB element, as presented in **Figure 5.8**, is defined as a shear spring in a frame with the bi-linear hysteresis and initial stiffness, K_1, and secondary stiffness of, K_2.

5.7 Performance evaluation of target building

5.7.1 Pushover analysis

The strength capacity and story drift distribution of the target building are evaluated using the non-linear static pushover analysis. The model is pushed horizontally until the drift ratio at the equivalent height of the model reached 1/50 using the lateral load distribution given by the Japanese standard [16,77]. The relationship between the base shear coefficient and the drift ratio at the equivalent height of the model, for both cases; without and with supplemented BRBs, are illustrated in **Figure 5.9**. The result indicates that the

lateral strength of the target frame is increased for the frame with supplemented BRBs by 135%, 115%, and 120% when the building pushover reaches 0.5%, 1.0%, and 2.0% of drift ratio, respectively.

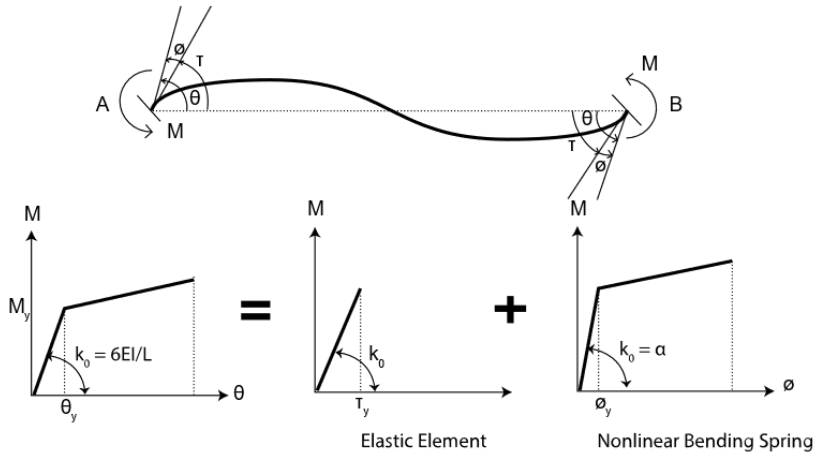

Figure 5.7. Hysteresis model of nonlinear bending spring of steel column and beam.

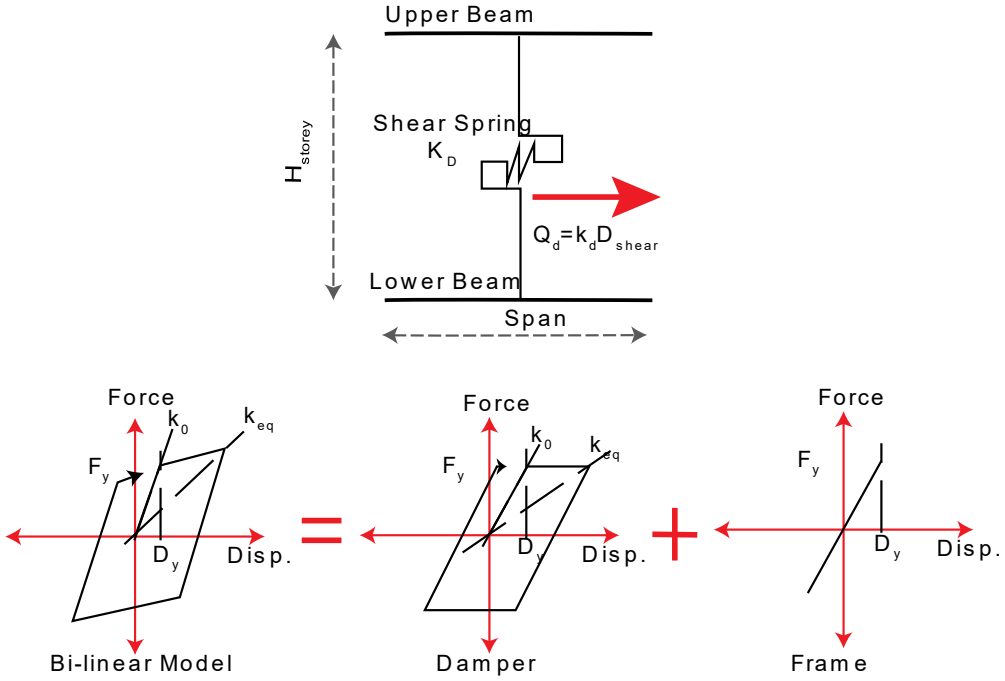

Figure 5.8. Configuration scheme and bilinear hysteresis model of nonlinear shear springs for BRBs.

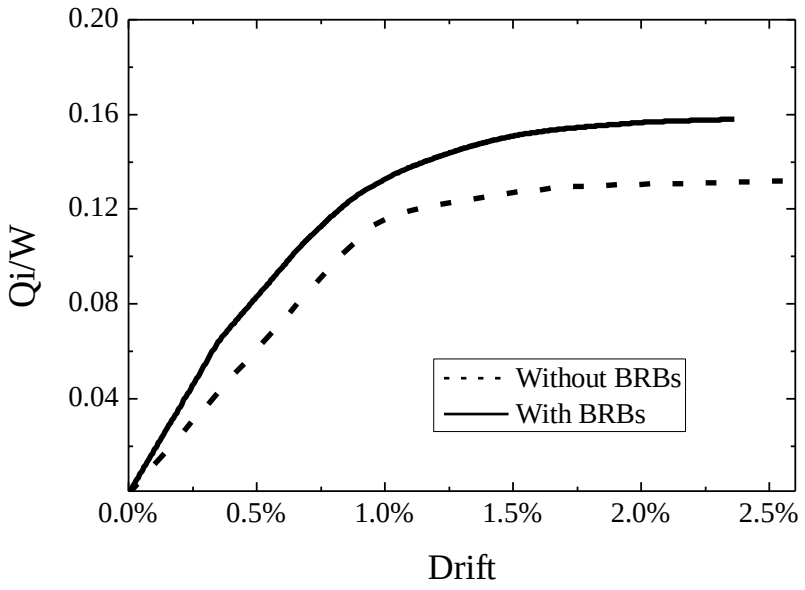

Figure 5.9. Base shear coefficient and drift ratio at the equivalent height of target model

5.7.2 Eigenvalue analysis

The dynamic characteristics of the target frame corresponding to the 1st to 3rd modes of vibration are obtained by eigenvalue analysis. As shown in **Figure 5.10**, the natural period becomes shorter after installing BRBs while the mode shape is not changed significantly.

5.7.3 Time history analysis under design loads

The target frame is analyzed under the design earthquakes and wind loads prescribed in the Japanese standard [15] to validate the design procedure and evaluate the contribution of BRBs. Five sets of earthquake ground motions are considered as listed in **Table 5.6**. Three of them are the observed earthquake ground motions scaled to Level 2 to have the maximum velocity of 50 cm/sec. The other two earthquakes are artificial earthquake ground motions to have the response spectra to be compatible with the Level 2 design spectrum of the Japanese standard [16] and the phase spectra of historical earthquakes. The acceleration response spectra of selected earthquakes are illustrated in **Figure 5.11**. As for the wind load, four sets of design wind load of the different average speeds of 17, 20, 25, and 31 m/s are generated according to the AIJ recommendations [15]. Since the shape of the building is regular, the wind loads are applied at the center of gravity on each floor, while the distribution of the wind loads along the height of the building is decided according to the Japanese standard [16].

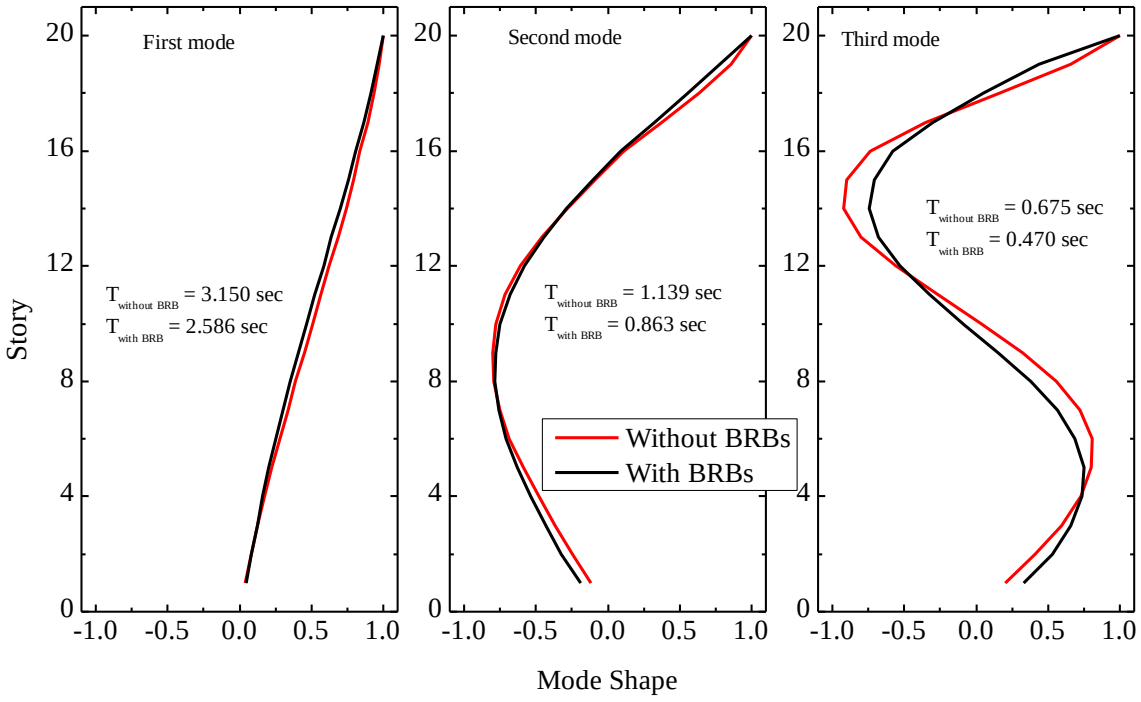

Figure 5.10. Normalized mode shape of the target high-rise building with and without BRBs devices.

Table 5.6. List of selected earthquake ground motions.

Categories	No.	Event	Year	Station
Scaled earthquake to be compatible of 50 cm/sec	1	Imperial Valley	1940	El Centro
	2	Kern County	1952	Taft
	3	Kobe	1995	JMA
Artificially generated earthquake to be compatible with Level 2	4	Tohoku	1978	Tohoku Univ.
	5	Tokachi Oki	1968	Hachinohe

The maximum story drift ratio of the target frame with and without BRBs under the design earthquake and wind loads is presented in **Figure 5.12**. For the design earthquake loads, the maximum story drift is controlled to satisfy the 1% design drift, while the average result indicates a 50% decrease in the critical stories compared to the target frame without BRBs. On the other hand, the maximum story drift under the wind loads also indicated an improvement of 50% in contrast to the model without BRBs which reaches the 1.2% story drift in critical floors, in the case of design wind load of 31m/sec. Hence, the design

procedure is a straightforward tool that can determine the amount of additional stiffness to be provided by BRBs without any iteration to satisfy the design targets.

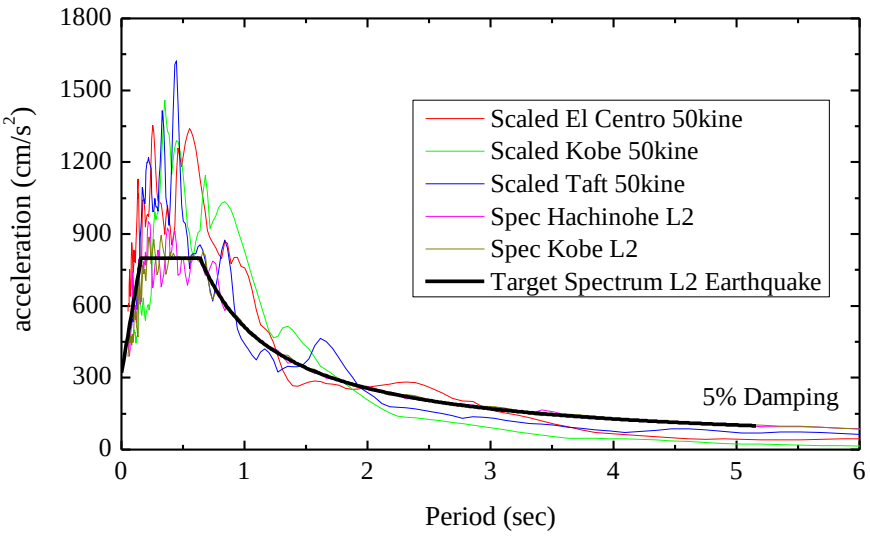

Figure 5.11. Response acceleration spectrum of selected ground motions (5% damping).

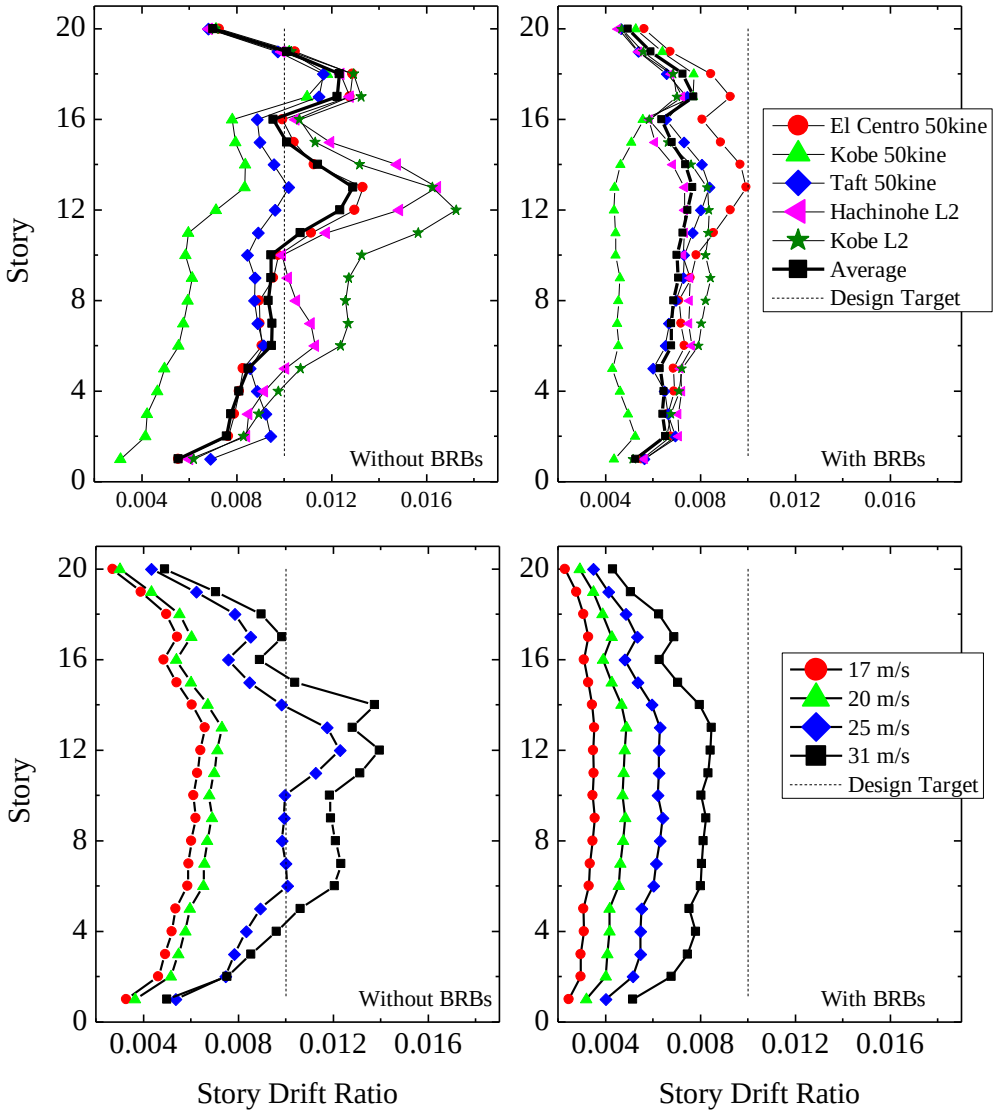

Figure 5.12. Maximum story drift ratio of high-rise steel building with and without BRBs under design earthquake and wind loads.

Furthermore, in **Figure 5.13**, for the earthquake and wind loads, the maximum ductility factor and the amount of dissipated energy of each BRB along the height of the building are evaluated. For most of the earthquake loads, the ductility factor of BRBs is in the range of the pre-defined design drift, which is considered to be (μ=7), except the lower stories which is exceeded. In the case of design wind loads, the ductility factor is decreasing significantly in upper stories. As for the amount of dissipated energy, in both cases, the BRBs in the upper floors are less effective to dissipate the earthquake or wind loads.

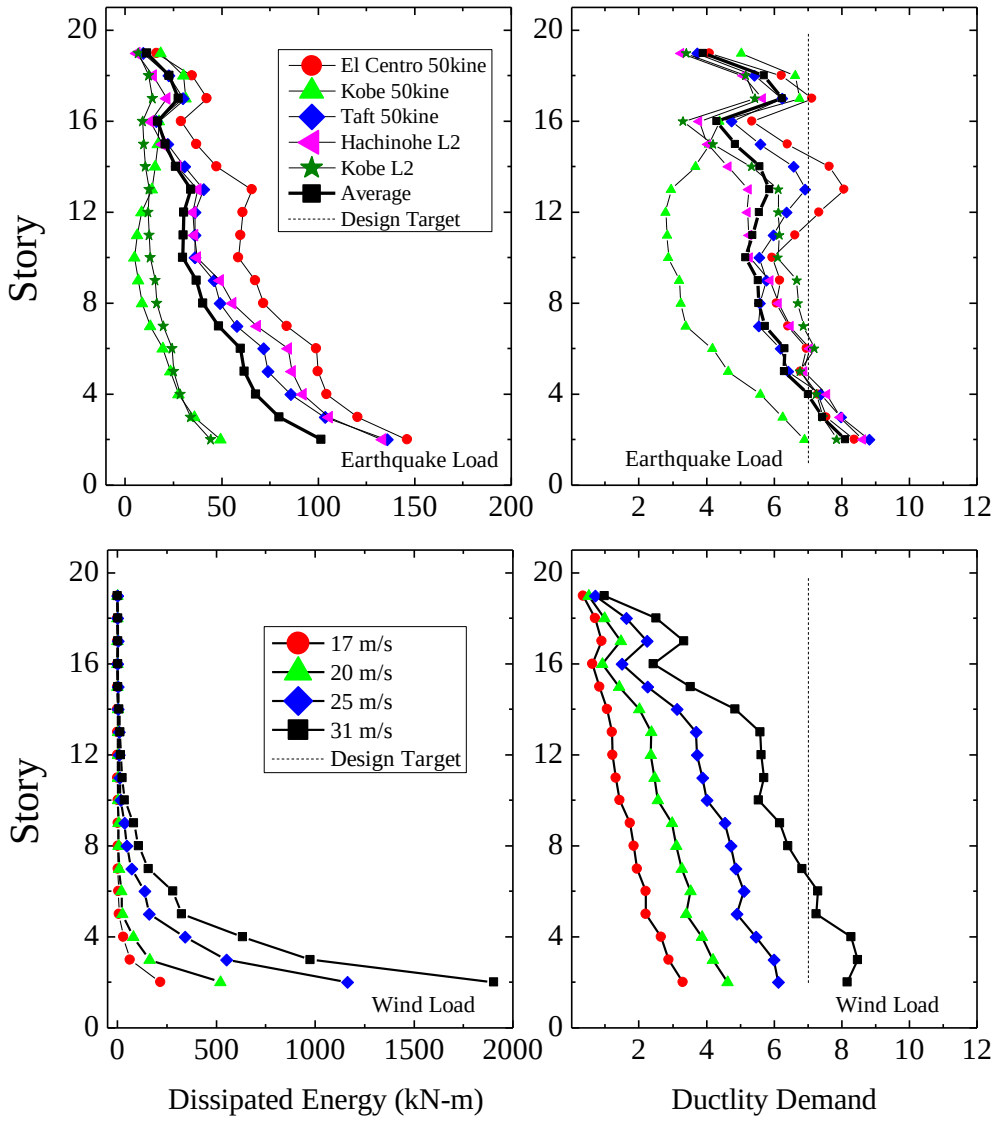

Figure 5.13. Ductility demand and energy dissipation rate of BRBs along with the height of high-rise steel building under earthquake and wind loads.

5.7.3 Multi-hazard timeline for the target building

Five random timelines are developed from the earthquake and wind events of different return periods, as discussed in previous sub-sections, and presented in **Figure 5.14**. In each timeline, an average of ten earthquakes of different PGA (range from 250 to 1100 gal), is anticipated, where the earthquake events detail and sequence are summarized in **Table 5.2**. Similarly, in each sets an average of 43 wind events (range from 16-31 m/sec) is expected to occur.

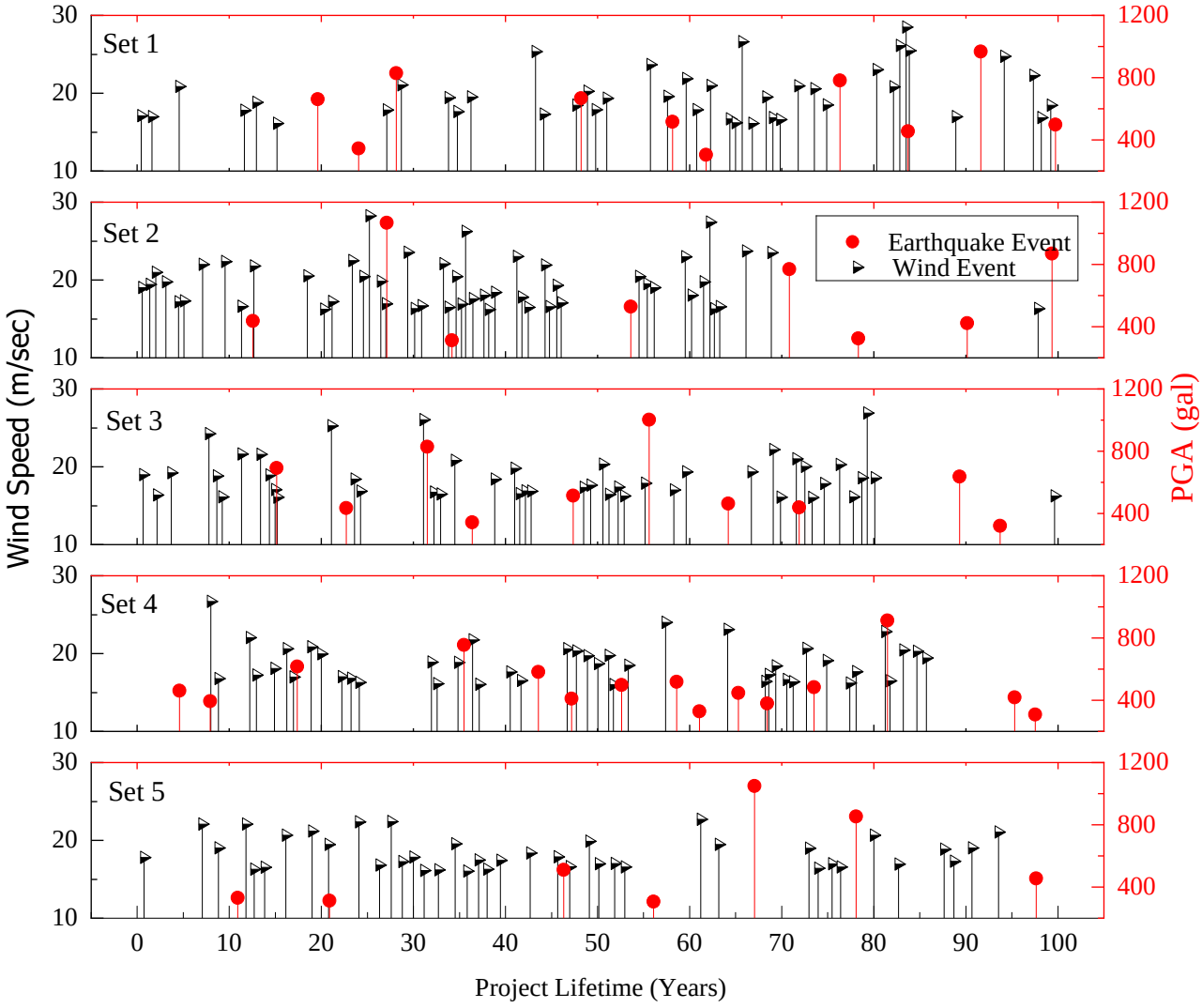

Figure 5.14. Probable Multi-hazard scenarios in the target building lifetime.

5.8 Result and discussion

5.8.1 Cumulative damage index (CDI)

Figure 5.15 demonstrates the estimated CDI for the selected BRBs (in 2nd, 5th, 10th, 15th, and 19th stories, **Figure 5.6**) under the application of five sets of multi-hazard scenarios, generated according to the procedure presented in Section 4 and **Figure 5.1**. It was noted, the BRB1, located on the 2nd floor, with an average strain of 0.05% has reached the CDI = 0.6 in the projected lifetime under the combined application of low-cycle high-strain and high-cycle low-strain of earthquake and wind loads. While the BRBs located

in upper stories indicating an average strain of $\geq 0.03\%$ and the estimated CDI is about 0.2. It is observed, that BRBs with an average strain of 0.05% is an optimal design for multi-hazard scenarios. It is important to be mentioned, the wind excitation pushes the building parallel to the wind direction at the rate of average wind speed, while the fluctuating wind speed acts as cyclic. This is evaluated as the fact the BRB's performance under wind loads is ineffective in the flexural sensitive stories.

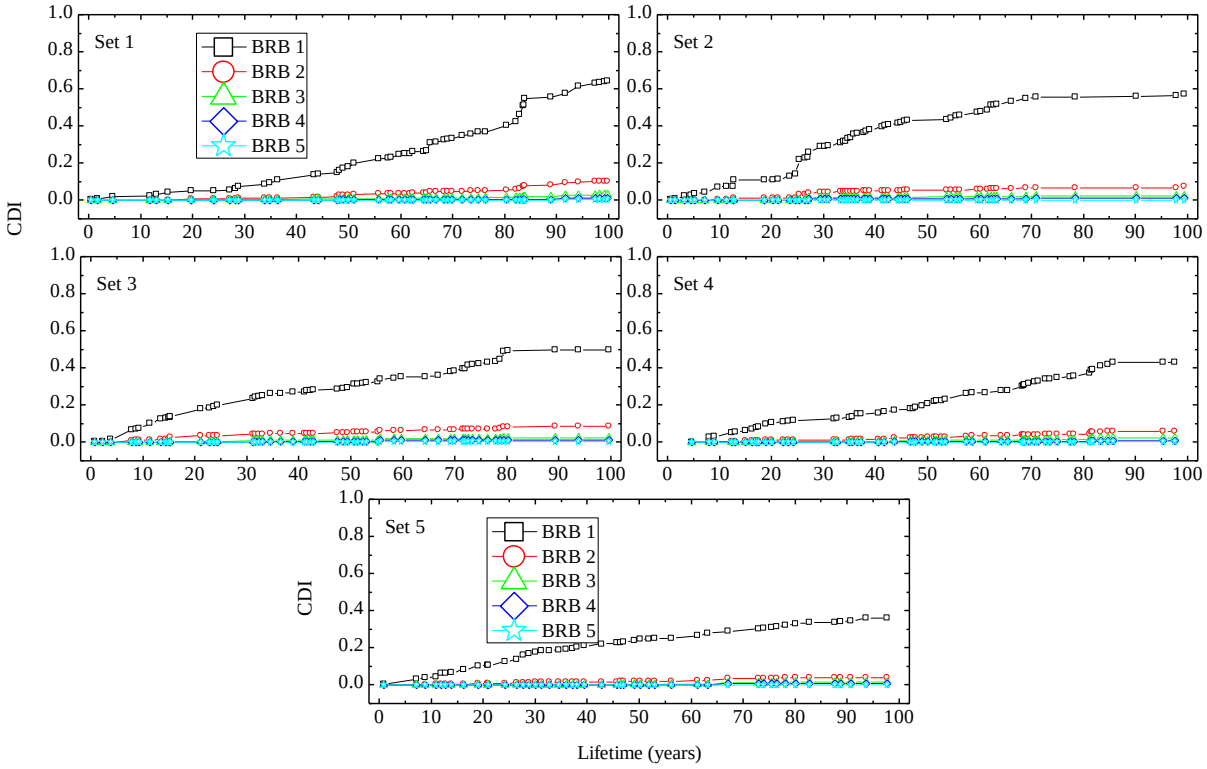

Figure 5.15. Cumulative damage index (CDI) of selected BRBs in the target building.

5.8.2 Story drift ratio of the target building

Figure 5.16 presents the envelope of maximum story drift and shear force of the target building under the five sets of multi-hazard scenarios. Comparing the maximum story drift ratio with the design target of 1%, the maximum story drift obtained from multi-hazard timelines is 2.0~5.5 times larger than the design target. Although the story drift amplification for the lower story in contrast to the upper story is 3 times larger, the upper stories are not able to endure the design drift, as well. Also, the distribution of the maximum story

shear force is approximately equal to the distribution of the story shear force (dotted line) when the seismic base shear is C_S=0.2W, where W is the weight of the building.

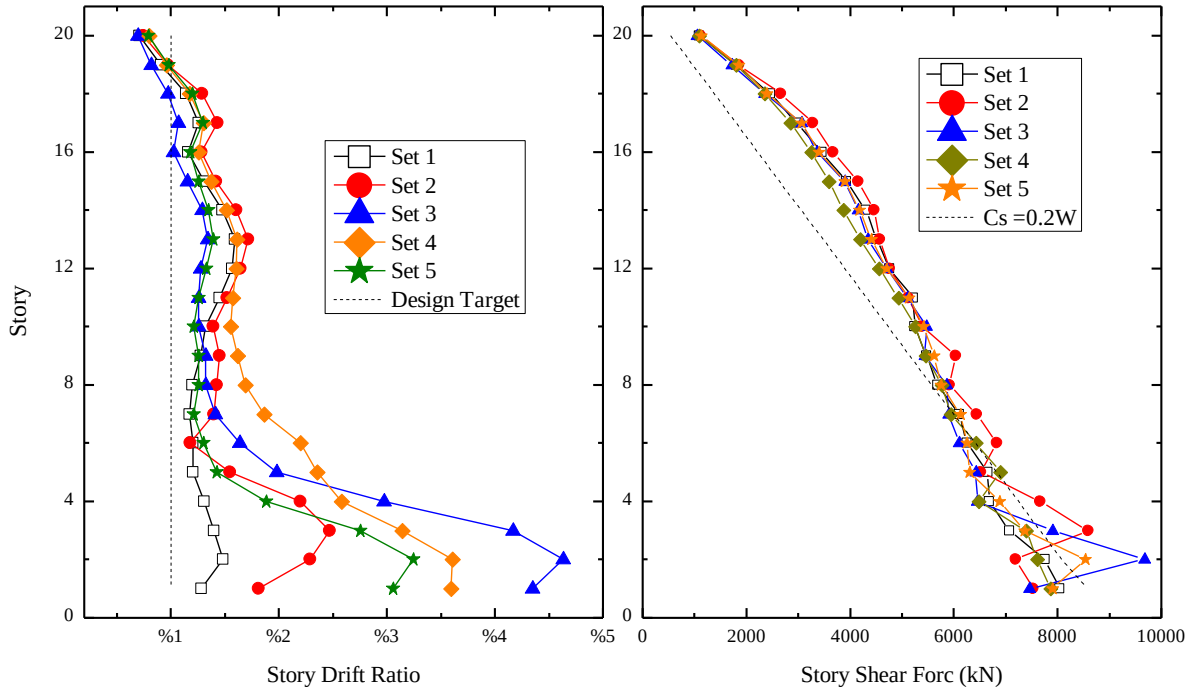

Figure 5.16. Maximum story drift ratio of target building under successive analysis multi-hazard scenarios.

5.8.3 Plastic strain energy (PSE) of the target building

The study conducts by Chung and Lee (1994) [94] introduces the plastic strain energy as a damage criterion, because, in each cycle of excitation an irrecoverable amount of PSE is inserted into the steel elements, which in response initiate and propagate the fatigue crack. Therefore, the cumulative damage of BRBs is further evaluated in the term of plastic strain energy (PSE) which is defined as the ratio of the area of plastic strain energy (E_t) by the triangular area (E_y) shaped by the yield and deformation strengths of RBR, **Figure 5.17a**.

The experimental study conducted by Iwata and Murai (2006) [57] introduces the PSE as a suitable indicator for the performance evaluation of BRBs in moment frames. The study recommends **Eq. (5.16)** as a threshold to evaluate the safety of BRB in terms of cumulative plastic strain energy [57].

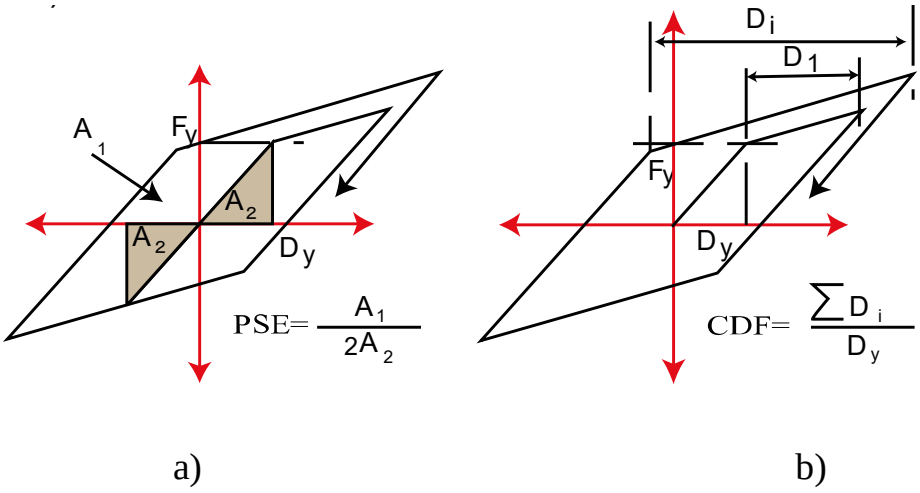

Figure 5.17. a) Plastic Strain Energy (PSE), b) Cumulative Ductility Factor.

$$CPSE = 150\,R \tag{5.16}$$

$$R = \frac{P_E}{P_y} \tag{5.17}$$

In the equation, P_E is the buckling strength of the restrainer and P_y is the yield strength of the steel core plate. The R factor is an indicator of the stable energy absorption capacity of BRBs. In **Figure 5.18**, the result of cumulative plastic strain energy is compared with the different ratios of (R=1, 2, 3, and 4), where the safety limit of PSE is estimated to be 150, 300, 450, and 600, accordingly. It is observed, BRBs with $R \geq 4$ can resist the cumulative plastic strain energy within the building lifetime, and the of BRBs with $R < 4$ have the potential to fail under cumulative PSE in the building lifetime. In case the BRB has the minimum capacity (R=1) the possibility to reach the PSE threshold is about 20-, 40- and 60-years in the 1st, 5th, and 10th floors. In contrast to the CDI, the cumulative PSE reveals that even the BRBs with an average strain of about 0.03% (e.g. BRB 2 and BRB 3) is possible reaching the PSE criteria which can lead to fatigue failure of the device. It is important to be mentioned, although almost all the BRBs are satisfying the cumulative damage index (CDI), under Miner's damage rule, the BRB's cumulative PSE performance indicates the device fatigue life must be examined under multiple criteria. Therefore, the current research recommends a multiple-criteria base investigation of BRBs damper which are objects to install the region prone to the multi-hazard scenarios.

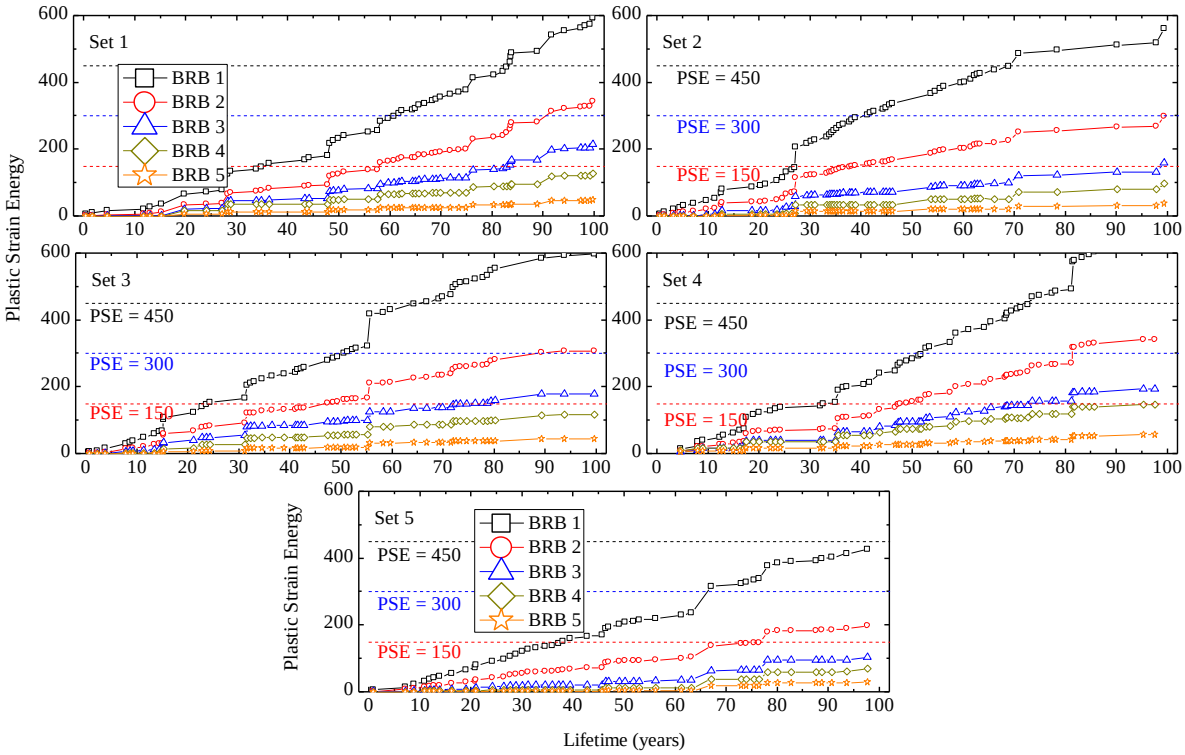

Figure 5.18. The plastic strain energy of selected BRBs under the successive analysis of 5-sets of Multi-hazard timelines.

5.8.4 Cumulative ductility factor (CDF) of the target building

Similarly, the accumulative damage of BRBs in the high-rise steel building under successive application of multi-hazard scenarios is investigated in terms of CDF. The CDF is an important indicator that describes the plastic deformation capability of the BRB devices before resulting in structural destruction. As presented in **Figure 5.17b**, the CDF is the normalized summation of total plastic deformation to the yield strength of BRB, **Eq. (5.18)**.

$$CDF = \frac{\sum(D_i)}{\mathrm{D}_y} \tag{5.18}$$

$$CDF = 75\,R \tag{5.19}$$

Researchers extensively examined the low-cycle fatigue capacity of BRBs in terms of cumulative ductility demands [95-100] and recommends the minimum criteria. FEMA-450 [97] and ANSI/AISC [100] recommend the CDF to not be less than 140 and 200, respectively, to ensure the cumulative ductility capability of the device. In the current research study, the result of the experimental study conducted by

Iwata and Murai (2006) [57], as given in **Eq. (5.18)**, is utilized to further evaluate the BRB's performance in the building lifetime. Accordingly, as given in **Eq. (5.19)**, for the (R=1, 2, 3, and 4, where $R= P_E/P_y$) the CDF threshold is estimated to be 75, 150, 225, and 300 as indicated by horizontal lines in **Figure 5.19**.

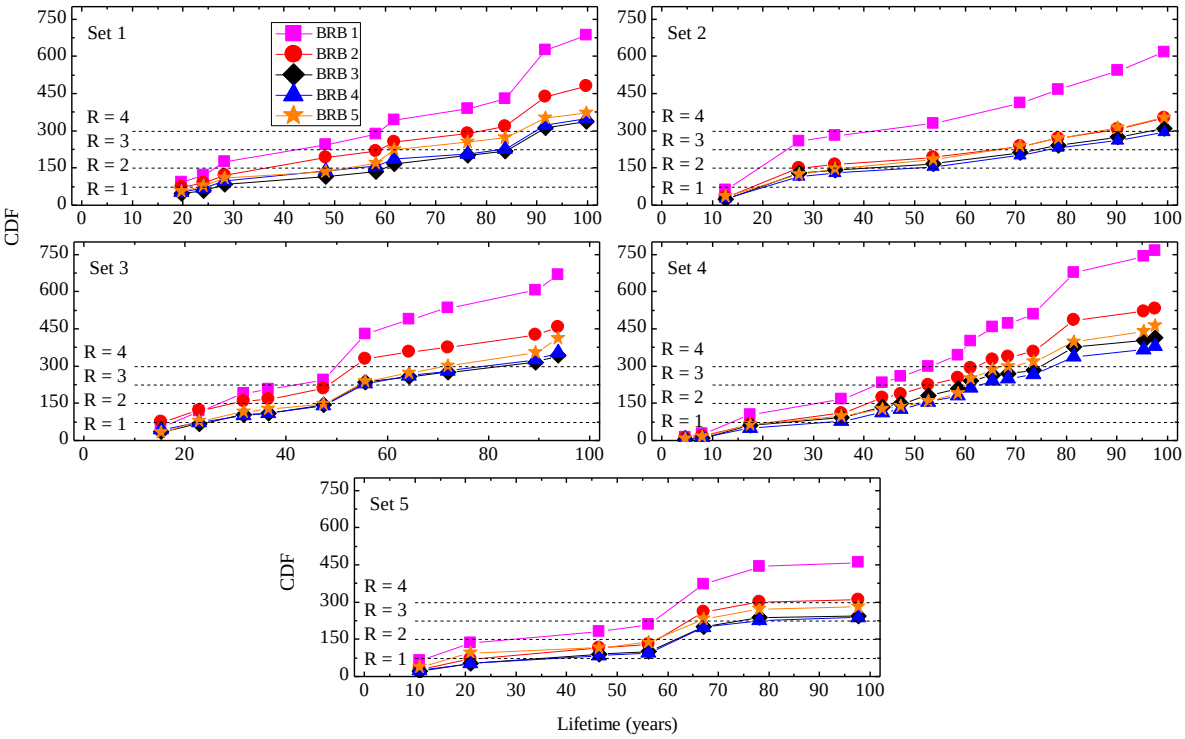

Figure 5.19. Cumulative ductility factor of selected BRBs under the successive analysis of 5-sets of Multi-hazard timelines.

In the figure, the CDF is estimated for the successive application of five sets of multi-hazard scenarios. It is observed, corresponding to the number and earthquake sequence in each timeline the CDF varies and almost for R=1, all the BRBs reaching the criteria within the 15-years. While this measurement for R=4 indicates that even the BRBs with the smallest strain amplitude have the potential to be failed in terms of CDF within 70-years of their life. Among the five generated timelines, considering set-4 which has the highest number of earthquakes, and set-5, which has the lowest number of earthquake events, the estimated CDF is almost 1.5 times larger. Comparing the results of Cumulative Damage Index and Plastic Strain Energy with Cumulative Ductility Factor, it is important to be pointed that the BRBs which look safe under one type of criteria could be easily damaged under another criterion. Therefore, the current study recommends precisely evaluate the fatigue life BRBs under different scenarios in terms of different criteria.

5.8.5 Maximum ductility of BRBs of the target building

The maximum ductility factor under successive application of multi-hazard scenarios is presented in **Figure 5.20**, for the selected BRBs.

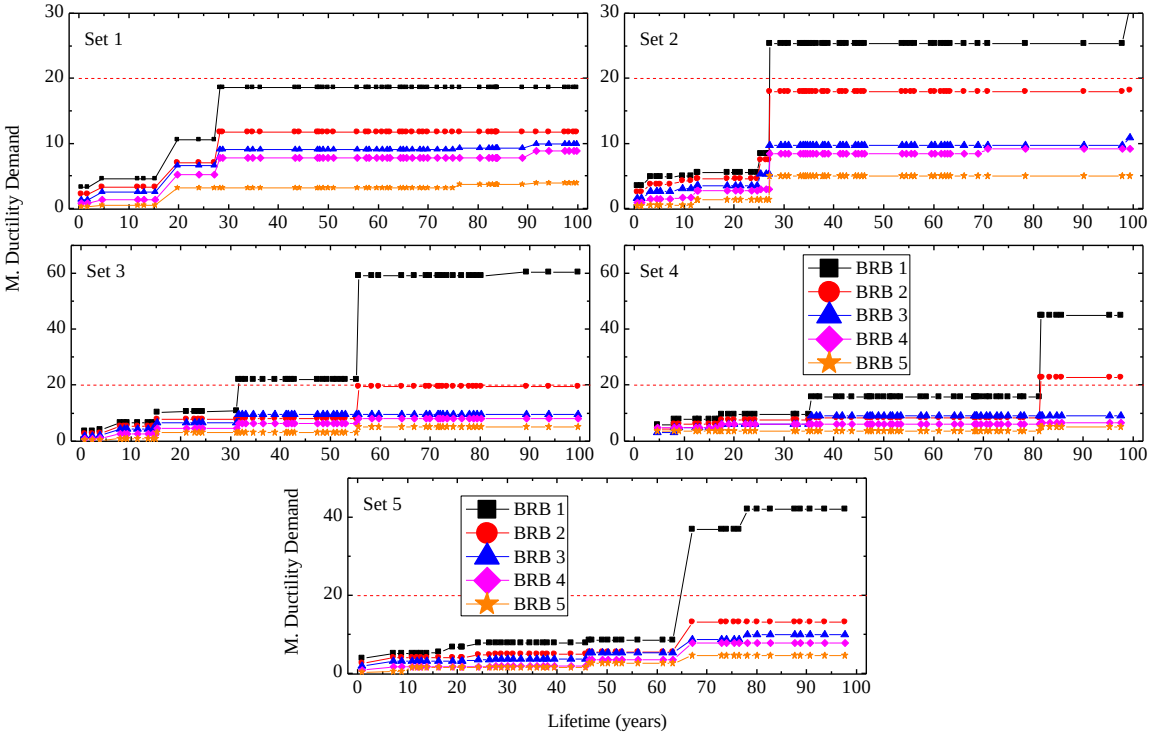

Figure 5.20. Maximum ductility demand of selected BRBs under the successive analysis of 5-sets of the multi-hazard timeline.

Then the maximum ductility is evaluated by comparing it to the experimental result obtained from previous research studies conducted for the common types of BRB in Japan [57,94,96]. Accordingly, the maximum ductility demand for BRBs with different configuration and cyclic loading protocols are reported to range (20-24) before exceeding the ultimate capacity of BRB. Now in **Figure 5.20**, considering the ductility of 7 and 20 as initial design target and ultimate ductility demand of BRBs it is observed, the successive application of multi-hazard events amplifies the BRBs deformation and increases the ductility demand. In contrast to the design earthquake, which indicates, the ductility demand of the target building is in the range of the initial design target for the level-two earthquakes and wind loads of different intensity, **Figure 5.20** reveals the cumulative deformation significantly increases the ductility demand. Although, this amplification, which is due to severe earthquakes, can significantly increase the maximum ductility demand

of BRBs is not affected under the successive analysis of the building under multi-hazard events. Therefore, it is found that the maximum ductility factor cannot be used to measure the fatigue life of the device. In contrast, the cumulative ductility factor can be a suitable measurement to assess the low-cycle fatigue life of the BRB while the maximum ductility can be used in the initial design phase.

5.9 Recommendation

The current chapter investigated the fatigue life of BRBs element and their effect on the overall performance of high-rise steel buildings, by predicting the sequence of multi-hazard scenarios in the project lifetime. Toward this objective, first, a 20-story moment resisting frame is designed to resist the gravitational loads, then, the simplified method presented in the JSSI manual is applied to design the required BRB elements to satisfy the 1% story drift ratio (design target) imposed by the lateral excitation. In the next step, the Passion process-based procedure is used to randomly approximate the probable multi-hazard scenarios during the project lifetime. The proposed concept is applied to generate five random scenarios and the target building performance under multi-hazard scenarios is assessed. applied to evaluate the 20-story high-rise steel building and BRBs performances. The main conclusions of the study are drawn as follows.

- Although for the design earthquake and wind loads, recommend by AIJ (2019), the target building satisfies the 1% story drift ratio, but it is observed the building performance under multi-hazard events is about 1.5~2.0 times larger. It is because the estimated intensities of multi-hazard events from the proposed procedure are slightly larger in comparison to the design earthquake and wind loads. Hence, the multi-hazard scenario must be considered in the design life of structures in regions where multiple hazards dominate.

- Under multi-hazard events, the contribution of BRBs which are located in upper stories is ineffective in comparison to the BRBs located in lower stories. Furthermore, the contribution of BRBs under the high-cycle and low-strain loads are significantly smaller than the low-cycle but high-strain loads.

- The cumulative deformation of BRBs under multi-hazard scenarios, which is studied in terms of Cumulative Damage Index (CDI), Cumulative Ductility Factor (CDF), Plastic Strain Energy (PSE), and Maximum Ductility, reveal the fatigue life of BRB is a multi-criteria issue. It is found, although the BRBs can satisfy one or two of the threshold, under successive application of wind and earthquake excitation the devices fail to endure all the aforementioned criteria. Corresponding to the designated criteria, the fatigue life is variable, as well. Therefore, the current study recommends the multi-criteria to be incorporated in the design of phase of passively controlled building with BRBs.

- Considering the multi-criteria investigated in this study, this study observed the effective service life of BRBs is about 20-years.
- It is determined, the BRB with an average strain of 0.05% is an optimal design criterion for the low-cycle fatigue design of BRBs device. The BRB with a higher value average strain is unable to satisfy the cumulative damage index, while the BRB with a lower value of average strain is less effective to effectively contribute to the overall performance of the buildings.

Chapter 6: Conclusion and remarks

6.1 Research summary

In this research, the seismic performance of conventional and passively controlled buildings was analyzed and studied. In the case of conventional buildings, the simplified procedure presented in Japanse standard for seismic evaluation of existing buildings is modified to become applicable to the conventional building (such as unreinforced and reinforced masonry block). The proposed methodology is further elaborated for the two cases; low-rise reinforced concrete block walls and mid-rise reinforced masonry concrete buildings. The accuracy of the proposed method is affirmed using the time history analysis and capacity spectrum methods.

In the case of a passively controlled building, a simplified methodology is developed to evaluate the seismic performance of an existing building with additional damping devices. The proposed methodology is a capacity spectrum-based method that determines the performance of the building corresponding to the demand response spectrum. Following the literature examination, except for the oil damper, the application of CSM to different types of response control buildings was explored by researchers. On the other hand, the CSM-base seismic assessment of structures is related to equivalent damping of damping devices and buildings. Since the additional damping inserted by the oil damper is proportional to the relieve velocity, a simplified method is presented to estimate the equivalent damping ratio of the system. The accuracy of the proposed methodology is examined for an equivalent SDOF and two; 4- and 10-story steel frames with oil dampers.

In the next phase, the passive-controlled building's performance under the successive application of multi-hazard scenarios is investigated. Considering the regions, which has more than two types of natural disaster are prone to multi-hazard events. For instance, Japan which is well-known for its tsunami, earthquake, and typhoon is an example of a region where the buildings are prone to multi-hazard scenarios. Although the current design manual and regulation recommends incorporating the maximum of an earthquake or wind load, it is indicated that the building performance under combined application of wind-earthquake, or vice-versa is crucial. Thus, in this research, the contribution of preceding events to succeeding events for an RC high-rise building with buckling-restrained brace is examined. It is demonstrated, that the multi-hazard scenarios have the capabilities to modify the building performance while increasing the progressive damage of response control devices.

As observed, the contribution of multi-hazard scenarios to the overall building's performance and progressive damage of response control devices are crucial issues, thus the research further elaborates the multi-hazard events. In this regard, a practical methodology is proposed to anticipate the likely occurrence of multi-hazard scenarios during the building's lifetime. The Poisson Process is used to develop the procedure to anticipated the earthquake and wind loads distribution considering the natural disaster return period and intensities. It is demonstrated, the proposed method is capable to randomly anticipate the multi-hazard scenarios in the service period of the buildings. Later on, using Miner's rule, *S-N* Curve, and rainflow methods a model is introduced to estimate the damping device's progressive damage under the multi-hazard timeline.

6.2 Recommendation

6.2.1 Damage assessment of conventional buildings

The Screening Procedure defined by "Japanese Standard for Seismic Evaluation of Existing Reinforce Concrete Building" is a practical procedure that enables the structural engineers to determine the vulnerable conventional buildings. The method is enough sufficient to assess the seismic demands of low-rise masonry buildings and mid-rise RC frame buildings. Among the three procedures defined by the standard, the first level of screening procedure which uses the load-carrying element cross-sectional dimension gives an excellent solution to assess the seismic performance of existing unreinforced conventional masonry buildings. Since the main objective of this section was to introduce a simplified methodology to promptly assess the seismic performance of a conventional building, it is observed the first level of screening method has the capability. Consequently, besides the reinforced concrete buildings, this study made the procedure applicable in the case of reinforced masonry structures, as well. Hence, the main points of this section are concluded and outlined as bellow:

- The seismic Screening Method is a practical procedure that could be used for the seismic demand assessment of low-rise and mid-rise buildings with a maximum of five stories. This method has the potential to be incorporated for the seismic demand assessment of reinforced concrete buildings and reinforced masonry structures.
- From the result of low-rise buildings with reinforced masonry walls in Afghanistan, it is observed the building with the seismic index of larger than or equal $I_s \geq 0.5$ can withstand the seismic demand given in Afghan Structural Codes. While a similar result is obtained for the RC mid-rise buildings. Therefore, the study recommends the seismic judgment index to be $I_s \geq 0.5$, for the conventional buildings in Afghanistan.

- The seismic index of six reinforced concrete mid-rise buildings is in the range of (0.12 to 0.33) and (0.13 to 0.30) on the ground floor for longitudinal and transverse directions, respectively. It was noted that neither Building No. 06 with a maximum of the seismic index (0.33) in the longitudinal direction and Building No. 05 with a maximum of the seismic index (0.30) in the transverse direction can confirm the required story drift ratio presented by standards. Therefore, the reference buildings are prone to damage under the demand earthquake given in ASC.

6.2.2 Damage assessment of passively controlled buildings

The Capacity spectrum method, which is frequently practiced by research to observe the seismic performance of almost all types of structures, gives an excellent estimation of building's performance under design earthquake loads as well as historical ground motions. It is demonstrated in the literature review, the CSM method can accurately predict the seismic performance of passively controlled buildings. Researchers have been evaluating the performance of buildings that are enhanced by metallic and viscous dampers using the CSM. Thus, in this section, the seismic performance of steel buildings with oil dampers is explored. A simplified procedure is introduced to determine the equivalent damping ratio of bi-linear type oil damper. It is indicated the modified CSM-procedure presented in this study can precisely predict the seismic performance of bi-linear type oil damper. The main finding of the damage assessment of passively controlled buildings is summarized as follow,

- To make the CSM applicable to the oil dampers, a simplified method to estimate the effective damping ratio is introduced. The proposed method estimates the effective damping ratio from the damping ratio of viscous and hysteresis of the system using the square root sum of square (SRSS) technique. The accuracy of the proposed SRSS is compared with the equation recommend by Kasai et al. [15], which is adopted in the JSSI manual [8]. It is revealed, the accuracy of the proposed method is relatively high in comparison to the Kasai et al. [15] equation.
- For the proposed CSM, the essential steps are outlined for an equivalent SDOF system. Accordingly, the estimated maximum displacement of ESDOF is about 6.15 cm for the design response spectrum of level 2 earthquakes, which in comparison to the result of time history analysis of historical earthquakes it indicates 20% differences. It is because the result of THA is obtained from the average result of six historical earthquakes.
- Furthermore, the accuracy of the method is investigated for two steel frames of 4- and 10-story buildings enhanced with oil dampers in each story. For this purpose, six historical earthquakes are selected and scaled to be compatible with the level 2 earthquake recommend by Japanese standards. The comparison of the proposed CSM and THA indicates a 90% correlation between the two methods.

6.2.3 Damage assessment of passively controlled buildings under multi-hazard Scenarios

From the literature review, it is observed the response control devices are an excellent technique to reduce the seismic damage of vertical load-carrying members and non-structural members. Under the maximum earthquake and wind loads, the high-rise building performance is studied widely by researchers, and the excellent performance of response control devices is reported. Since the high-rise is expected to have a longer service period, the possibility of damping devices to experience a huge number of cycling loading is high. On the other hand, considering the region which is prone to multi-hazard scenarios, dampers are prone to not only maximum earthquake or wind load, which is recommended in design provisions, but also they are susceptible to the high-cycle of low-strain wind and low-cycle of high-strain earthquake excitations. Therefore, in this section, first, a practical procedure is introduced to anticipates the likely occurrence of multi-hazard events. Then, the fatigue and progressive damage model of the response control device is generated to investigate the influence of multi-hazard events on each other. The main scientific contribution of this section is outlined below.

- The proposed methodology based on the Poisson Process is a practical tool to randomly anticipates the occurrence of multi-hazard scenarios in the building lifetime.
- According to the anticipated multi-hazard timelines, it is observed the possibility of earthquake and wind loads to succeed each other is extremely high.
- Therefore, the performance of high-rise RC buildings with BRB under successive application of wind-earthquake and/or earthquake-wind multi-hazard scenarios indicates the overall building's performance and the cumulative damage of response control devices are increase.
- The proposed fatigue model to evaluate the progressive damage of BRBs under lifetime multi-hazard scenarios is a practical method that enables the engineers to precisely track the lifetime damage of damping devices as well as building performance.
- The seismic performance of the high-rise steel model under maximum design loads and successive application of multi-hazard scenarios reveal that the building performance under multi-hazard cases is 1.5-2.0 larger.
- Although the model is capable to withstand the design loads, it is indicated under multi-hazard cases the building cannot endure the designated target considered in the initial design phase.
- Under the multi-hazard scenarios, the progressive damage of BRBs which are in upper stories is considerably smaller than to the BRBs located in lower stories. This is indicating that the BRBs in lower stories are severely prone to low-cycle fatigue damage in the building service period.

- The progressive damage of BRBs under multi-hazard scenarios, which is studied in terms of Cumulative Damage Index (CDI), Cumulative Ductility Factor (CDF), Plastic Strain Energy (PSE), and Maximum Ductility, reveal that the fatigue life of BRB is a multi-criteria issue. It is found, although the BRBs can satisfy one or two of the thresholds, under successive application of wind and earthquake excitation, the devices fail to endure all the aforementioned criteria. Corresponding to the designated criteria, the fatigue life is variable, as well. Therefore, the current study recommends the multi-criteria be incorporated in the design phase of the high-rise building with BRBs.
- Considering the multi-criteria investigated in this study, this study observed the effective service life of BRBs is much smaller than the design service life.
- Under the successive analysis of multi-hazard scenarios, the ductility demand of BRBs is three times larger than the Level 2 earthquakes.

References

[1] Kobori, T.; New proposal of research and development for seismic response-controlled structure Memorial Proc. for the Centenary of the Birth of Tachu Naito (Waseda University), **1986**.

[2] Roy, T., Saito, T., Matsagar, V.; Multihazard framework for investigating high-rise base-isolated buildings under earthquakes and long-duration winds. *Earthquake Engineering and Structure Dyn*amic, **2020**. Article in press.

[3] Roy, T. and Matsagar, V.; Effectiveness of passive response control devices in buildings under earthquake and wind during design life, *Structure and Infrastructure Engineering*, 15(2), 252-268, **2019**.

[4] Takeuchi, T. and Wada, A.; Review of buckling-restrained brace design and application to tall buildings. *Key Engineering Materials*, 763. 50-56, **2018**.

[5] Watanabe, A.; Design and application of buckling-restrained braces. *International Journal of High-Rise Building*, 7(3), 215-221, **2018**.

[6] RSMC Tokyo-Typhoon Center: Best Track Data (1951–2020), Japan Meteorological Agency (JMA), available at, https://www.jma.go.jp/jma/jma-eng/jma-center/rsmc-hp-pub-eg/besttrack.html (last access: 3 Feb 2021).

[7] Duthinh, D., and Simiu, E.; Safety of structures in strong winds and earthquakes: Multihazard considerations. *Journal of Structure Engineering*, 136(3). 330-333, **2010**.

[8] JSSI, Report of investigation committee on response control buildings. The Japan Society of Seismic Isolation. **2012**.

[9] The standard for seismic evaluation of existing reinforced Concrete Buildings, English Version 1st, The Japan Building Disaster Prevention Associating, Translated by Building Research Institute, **2001**.

[10] Afghan Structural Code (ASC), ABC/079, Afghan Building Code, *ANSA*, **2021**.

[11] Shing P. B., Klameru E., Spaech H., and Noland J. L.; Seismic Performance of Reinforced Masonry Shear wall, *9th WCEE*, Tokyou-Kyouto, Japan, VI103-108, **1988**.

[12] Akira, M.; Shear strength of reinforced masonry walls, *9th WCEE*, Tokyo-Kyoto, Japan, VI121-126, **1988**.

[13] Saito, T.; STructural Earthquake Response Analysis 3D, version 10.5 (STERA_3D v10.5). **2020**. http://www.rc.ace.tut.ac.jp/saito/software-e.html , (accessed on Saturday, 27 February 2021).

[14] Building Code Requirement for masonry structure, *TMS 402-13/ACI 530.1-13/ASCE 6-13*.

[15] AIJ, Recommendations for loads on buildings. *Architectural Institute of Japan*. **2019**.

[16] BSL, The building standard law of Japan, *The building center of Japan*, Tokyo, **2004**.

[17] Kasai, K., Baba, Y., Fu, Y. and Watanabe, A.; Passive control system for seismic damage mitigation, *Journal of Structural Engineering*, 124, 501-5121, **1998**.

[18] Kasai, K., and Kibayashi, M.; JSSI manual for building passive control technology part-1 manual contents and design/analysis methods, *13th WCEE*, Vancouver Canada, Paper 2989, Aug. 1-6 **2004**.

[19] Kibayashi, M., Kasai, K., Tsuji, Y., Kikuchi, M., Kimura, Y., Kobayashi, T., Nakamura, H. and Matsuba, Y.; JSSI manual for building passive control technology part-2 criteria for implementation of energy dissipation devices, *13th WCEE*, Vancouver Canada, Paper 2990, Aug. 1-6, **2004**.

[20] Tsuyuki, Y., Gofuku, Y., Iiyama, F., and Kotake, Y.; JSSI manual for building passive control technology part-3 performance and quality control of oil damper, *13th WCEE*, Vancouver Canada, Paper 2468, Aug. 1-6, **2004**.

[21] Tanaka, Y., Kawaguchi, S., Sukagawa, M., Masaki, N., Sera, S., Washiyama, Y., and Mitsusaka, Y.; JSSI manual for building passive control technology part-4 performance and quality control of viscous dampers, *13th WCEE*, Vancouver Canada, Paper 1387, Aug. 1-6, **2004**.

[22] Ishikawa, K., Okuma, K., Shimada, A., Nakamura, H.; and Masaki, N.; JSSI manual for building passive control technology part-5 performance and quality control of viscoelastic dampers, *13th WCEE*, Vancouver Canada, Paper 1449, Aug. 1-6, **2004**.

[23] Nakata, Y., Hirota, M., Shimizu, T., and Iida, T.; JSSI manual for building passive control technology part-6 design of steel damper, *13th WCEE*, Vancouver Canada, Paper 3451, Aug. 1-6, **2004**.

[24] Tran, B. T., Kasai, K., Sato T., Oohara, K., and Shao, L.; JSSI manual for building passive control technology part-7 stepping column system, *13th WCEE*, Vancouver Canada, Paper 5059, Aug. 1-6, **2004**.

[25] Kasai, K. and Ito, H.; JSSI manual for building passive control technology part-8 peak response evaluation and design for elasto-plastically damped system, *13th WCEE*, Vancouver Canada, Paper 5056, Aug. 1-6, **2004**.

[26] Kasai, K., Ooki, Y., Tokoro, K., Amemiya, K., and Kimura, K.; JSSI manual for building passive control technology part-9 time-history analysis model for viscoelastic dampers, *13th WCEE*, Vancouver Canada, Paper 1507, Aug. 1-6, **2004**.

[27] Kasai, K., Takahashi, O., and Sekiguchi, Y.; JSSI manual for building passive control technology part-10 time-history analysis model for nonlinear oil dampers, *13th WCEE*, Vancouver Canada, Paper 1283, Aug. 1-6, **2004**.

[28] Kasai, K., Oohara, K., and Sekiguchi, Y.; JSSI manual for building passive control technology part-11 time-history analysis model for viscous dampers, *13th WCEE*, Vancouver Canada, Paper 1427, Aug. 1-6, **2004**.

[29] Ooki, Y., Kasai, K., Takahashi, O., and Sekiguchi, Y.; JSSI manual for building passive control technology part-12 velocity-dependent damper performance under extremely small excitation, *13th WCEE*, Vancouver Canada, Paper 1285, Aug. 1-6, **2004**.

[30] Freeman, S.A.; Review of the development of the capacity spectrum method. *ISET Journal of Earthquake Technology*, 4, 1–13, **2004**.

[31] ATC, Seismic Evaluation and Retrofit of Concrete Buildings; Report ATC-40; ATC: *Redwood City, CA, USA*, **1996**.

[32] Kim, H., Min, K.-W., Chung, L., Park, M., Lee, S.-H.; Evaluation of capacity spectrum method for estimating the peak inelastic responses. *Journal of Earthquake Engineering*, 9, 695–718, **2005**.

[33] Choi, H.H. Kim, J.; Evaluation of proper supplemental damping for a multi-story steel frame using capacity spectrum method. *Advanced Earthquake Engineering*, 9, 25–34, **2001**.

[34] Kim, J., Choi, H., Min, K.-W.; Performance-based design of added viscous dampers using capacity spectrum method. *Journal of Earthquake Engineering*, 7, 1–24, **2003**.

[35] Li, B., Liang, X.-W.; Design of supplemental viscous dampers in inelastic SDOF system based on improved capacity spectrum method. *Structure Engineering Mechanic*, 27, 541–554, **2007**.

[36] Chen, B.-J. Chung, L.L. Tsai, C.S. Chiang, T.-C.; Applications of capacity spectrum method for buildings with metallic yielding dampers. In Proceedings of the ASME 2005 Pressure Vessels and Piping Conference, Denver, CO, USA, Volume 8, pp. 299–306, 17–21 July **2005**.

[37] Han, J., Yan, R., Li, H.; Performance-based seismic design for structures with viscoelastic dampers. *Journal of Earthquake Engineering and Engineering Vibration*, 28, 175–181, **2008**.

[38] Benavent-Climent, A., Escolano-Margarit, D.; Shaking table tests of structures with hysteretic dampers: Experimental results versus prediction using non-linear static methods. *Bulletin of Earthquake Engineering*, 10, 1857–1883, **2012**.

[39] Kim, J., Kim, M., Eldin, M.N.; Optimal distribution of steel plate slit dampers for seismic retrofit of structures. *Steel and Composite Structures*, 25, 473–484, **2017**.

[40] Bantilasa, K.E., Kavvadias, I.E., Vasiliadisb, L.K.; Capacity spectrum method based on inelastic spectra for high viscous damped buildings. *Earthquake and Structure*, 13, 337–351, **2017**.

[41] João, M.C., and Estêvão.; An Integrated Computational Approach for Seismic Risk assessment of Individual Buildings. *Applied Science*, 9, 5088, **2019.**

[42] Ferraioli, M., and Lavino, A.; A displacement-based design method for seismic retrofit of RC buildings using dissipative braces. *Mathematical Problems in Engineering*, 1–28, **2018**.

[43] Naeem, A., and Kim, J.; Seismic retrofit of structures using rotational friction dampers with restoring force. *Advance in Structural Engineering*, 23, 3525–3540, **2020**.

[44] Ramirez, O.M., Constantinou, M.C., Gomez, J.D., Whittaker, A.S., and Chrysostomou, C.Z.; Evaluation of Simplified Methods of Analysis of Yielding Structures with Damping Systems. *Earthquake Spectra*, 18, 501–530, **2002**.

[45] Adachi, F., Yoshitomi, S., Tsuji, M., and Takewaki, I.; Nonlinear optimal oil damper design in seismically controlled multi-story building frame. *Soil Dynamics and Earthquake Engineering*, 4, 1–13, **2013**.

[46] Adachi, F., Fujita, K., Tsuji, M., and Takewaki, I.; Importance of interstory velocity on optimal along-height allocation of viscous oil dampers in super high-rise buildings. *Engineering Structure*, 56, 489–500, **2013**.

[47] Ji, X., Hikino, T., Kasai, K., and Nakashima, M.; Damping identification of a full-scale passively controlled five-story steel building structure. *Earthquake Engineering and Structural Dyn*amics, 42, 277–295, **2013**.

[48] Xie, L., Cao, M., Funaki, N., Tang, H., and Xue, S.; Performance study of an eight-story steel building equipped with oil dampers damaged during the 2011 great east japan earthquake part 1: Structural identification and damage reasoning. *Journal of Asian Architecture and Building Engineering*, 14, 181–188, **2015**.

[49] Takabatake, H., and Kitada, Y.; Approximate method of estimating seismic performance of high-rise buildings with oil-dampers. *Structural Design of Tall and Spec*ial *Building*, 27, 1–28, **2018**.

[50] Chopra, A.K.; Dynamics of Structures: Theory and Applications to Earthquake Engineering, Prentice Hall: Englewood Cliffs, NJ, USA, **2017**.

[51] Kasai, K., Fu, Y., and Watanabe, A.; Passive control systems for seismic damage mitigation. *Journal of Structural Engineering*, 124, 501–512, **1998**.

[52] Kasai, K., and Kawanabi, Y.; Equivalent linearization to predict dynamic properties and seismic peak responses of a structural system with high viscous damping and hysteretic damping. *Journal of Structure and Construction Engineering*, 591, 43–51, **2005**. (In Japanese)

[53] Kuramoto, H., Teshigawara, M., Lkuzono, T., Koshika, N., Takayama, M., and Hori, T.; Predicting the earthquake response of buildings using equivalent single degree of freedom system. In Proceedings of the *12th World Conference on Earthquake Engineering*, Auckland, New Zealand, 30 January–4 February **2000**, Paper No.1039.

[54] Fu, Y., and Kasai, K.; Comparative study on frames using viscoelastic and viscous dampers. *Journal of Structural Engineering*, 124, 513–522, **1988**.

[55] Sekiya, E., Mori, H., Ohbuchi, T., Yoshie, K., Hara, H., Arima, F., Takeuchi, Y., Saito, Y., Ishii, M., and Kasai, K.; Details of 4-, 10-, and 20-story theme structure used for passive control design examples. In The JSSI Response Control Committee Symposium on Passive Vibration Control, JSSI: Tokyo, Japan, **2004**. (In Japanese)

[56] Vidal, F., Navarro, M., Aranda, C., and Enomoto, T.; Changes in dynamic characteristics of Lorca RC buildings from pre- and post-earthquake ambient vibration data. *Bulletin of Earthquake Engineering*, 12, 2095–2110, **2014**.

[57] Iwata, M., and Murai, M.; Buckling-restrained brace using steel mortar planks, performance evaluation as a hysteretic damper. *Earthquake Engineering and Structure Dynamic*, 35 (14), 1807-1826, **2006**.

[58] Fujimoto, M., Wada, A., Saeki, E., Watanabe, A., and Hitomi, Y.; A study on the unbounded brace encased in buck-ling-restraining concrete and steel tube. *Journal of Structural Engineering*, 34(B), 249-258, **1988**. (in Japanese)

[59] Takeuchi, T.; Buckling-Restrained brace: Historey, design, and application. *Key Engineering Materials*, 763, 50-56, **2018**.

[60] Black, C. J., Makris, N., and Aiken, I. D.; Component testing, seismic evaluation and characterization of buckling-restrained braces. *Journal of Structural Engineering*, 130(6). 880-894, **2004**.

[61] Tremblay, R., Bolduc, P., and DeVall, R.; Seismic testing and performance of buckling-restrained bracing systems. *Canadian Journal of Civil Engineering*, 33(2). 183-198, **2006**.

[62] Ju, Y. K., Kim, M. H., Kim, J. and Kim S. D.; Component test of buckling-restrained braces with unconstrained length. *Engineering Structure*, 31(2). 507-516, **2009**.

[63] Fahnestock, L. A., Ricles, J. M. and Sause, R.; Experimental evaluation of large-scale buckling-restrained braced frame. *Journal of Structural Engineering*, 133(9). 1205-1214, **2007**.

[64] Tsai, C. S., Chen, W. S., Lin, Y. C., Yang, C. T. and Tsou, C. P.; Seismic response of a full-scale steel structure using multi-curved buckling restrained brace. *American Society of Mechanical Engineers*, Pressure Vessels, and Piping Division, PVP8, 55-61, **2008**.

[65] Kaneki, Y., Hikone, S., Yamashita, T., and Iwata, M.; Seismic Strengthening by buckling restrained braces arranged diagonally, *Journal of structural and construction engineering*, 73(634). 2215-2222, **2008**. (in Japanese)

[66] Shima, Y., Ding, Y. and Zhao, J.; Proposal for the structural design method of a sustainable building structure system. *Journal of structural and construction engineering*, 74(640). 1179-1185, **2009**. (in Japanese)

[67] Alemayehu, R.W., Kim, Y., Bae, J., and Ju, Y.K.; Cyclic Load Test and Finite Element Analysis of NOVEL Buckling-Restrained Brace. *Materials*, 13(22). 5103-5118, **2020**.

[68] Guerrero, H., Ji, T., Teran-Gilmore, A., and Escobar, J. A.; A method for preliminary seismic design and assessment of low-rise structures protected with buckling-restrained braces. *Engineering Structure*, 123. 141-154, **2016**.

[69] Çelebi, M., Kashima, T., Ghahari, F., Koyama, S., Taciroğlu, E., and Okawa, I.; Before and after retrofit behavior and performance of a 55-storey tall building inferred from distant earthquake and ambient vibration data. *Earthquake Spectra*, 34(4). 1599-1626, **2017**.

[70] Di Sarno, L., and Manfredi, G.; Seismic retrofitting with buckling restrained braces: Application to an existing non-ductile RC framed building. *Soil Dynamics and Earthquake Engineering*, 30(11). 1279-1297, **2010**.

[71] Almeida, A., Ferreira, R., Proença, J.M., and Gago, A.S.; Seismic retrofit of RC building structures with Buckling Restrained Braces. *Engineering Structure*, 130. 14-22, **2017**.

[72] Saingam, P., Sutcu, F., Terazawa, Y., Fujishita, K., Lin, P., Celik, O.C., and Takeuchi, T.; Composite behavior in RC buildings retrofitted using buckling-restrained braces with elastic steel frames. *Engineering Structure*, 219. 110896, **2020**.

[73] Castaldo, P., Tubaldi, E., Selvi, F., and Gioiella, L.; Seismic performance of an existing RC structure retrofitted with buckling restrained braces. *Journal of Building Engineering*, 33. 101688, **2021**.

[74] Usami, T., Wang, C., and Funayama, J.; Low-cycle fatigue tests of a type of Buckling Restrained Braces. *Procedia Engineering*, 14. 956-964, **2011**.

[75] Wang, C.-L., Usami, T., and Funayama, J.; Improving low-cycle fatigue performance of high-performance buckling-restrained braces by toe-finished method. *Journal of Earthquake Engineering*, 16(8). 1248-1268, **2012**.

[76] Chen, K., Li, G., Liu, Y., Guo, X., and Sun, F.; Low-Cycle Fatigue Performance of Buckling Restrained Braces and Assessment of Cumulative Damage under Severe Earthquakes. *Progress in Steel Building Structures*, 19(1). 43-50 and 84, **2017**.

[77] Xu, Z.-D., Dai, J., and Jiang, Q.-W.; Study on fatigue life and mechanical properties of BRBs with viscoelastic filler. *Steel and Composite Structures*. 26(2). 139-150, **2018**.

[78] Tong, C., Wu, J., Hua, K., and Xie, L.; Low-Cycle Fatigue Life Estimation Curve for Buckling-Restrained Braces Based on Cumulative Plastic Deformation. *Journal of Earthquake Engineering*, **2020**. article in press.

[79] Repetto, M. P., and Solari, G.; Wind-induced fatigued collapse of real slender structures. *Engineering Structure*, 32(12). 3888-3898, **2010.**

[80] Jia, J.; Wind and structural modeling for an accurate fatigue life assessment of tubular structures. *Engineering Structure*, 32(2). 447-491, **2011**.

[81] Fang, Z., Li, A., Li, W., and Shen, S.; Wind-induced fatigue analysis of high-rise steel structures using equivalent structural stress method. *Applied Sciences*. 7(1). 71, **2007**.

[82] Hoveidae, N.; Ultra-low cycle fatigue fracture life of a type of buckling restrained brace. *Journal of Rehabilitation in Civil Engineering*. 6(2). 29-42. **2018**.

[83] Saito, T.; STructural Earthquake Response Analysis WAVE version 1.0 (STERA_WAVE v1.0). **2019**. http://www.rc.ace.tut.ac.jp/saito/software-e.html (accessed on Saturday, 27 February 2021).

[84] Jennings, P.C., Housner, G.W., and Tsai, N.C.; Simulated earthquake motions for design purpose. *Proceedings of 4th World Conference on Earthquake Engineering*. 145-160. **1969**.

[85] Deodatis, G., and Shinozuka, M.; Weighted integral method. II: response variability and reliability. *Journal of Engineering Mechanics*,117(8), 1865-1877, **1991.**

[86] Deodatis, G.; Simulation of ergodic multivariate stochastic processes. *Journal of Engineering Mechanics*, 122(8), 778-787, **1996**.

[87] Marsh, G., Wignall, C., Thies, P.R., Barltrop, N., Incecik, A., Venugopal, V., and Johanning, L.; Review and application of Rainflow residue processing techniques for accurate fatigue damage estimation. *International Journal of Fatigue*. 82. 757–765. **2016**.

[89] Hasegawa, H., Takeuchi, T., Iwata, M., Yamada, S., and Akiyama, H.; Dynamic performances of unbonded braces. *AIJ Technical Report*, 9. 103–106, **1999**. (in Japanese).

[90] Nakamura, H., Takeuchi. T., Maeda, Y., Nakata, Y., Sasaki, T., Iwata, M., and Wada, A.; Fatigue properties of practical-scale un-bonded braces. *Nippon steel technical report*. 82. 51-57. **2000**.

[91] Yamaguchi, M., Yamada, S., Takeuchi, T., and Wada, A.; Seismic performance of buckling resistant brace within a steel frame in the case of ultimate earthquake. *Journal of Condition Steel*. 12. 207–210, **2004**. (in Japanese).

[92] Takeuchi, T., Uchiyama, T., Suzuki, K., Ookouchi, Y., Ogawa, T., and Kato, S.; Seismic retrofit of truss tower structures using buckling restrained braces. *Journal of Structure and Construction Engineering*, 589. 129–136, **2005**. (in Japanese).

[93] Takeuchi, T., Ida, M., Yamada, S., and Suzuki, K.; Estimation of cumulative deformation capacity of buckling restrained braces. *Journal of Structure Engineering*, 134(5). 822-831, **2008**.

[94] Chung, Y.W., and Lee, W.J.; Cyclic plastic strain energy as a damage criterion and environmental effect in Nb-bearing high strength, low alloy steel. *Material Science Engineering*, 186 (1-2). 121-128, **1994**.

[95] Takeuchi, T., Ohyama, T., and Ishihara, T.; Cumulative cyclic deformation capacity of high-strength steel frames with energy dissipation braces – Seismic performance of high-strength steel frames with energy braces part 1. *Journal of Structure and Construction Engineering*, 75(655). 1671-1679, **2010.**

[96] Takeuchi, T., Hajjar, J. F., Matsui, R., Nishimoto, K., and Aiken, I. D.; Effect of buckling core plate restraint in buckling restrained braces. *Engineering Structure*, 44. 302-311, **2012**.

[97] FEMA-450; NEHRP Recommended Provisions for Seismic Regulations for New Buildings and Other Structures, *Federal Emergency Management Agency*, Washington, DC, USA, **2003**.

[98] R. Sabelli; Research on Improving the Design and Analysis of Earthquake-Resistant Steel Braced Frames, EERI, Oakland, CA, USA, **2001**.

[99] Usami, T., Kasai, A., and Kato, M.; Behavior of buckling restrained brace members," in *Proceedings of 4th International Conference on STESSA 2003-Behavior of Steel Structures in Seismic Areas*, 211–216, Naples, Italy, June **2003**.

[100] ANSI/AISC 360-10; Seismic Provisions of Structural Steel Buildings, *American Institute of Steel Construction*, Chicago, IL, USA, **2010**.

Appendix A: Preliminary design of passively controlled buildings

A1.1 Overview passively controlled building

Natural disaster, which is well-known by human since long time ago, is still a challenging issue which is impossible to predict the next occurrence. Therefore, conventional buildings were designed in such a way to provide the minimum level of safety to protect human lives. The required amount of safety is mainly obtained by the means of the load-carry element's strength or ductility. Therefore, a certain amount of damage is inevitable which in response the conventional building cannot sufficiently overcome the latest demands for the building performance and safety. To overcome the problem, the seismic response control building, which was originally initiated by Kobori in 1986 [A1], as the main load-carry element is employed extensively. Since that time, wide-range response control system introduced and examined by research to overcome the limitation exist in conventional buildings. Overall, the response control system is classified as active, semi-active, and passive technologies. Among the different types of response control systems, passive technology has become popular and adopted widely.

Table A.1: Damping devise category and technical parameters.

Technical Parameter	**Viscous Damper**	**Oil Damper**	**Viscoelastic Damper**	**Steel Damper**
Material	Silicon Fluid	Oil	Acryl, Butadiene	Steel, Lead, Friction Pad
Possess configuration	The plane, Box, Tube Shapes	Tube shape	Tube or Plane Shapes	Tube or Plane Shapes
Hysteresis Loop	Combined Ellipse and Rectangle hysteresis	Ellipse Hysteresis	Inclined Ellipse	Bilinear
Damper Force	Shear resistance, Flow resistance	Orifice Flow resistance	Shear Resistance	Yielding Resistance, Slipping resistance
	$F = C\dot{u}^{\alpha}$	$F = C\dot{u}$	$F = K(\omega) \cdot u + C(\omega) \cdot \dot{u}$	$F = K \cdot f(u)$

In Japan, the passive control systems become more popular after the Kobe earthquake in 1995 [A2]. In the case of passively controlling the buildings, the structural damping and stiffness are augmented by install damping devices. A wide range of damping devices of the different mechanisms are manufactured,

currently. Therefore, the Japanese manual for the Design of passively controlled buildings (JSSI) [A3] classified the dampers into four major categories, as listed and summarized in **Table A.1**.

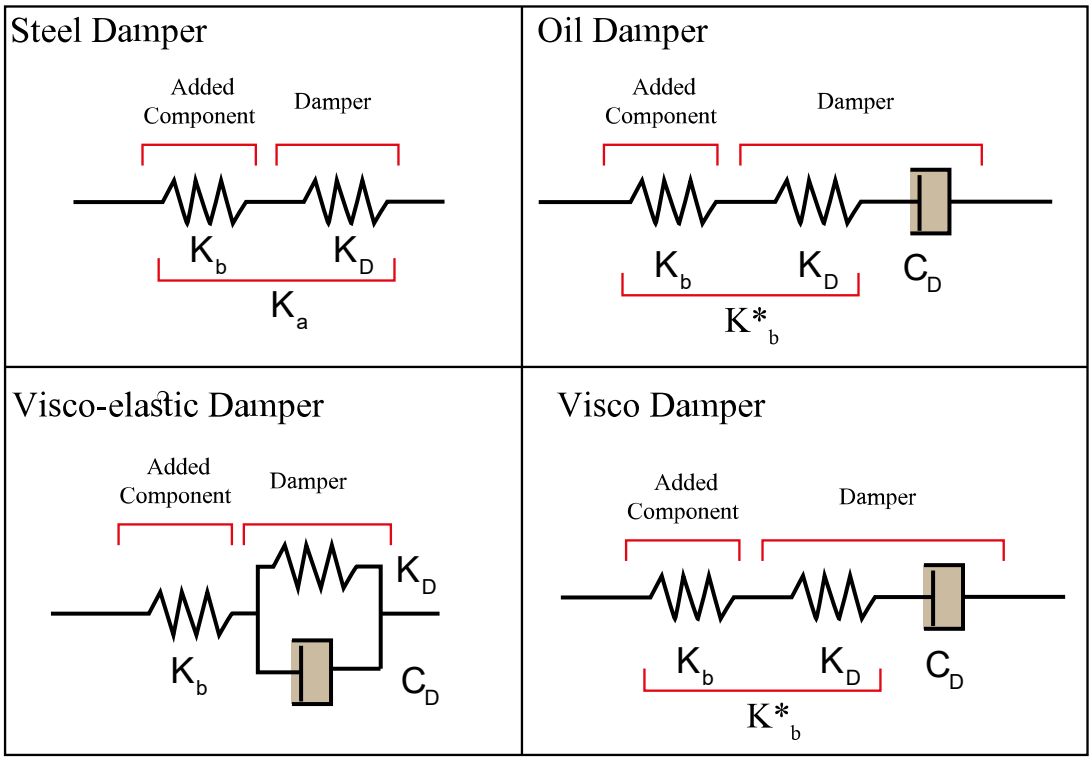

Figure A.1: Damping devices and added component modeling according to JSSI.

As mentioned earlier, the dampers are installed along the height of the structure to insert additional stiffness and damping. The damper can be connected directly, indirectly, or with a special system to the main structure. In the case of direct connection, the two ends of the damper are directly connected to the upper and lower frame through relatively stiff support. In the indirect connection, the damper ends are connecting to the main frame indirectly by the support of an additional stud, bracket, or connector. A special connection system is the installation mechanism of a damper into a disconnected zone of column or beam, which makes the damping devices part of the column or beam. As a result of the damper connection to the main frame, the damper technical parameters (such as energy dissipation capacity, stiffness, or damping ratio) can be affected due to the additional stiffness which is inserted from the connector elements. Therefore, the JSSI manual defines the modeling schemes of dampers and their connection system (hereafter it is called “added component”). **Figure A.1** represents the dampers and their added components modeling defined in the JSSI manual.

A brief description of each classification are given as below;

Steel Damper: The damper energy dissipator system is defined by an elastic-plastic spring with elastic stiffness of K_D, which is connected in series with the elastic stiffness of added component, K_b.

Viscous Damper: Similarly, the viscous damper energy dissipator system is defined by a nonlinear dashpot with the viscous coefficient of C_D, which is connected in series with the elastic stiffness of damper K_D and added component, K_b. Where the equivalent stiffness of the system is denoted by K_b*.

Visco-elastic Damper: the damper energy dissipator is express by a dashpot and spring connected in parallel. The system damping coefficient C_D and elastic stiffness K_D are frequency dependent. Where the elastic stiffness of added component K_b are connected in series, **Figure A.1**.

Oil Damper: The damper energy dissipator system is defined by a bilinear dashpot with the viscous coefficient of C_D, which is connected in series with the elastic stiffness of damper K_D and added component, K_b. Where the equivalent stiffness of the system is denoted by K_b*.

As illustrated in **Figure A.1**, due to added components including the damper brace, the force-displacement relationship of the damper will change differently for each category of the damper. **Figure A.2** compares the hysteresis curves of the damper when the added component and frame are combined. In the figure, the peak deformation, peak force, and zero deformation are denoted by black, red, and blue dots. Where the equivalent stiffness and loss stiffness can be determined by dividing the maximum force by maximum deformation and force at zero-deformation by maximum deformation, respectively. In the figure, the equivalent stiffness for damper, added component, and system is denoted by K_D', K_b', and K'which are defined in **Table A.2**. Similarly, $K_D^{"}$, $K_b^{"}$, and $K^{"}$represents the loss stiffness of damper, added component, and system, which are given by equations presented in **Table A.3**.

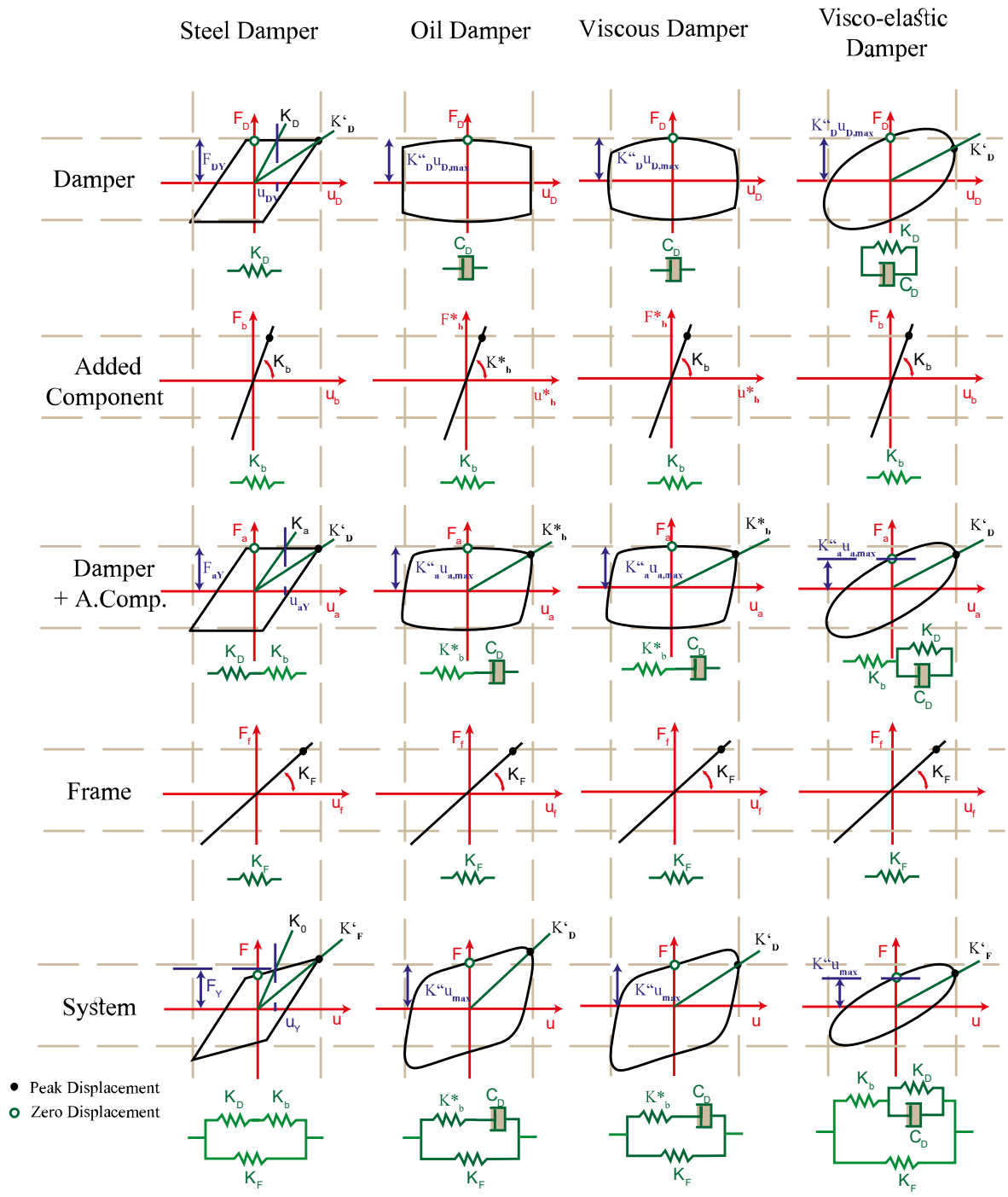

Figure A.2: Damping devices and added component configuration scheme.

Table A.2: Equivalent stiffness definition for the four types of the passive control device.

Damper type	Damper	Added Component	System
Steel damper	K_D $K_D' = \frac{F_{Dy}}{u_{d,max}}$	$K_a' = \frac{K_a}{\mu_a}$ $K_a = \frac{1}{\frac{1}{K_b} + \frac{1}{K_D}}$	$K = K_a + K_f$ $K' = K_a' + K_f$
Oil damper	$K_D' = 0$	$K_a'(\mu_D \le 1) = \frac{\lambda}{1+\lambda^2} C_D \omega$ $K_a'(\mu_D \ge 1) = \frac{\zeta\lambda}{1+(\zeta\lambda)^2} \zeta C_D \omega$	$K' = K_a' + K_f$
Viscous damper	$K_D' = 0$	$K_a' = K_b^* \frac{\left(\frac{K_D^{"}}{K_D^*}\right)^{1+\alpha}}{1+\left(\frac{K_D^{"}}{K_D^*}\right)^{1+\alpha}}$	$K' = K_a' + K_f$
Visco-elastic damper	K_D'	$K_a' = \frac{\{(1+\eta_d^2)K_D' + K_b\}K_D' K_b}{(K_D' + K_b)^2 + (\eta_d K_D')^2}$	$K' = K_a' + K_f$

Table A.3: Loss stiffness definition for the four types of the passive control device.

Damper type	Damper	Added Component	System
Steel damper	$K_D^{"} = K_D'$	$K_a^{"} = K_a'$	$K^{"} = K_a'$
Oil damper	$K_D^{"}(\mu_D \le 1) = C_D \omega$ $K_D^{"}(\mu_D \ge 1) = \{p + \frac{1-p}{\mu_D}\} C_D \omega$	$K_a^{"}(\mu_D \le 1) = \frac{1}{1+\lambda^2} C_D \omega$ $K_a^{"}(\mu_D \ge 1) = \min(1), (2)$ $(1) = \frac{\zeta}{1+(\lambda\zeta)^2} C_D \omega$ $(2) = \left(p + \frac{1-p}{\mu_D\sqrt{1+\lambda^2}}\right) C_D \omega$	$K^{"} = K_a^{"}$
Viscous damper	$K_D^{"} = \frac{C_D \omega^{\alpha}}{u_{d,max}^{1-\alpha}}$	$K_a^{"} = \frac{\min(K_D^{"} \; or \; (K_b^*)^{1-\alpha}(K_D^*)^{\alpha})}{1+\left(\frac{K_D^{"}}{K_D^*}\right)^{1+\alpha}}$	$K^{"} = K_a^{"}$
Visco-elastic damper	$K_D^{"} = \eta_d K_D'$	$K_a^{"} = \frac{\eta_d K_D' K_b^2}{(K_D' + K_b)^2 + (\eta_d K_D')^2}$	$K^{"} = K_a^{"}$

Table A.4: Maximum and yield deformation and maximum force definition for the four types of the passive control device.

Damper type	Damper	Added Component	System
Steel damper	$u_{Dy} = \frac{F_{Dy}}{K_D}$ $F_{D,max} = F_{Dy}$ $u_{D,max}$	$u_{ay} = \frac{F_{Dy}}{K_a}$ $F_{a,max} = F_{D,max}$ $u_{a,max} = \frac{F_{Dy}}{K_a} + u_{D,max}$	$u_y = u_{ay}$ $F_{max} = K' u_{max}$ $u_{max} = u_{a,max}$
Oil damper	$u_{Dy} = \frac{F_{Dy}}{C_D \omega}$ $F_{D,max} = K_D^{"} u_{D,max}$ $u_{D,max}$	$u_{ay} = u_{Dy}\sqrt{1+\lambda^2}$ $F_{a,max} = F_{D,max}$ $u_{a,max}(\mu_D \le 1) = u_{D,max}\sqrt{1+\lambda^2}$ $u_{a,max}(\mu_D \ge 1) = u_{D,max}\sqrt{1+\lambda^2}\left(\frac{\mu_a}{\mu_D}\right)$	$u_y = u_{ay}$ $F_{max} = \sqrt{K'^2 + K"^2}\, u_{max}$ $u_{max} = u_{a,max}$
Viscous damper	$F_{D,max} = K_D^{"} u_{D,max}$ $u_{D,max}$	$F_{a,max} = F_{D,max}$ $u_{a,max} = u_{D,max}\left[\left(\frac{K_D^{"}}{K_D^{*}}\right)^{1+\alpha}\right]^{1-0.5\alpha}$	$F_{max} = \sqrt{K'^2 + \alpha K"^2}\, u_{max}$ $u_{max} = u_{a,max}$
Visco-elastic damper	$F_{D,max} = \sqrt{1+\eta_d{}^2} K_D' u_{D,max}$ $u_{D,max}$	$F_{a,max} = F_{D,max}$ $u_{a,max} = u_{D,max}\sqrt{\frac{K_D^{"}}{K_a^{"}}}$	$F_{max} = \sqrt{1+\eta^2}\, K'\, u_{max}$ $u_{max} = u_{a,max}$

A1.2 Design of passively controlled buildings

The manual for the design of buildings with passive control devices (JSSI, 2014) [A3] adopts the procedure developed by Kasai et al. (1998) [A4] to simplify the design procedure of building with added damping devices. The method idealizes the multi-story building as an equivalent single degree of freedom (SDOF) system and estimates the amount of additional damping and stiffness to be supplemented for achieving the target performance. An idealized SDOF with hysteresis damper, as shown in 0, consists of an effective mass, M_{ef}, effective height, H_{ef}, and two springs representing the bare model elastic stiffness, K_f, and damper elastic stiffness, K_d. The performance of the idealized SDOF with the damper can mathematically be presented by its elastic stiffness, K_0, natural period, T_0, ductility factor, μ, equivalent natural period, T_{eq}, equivalent secant stiffness, K_{eq}, and equivalent damping ratio, h_{eq}, which are obtained as follows.

$$K_0 = K_f + K_d \tag{A.1}$$

$$T_0 = T_f \sqrt{\frac{K_f}{K_0}} \tag{A.2}$$

$$T_{eq} = T_f \sqrt{\frac{K_f}{K_{eq}}} = T_f \sqrt{\frac{p\mu}{1 + p(\mu - 1)}} \tag{A.3}$$

$$K_{eq} = K_f + \frac{K_d}{\mu} = \frac{1 + p(\mu - 1)}{\mu} K_0 \tag{A.4}$$

$$p = \frac{K_f}{K_f + K_d} \tag{A.5}$$

$$h_{eq} = h_0 + \frac{2}{\mu\pi p} \ln\left[\frac{1 + p(\mu - 1)}{\mu^p}\right] \tag{A.6}$$

The JSSI manual [A3] introduces the damped effect factor, D_h, which is an average reduction of the spectral response of observed earthquakes, as shown in **Eq. (A.7)**.

$$D_h = \sqrt{\frac{1 + 25h_0}{1 + 25h_{eq}}} \tag{A.7}$$

The displacement and the shear force reduction factor, R_d and R_a, to be provided by the damping device, can be evaluated as **Eqs. (A.8)-(A.9)**. For the models of medium to long natural period, Velocity Dependent, the spectral velocity is assumed to be period-independent and the reduction factors are defined as below,

$$R_d = D_h \frac{T_{eq}}{T_f} \tag{A.8}$$

$$R_a = D_h \frac{T_f}{T_{eq}} \tag{A.9}$$

While for models having a short period, Acceleration Dependent Model, the spectral acceleration is time-dependent and hence, **Eqs. (A.8) and (A.9)** can be rewritten as,

$$R_d = D_h \frac{T_{eq}}{T_f} \frac{T_{eq} + T_0}{2T_f} \tag{A.10}$$

$$R_a = D_h \frac{T_f}{T_{eq}} \frac{T_{eq} + T_0}{2T_f} \tag{A.11}$$

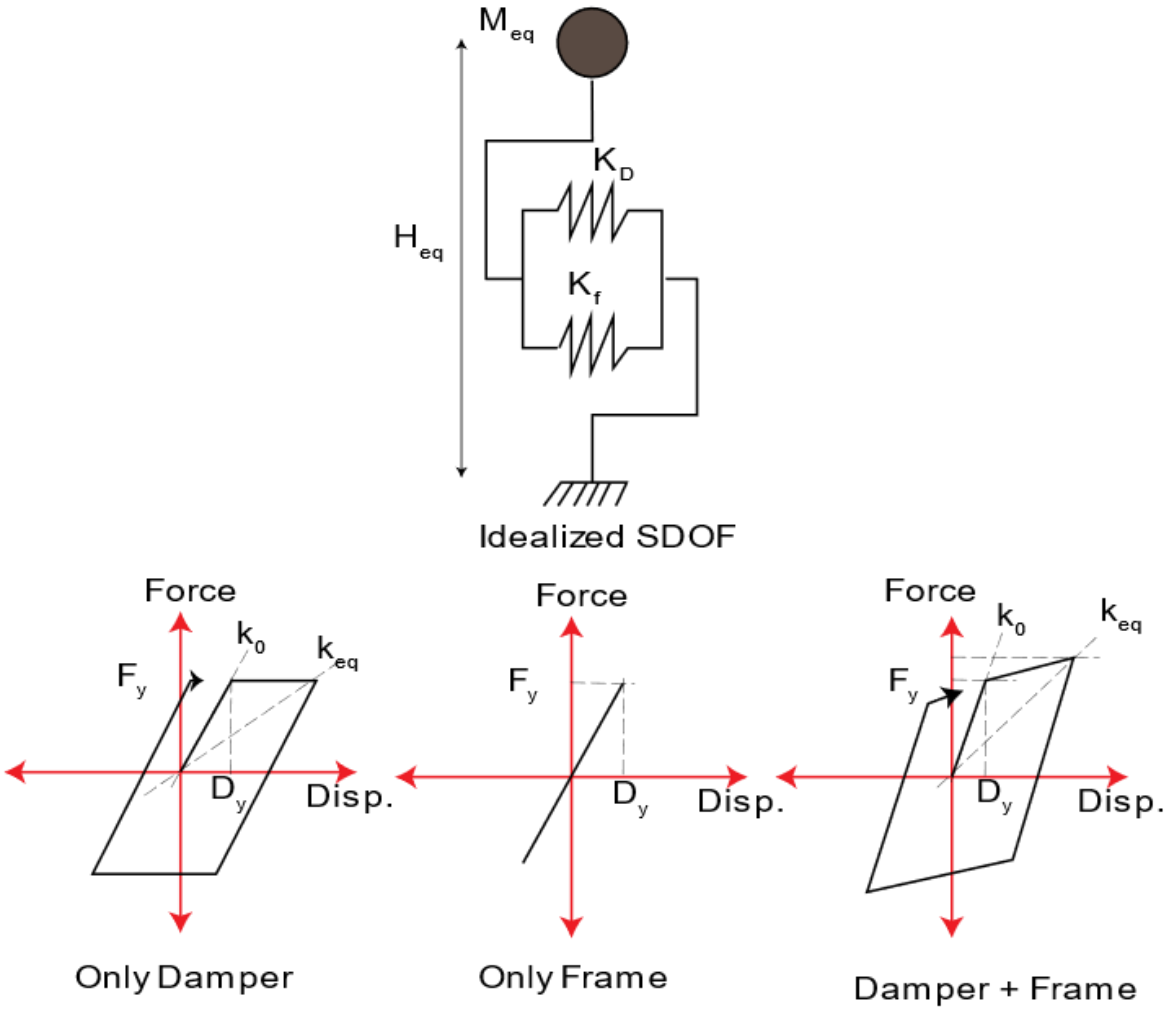

Figure A.3. Idealized SDOF and force-displacement relationship of BRB system.

For a certain ductility factor, μ, and a stiffness ratio, K_d/K_f, the amount of displacement and shear force reduction factors are plotted (which after this point is called Control Performance Curve – CPC) [A4], as shown in **Figure A.4**. The CPC plot serves as a practical tool that simplifies the preliminary design of the damping device by optimizing the ratio of damper stiffness to the bare frame. Once the stiffness ratio, K_d/K_f, for the equivalent SDOF is obtained, then, the required amount of BRB's stiffness will be distributed

over the height of the MDOF system. For this purpose, it is assumed, first, the equivalent damping ratio of the MDOF system is the same as of the equivalent SDOF system. Secondly, under the design shear force, the drift angle and the ductility demand of the MDOF system are assumed to be uniform. And lastly, the yield drift angle of each story is assumed to be uniform, as well. Based on the assumption, the JSSI manual introduces the **Eq. (A.12)** to estimate the amount of required supplemented stiffness, K_{ai}, where Q_i, is the i^{th} story shear force.

$$D_h = \sqrt{\frac{1 + 25h_0}{1 + 25h_{eq}}} \tag{A.12}$$

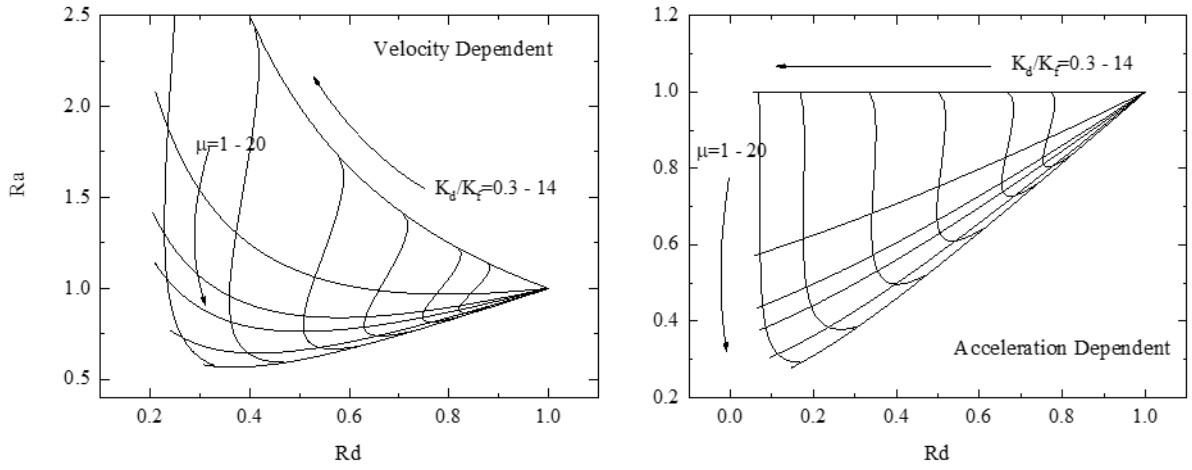

Figure A.4. Control performance curve (CPC), a) velocity-dependent, b) acceleration dependent.

The design procedure and steps discussed in this section are briefly presented in the flowchart of **Figure A.5.**

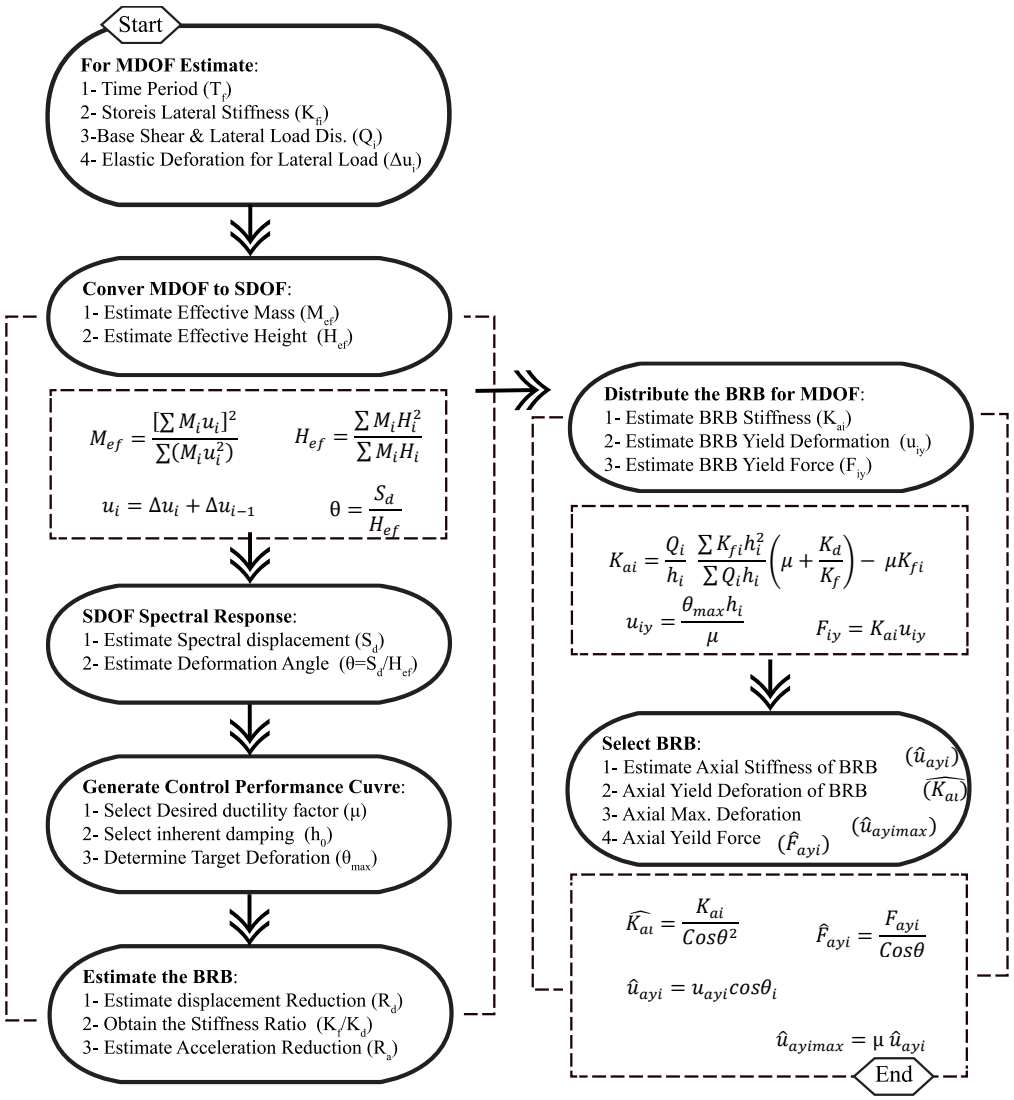

Figure A.5. Flow chart of the preliminary design of a passively controlled building

A1.3 Appendix references

[A1] Kobori, T.; New proposal of research and development for seismic response-controlled structure Memorial Proc. for the Centenary of the Birth of Tachu Naito (Waseda University), **1986**.

[A2] Kasai, K., and Kibayashi, M.; JSSI manual for building passive control technology part-1 manual contents and design/analysis methods, *13th WCEE*, Vancouver Canada, Paper 2989, Aug. 1-6 **2004**.

[A3] JSSI, Report of investigation committee on response control buildings. The Japan Society of Seismic Isolation. **2012**.

[A4] Kasai, K., Baba, Y., Fu, Y. and Watanabe, A.; Passive control system for seismic damage mitigation, *Journal of Structural Engineering*, 124, 501-5121, **1998**